Vegard Leistad

Triangular and tetrahedral assumed natural strain finite element formulations for Seth-Hill strain tensors

June 2022

Master's thesis

2022

Vegard Leistad

NTNU
Norwegian University of
Science and Technology
Faculty of Engineering
Department of Mechanical and Industrial Engineering

Master's thesis

NTNU
Norwegian University of
Science and Technology

NTNU
Norwegian University of
Science and Technology

NTNU
Norwegian University of
Science and Technology

Triangular and tetrahedral assumed natural strain finite element formulations for Seth-Hill strain tensors

Vegard Leistad

Mechanical Engineering
Submission date: June 2022
Supervisor: Bjørn Haugen

Norwegian University of Science and Technology
Department of Mechanical and Industrial Engineering

Abstract

Does a cylinder subjected to torsion elongate or shorten?

Models using Seth-Hill strain tensors are capable of modeling both elongation and shortening through the use of a single parameter (m). This master thesis has investigated different element formulations with Seth-Hill strain tensors. Both conventional elements and assumed natural strain elements have been created based on triangular and tetrahedral element geometries.

The assumed natural strain formulations give formulations capable of modeling the whole range of the Seth-Hill strain tensors, thus giving elongation and shortening capabilities to the element formulations. Commercial softwares often use conventional element formulations. These element formulations are practical for implementing the Green-Lagrange strain tensor ($m = 1$) and were used for creating a comparative basis. Two- and three-dimensional geometries have been collected from the Abaqus software and put into an element solver based on previous master theses. Ultimately the element formulations have been compared for elastic and plastic conditions with different strain tensors.

Sammendrag

Blir en sylinder kortere eller lengre når den vris?

Modeller som bruker Seth-Hill tøyningsuttrykk evner å modellere både forkortning og økning ved hjelp av en parameter (m). I denne masteroppgaven har Seth-Hill tøyningsuttrykk blitt brukt for å lage elementformuleringer for store tøyningsuttrykk. Dette ved hjelp av både konvensjonelle elementformuleringer og antatt naturlig tøyningsformuleringer basert på trekant og tetraeder analogien.

De antatt naturlig tøyningsformuleringene har egenskaper som gir fritt valg tøyningstensor (m) slik at sylinderen kan modelleres både kortere og lengre. Dagens kommersielle programvarer bruker i stor grad de konvensjonelle formuleringene, og for å få et sammenligningsgrunnlag har disse også blitt programmert opp med Green-Lagrange tøyning ($m = 1$). To- og tredimensjonale geometrier har blitt hentet ut fra Abaqus programvaren og satt inn i en elementsolver basert på tidligere masteroppgaver. Deretter har formuleringene blitt sammenlignet for elastisitet, plastisitet og tøyningstensorer.

Preface

My two-year mechanical engineering study program at the Norwegian University of Science and Technology ends with this master thesis carried out throughout the winter and spring of 2022. The work bases itself upon previous master theses and has created possibilities for learning about computer structures, finite element methods, and plasticity formulations.

First and foremost, I would like to show my gratitude to my supervisor Bjørn Haugen. His previous finite element courses are the main reason for choosing this subject. Countless hours have been put down by him answering different finite element method-related questions, and many clever approaches have been the product of his presence.

My computer science friends Brage Lytskjold and Jakob Vaardal also deserve recognition for their helpfulness. They have been of great help answering different programming-related questions throughout the winter, and their help has improved the code significantly.

At last, I would like to thank the predecessors of this thesis, Maren Eriksen Eia, Heidi Igland Jacobsen; and Anders Østebø, for putting down a solid foundation for this work.

Contents

List of Figures

List of Tables

Notations and acronyms

Bold straight letters showcase the matrix notation, while light skew letters showcase tensor notation.

$\mathbf{X}$, $\mathbf{E}$: Matrix notation

X, E - Tensor notation

Forward subscript 0 and t is used for denoting tensors, bases and other properties seen at different times.

${}_0A$: Property A seen at time 0

${}_tA$: Property A seen at time t

Abbreviations and acronyms:

ANS:	assumed natural strain
Conv:	conventional element formulation
CST:	constant strain triangle/tetrahedron

Chapter 1

Introduction

Small strain theory is widely agreed upon for continuum mechanics and implemented in almost all finite element software. This approach gives a quick overview of stresses, strains, and displacements of a construction exhibiting small strains and rotations. Unlike the small strain tensor, there is no one and true large strain tensor.

Some of the most commonly used large strain tensors are the Green-Lagrange, Logarithmic/Henchy, and Eulerian/Almansi strain tensors. The Green-Lagrange strain tensor is practical in implementations based on the undeformed description. Negative stretch values of the Green-Lagrange strain tensor give a non-surjective function, meaning infinitely large compressive strains are not possible with the Green-Lagrange strain tensor. The same can be said for the Almansi strain tensor but based on the deformed system and elongation. The Logarithmic/Hencky strain tensor exhibits many attractive properties but is difficult to explicitly implement in finite element formulations.

The three strain tensors mentioned above can be generalized into a set of matrix polynomials, forming the Seth-Hill strain tensors. B.R. Seth proposed this idea during the 1960s [1], giving infinitely many large strain tensors. R. Hill expanded the idea further by suggesting work conjugate stresses for each strain tensor [2].

The most common way of solving partial differential equations in solid continuum mechanics today is through the finite element method. The finite element method assumes displacement field and position field inside a region, giving the weak/Galerkin formulation. Using the displacement and position field of the whole element for creating strain tensors gives the conventional approach. Another approach is the Assumed Natural Strain (ANS), assuming strain states at specified locations inside the element/region. An idea first introduced by K. Willam [3].

The works of M. Eia et. al [4] and A. Østebø [5] is the predecessor of this thesis, who based their work on the methodology of C. Felippa et al. [6]. They used conventional and ANS element formulations for expressing constant strain triangles and tetrahedrons. In this work, ANS linear strain triangles and tetrahedrons expanded the idea of the constant strain ANS element formulations. Different geometries were then tested in isotropic elasticity and associated plasticity and compared with the conventional element formulations.

Chapter 2

Preliminaries

2.1 Finite strain measures

In the finite element method, it is desirable to relate forces with displacements. Equation 2.1 shows the rank 1. displacement tensor as a function of the deformed ($_{\mathrm{t}}\mathbf{X}$) and undeformed system ($_0\mathbf{X}$), seen at time = t and time = 0.

$$\mathbf{u} = {}_{\mathrm{t}}\mathbf{X} - {}_0\mathbf{X} \tag{2.1}$$

The change of infinitesimal material fibers is of interest when looking at deformations of a solid. Equation 2.2 shows the Lagrangian deformation gradient described through the chain rule of the deformed solid differentiated with respect to the undeformed solid. Here (α) follows Einstein summation and sums up to the number of dimensions.

$$\delta_{\mathrm{t}}\mathbf{X} = \frac{\partial_{\mathrm{t}}\mathbf{X}}{\partial_0\mathbf{X}}\delta_0\mathbf{X} = {}_0F_{i\alpha}\ \delta_0 X_\alpha \tag{2.2}$$

The Lagrangian deformation gradient (hereby called the deformation gradient) can be inserted into the differentiated displacements, giving the displacement gradient in Equation 2.3. ($_0G_{ij}$) denotes the displacement gradient, ($_0F_{ij}$) the deformation gradient, and (δ_{ij}) the Kronecker delta. The displacement gradient also follows the pattern of Equation 2.4.

$$\frac{\partial \mathbf{u}}{\partial_0\mathbf{X}} = {}_0G_{ij} = {}_0F_{ij} - \delta_{ij} \tag{2.3}$$

$${}_0G_{ij} = \begin{bmatrix} \frac{\partial u}{\partial_0 X} & \frac{\partial u}{\partial_0 Y} & \frac{\partial u}{\partial_0 Z} \\ \frac{\partial v}{\partial_0 X} & \frac{\partial v}{\partial_0 Y} & \frac{\partial v}{\partial_0 Z} \\ \frac{\partial w}{\partial_0 X} & \frac{\partial w}{\partial_0 Y} & \frac{\partial w}{\partial_0 Z} \end{bmatrix} = \begin{bmatrix} g_1 & g_4 & g_7 \\ g_2 & g_5 & g_8 \\ g_3 & g_6 & g_9 \end{bmatrix} \tag{2.4}$$

The deformation gradient shown in Equation 2.2 can further be used for creating different deformation measures. Equation 2.5 shows the rank 2. symmetric right Cauchy-Green deformation tensor. Using the polar decomposition theorem for rewriting the deformation gradient creates a stretch tensor (U) and rotation/transformation (R). Figure 2.1 shows a principal sketch of the polar decomposition theorem. The polar decomposition of the left stretch tensor (counter-clockwise movement in Figure 2.1) rotates the rigid body firstly, then stretches the solid. The same goes for the polar decomposition of the right stretch

tensor (clockwise movement in Figure 2.1), but with stretching of the body initially, then rigid body rotations. From Equation 2.5, it can be seen that the right Cauchy-Green deformation tensor is independent of the rotation/transformation (R). A more thorough derivation can be found in F. Irgens's book on continuum mechanics ([7], p. 124).

$$ {}_0F_{\alpha i}\ {}_0F_{\alpha j} = R_{\alpha\beta}\ {}_0U_{\beta i}\ R_{\alpha\gamma}\ {}_0U_{\gamma j} = {}_0U_{\alpha i}\ {}_0U_{\gamma j}\delta_{\alpha\gamma} = {}_0U_{\alpha i}\ {}_0U_{\alpha j} \tag{2.5} $$

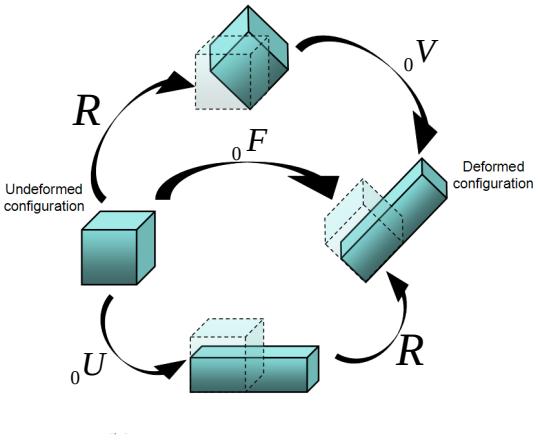

Figure 2.1: Polar decomposition of the right and left deformation tensors. [8]

2.2 Seth-Hill strain tensors and work conjugate stresses

The small strain tensor shown in Equation 2.6 is a popular choice in many solid mechanics applications. In contrast to the right Cauchy-Green deformation tensor, the small strain tensor does not create stretches independent of the rigid body rotations. Equation 2.7 shows the generalized form of the Seth-Hill strain tensors, an idea proposed by B.R Seth [1]. As the strain tensor is a function of the right Cauchy-Green deformation tensor, the stretches are independent of rotations. Here the values $m = \{-1, 0, 1\}$ correspond with the Almansi, Logarithmic/Hencky, and Green-Lagrange strain tensors.

$$ \varepsilon_{ij} = \frac{1}{2}(G_{ij} + G_{ji}) \tag{2.6} $$

$$ {}_0E_{ij} = \begin{cases} \frac{1}{2m}\left(({}_0F_{\alpha i}\ {}_0F_{\alpha j})^m - \delta_{ij}\right) & \text{if } m \neq 0 \\ \frac{1}{2}\ln\left({}_0F_{\alpha i}\ {}_0F_{\alpha j}\right) & \text{if } m = 0 \end{cases} \tag{2.7} $$

The idea of the generalized strain tensor was further expanded by R. Hill [2]. He introduced the idea of each Seth-Hill strain tensor having a corresponding conjugate stress tensor. The stress tensor had to be of such character that the work created by the Seth-Hill strain and stress conjugate pair had to be equal to any other conjugate pairs.

2.3 Covariant representation of 1-dimensional rod

Stresses, strains, displacements, and forces all need to be invariant for creating a meaningful representation of the physics in a solid. Strain tensors are rank 2. tensors, and thus need to obey Equation 2.8 for the 2-dimensional covariant representation. Here tilde represents a continuously differentiable basis.

$$\begin{bmatrix} \widetilde{E}_{\widetilde{X}\widetilde{X}} \\ \widetilde{E}_{\widetilde{Y}\widetilde{Y}} \\ \widetilde{E}_{\widetilde{X}\widetilde{Y}} \end{bmatrix} = \begin{bmatrix} \frac{\partial X}{\partial \widetilde{X}}\frac{\partial X}{\partial \widetilde{X}} & \frac{\partial Y}{\partial \widetilde{X}}\frac{\partial Y}{\partial \widetilde{X}} & \frac{\partial X}{\partial \widetilde{X}}\frac{\partial Y}{\partial \widetilde{X}} \\ \frac{\partial X}{\partial \widetilde{Y}}\frac{\partial X}{\partial \widetilde{Y}} & \frac{\partial Y}{\partial \widetilde{Y}}\frac{\partial Y}{\partial \widetilde{Y}} & \frac{\partial X}{\partial \widetilde{Y}}\frac{\partial Y}{\partial \widetilde{Y}} \\ \frac{\partial X}{\partial \widetilde{X}}\frac{\partial X}{\partial \widetilde{Y}} & \frac{\partial Y}{\partial \widetilde{X}}\frac{\partial Y}{\partial \widetilde{Y}} & \frac{\partial X}{\partial \widetilde{X}}\frac{\partial Y}{\partial \widetilde{Y}} \end{bmatrix} \begin{bmatrix} E_{XX} \\ E_{YY} \\ E_{XY} + E_{YX} \end{bmatrix} \tag{2.8}$$

Equation 2.9 shows the global cartesian coordinates differentiated in terms of the local basis. This expression can further used for creating the composure of the covariant transformation in Equation 2.8.

$$\begin{bmatrix} \delta X \\ \delta Y \end{bmatrix} = \begin{bmatrix} \frac{\partial X}{\partial \widetilde{X}} & \frac{\partial X}{\partial \widetilde{Y}} \\ \frac{\partial Y}{\partial \widetilde{X}} & \frac{\partial Y}{\partial \widetilde{Y}} \end{bmatrix} \begin{bmatrix} \delta \widetilde{X} \\ \delta \widetilde{Y} \end{bmatrix} \tag{2.9}$$

Now assuming two points can be used to describe the local orthonormal unit basis $(\widetilde{X}, \widetilde{Y})$, then Equation 2.9 can be rewritten into Equation 2.10. Where $(\Delta X, \Delta Y)$ denotes the difference between the X and Y coordinates for the two points, and L is the length between the two points.

$$\begin{bmatrix} \delta X \\ \delta Y \end{bmatrix} = \begin{bmatrix} \frac{\Delta X}{L} & -\frac{\Delta Y}{L} \\ \frac{\Delta Y}{L} & \frac{\Delta X}{L} \end{bmatrix} \begin{bmatrix} \delta \widetilde{X} \\ \delta \widetilde{Y} \end{bmatrix} = \begin{bmatrix} \mathbf{e} & \mathbf{n} \end{bmatrix} \begin{bmatrix} \delta \widetilde{X} \\ \delta \widetilde{Y} \end{bmatrix} \tag{2.10}$$

Assuming the local basis runs between positions $(1 \rightarrow 2)$ gives the basis vector $({}_0\mathbf{e}^1)$ shown in Equation 2.11. This single rod basis gives the covariant transformation between the normal strain $(\widetilde{X}\widetilde{X})$ and the global Cartesian strain tensor. The relation between the two strain tensors therefore follows Equation 2.12.

$${}_0\mathbf{e}^1 = (({}_0X_2 - {}_0X_1)^2 + ({}_0Y_2 - {}_0Y_1)^2)^{-1/2} \begin{bmatrix} {}_0X_2 - {}_0X_1 \\ {}_0Y_2 - {}_0Y_1 \end{bmatrix} \tag{2.11}$$

$$\begin{bmatrix} {}_0\widetilde{E}_1 \end{bmatrix} = \begin{bmatrix} {}_0e^{1X}{}_0e^{1X} & {}_0e^{1Y}{}_0e^{1Y} & {}_0e^{1X}{}_0e^{1Y} \end{bmatrix} \begin{bmatrix} {}_0E_{XX} \\ {}_0E_{YY} \\ {}_0E_{XY} + {}_0E_{YX} \end{bmatrix} \tag{2.12}$$

Equation 2.12 relates the local strain component ${}_0\widetilde{E}_1$ through the global Cartesian strain tensor, but this relation is not invertible. Hence two more directions are needed. Choosing three directions (1,2,3) such that the covariant transformation of each of the three directions is linearly independent gives Equation 2.13. This transformation assumes the local strain components $({}_0\widetilde{E}_1, {}_0\widetilde{E}_2, {}_0\widetilde{E}_3)$ follow the normal strains of $({}_0\mathbf{e}^1, {}_0\mathbf{e}^2, {}_0\mathbf{e}^3)$. The same derivation is also valid for the 3-dimensional case giving Equation 2.14.

$${}_0\widetilde{\mathbf{E}} = \widetilde{\mathbf{T}}\ {}_0\mathbf{E} = \begin{bmatrix} {}_0\widetilde{E}_1 \\ {}_0\widetilde{E}_2 \\ {}_0\widetilde{E}_3 \end{bmatrix} = \begin{bmatrix} {}_0e^{1X}{}_0e^{1X} & {}_0e^{1Y}{}_0e^{1Y} & {}_0e^{1X}{}_0e^{1Y} \\ {}_0e^{2X}{}_0e^{2X} & {}_0e^{2Y}{}_0e^{2Y} & {}_0e^{2X}{}_0e^{2Y} \\ {}_0e^{3X}{}_0e^{3X} & {}_0e^{3Y}{}_0e^{3Y} & {}_0e^{3X}{}_0e^{3Y} \end{bmatrix} \begin{bmatrix} {}_0E_{XX} \\ {}_0E_{YY} \\ 2{}_0E_{XY} \end{bmatrix} \tag{2.13}$$

$$\begin{bmatrix} {}_0\widetilde{E}_1 \\ {}_0\widetilde{E}_2 \\ {}_0\widetilde{E}_3 \\ {}_0\widetilde{E}_4 \\ {}_0\widetilde{E}_5 \\ {}_0\widetilde{E}_6 \end{bmatrix} = \begin{bmatrix} {}_0e^{1X}{}_0e^{1X} & {}_0e^{1Y}{}_0e^{1Y} & {}_0e^{1Z}{}_0e^{1Z} & {}_0e^{1Y}{}_0e^{1Z} & {}_0e^{1X}{}_0e^{1Z} & {}_0e^{1X}{}_0e^{1Y} \\ {}_0e^{2X}{}_0e^{2X} & {}_0e^{2Y}{}_0e^{2Y} & {}_0e^{2Z}{}_0e^{2Z} & {}_0e^{2Y}{}_0e^{2Z} & {}_0e^{2X}{}_0e^{2Z} & {}_0e^{2X}{}_0e^{2Y} \\ {}_0e^{3X}{}_0e^{3X} & {}_0e^{3Y}{}_0e^{3Y} & {}_0e^{3Z}{}_0e^{3Z} & {}_0e^{3Y}{}_0e^{3Z} & {}_0e^{3X}{}_0e^{3Z} & {}_0e^{3X}{}_0e^{3Y} \\ {}_0e^{4X}{}_0e^{4X} & {}_0e^{4Y}{}_0e^{4Y} & {}_0e^{4Z}{}_0e^{4Z} & {}_0e^{4Y}{}_0e^{4Z} & {}_0e^{4X}{}_0e^{4Z} & {}_0e^{4X}{}_0e^{4Y} \\ {}_0e^{5X}{}_0e^{5X} & {}_0e^{5Y}{}_0e^{5Y} & {}_0e^{5Z}{}_0e^{5Z} & {}_0e^{5Y}{}_0e^{5Z} & {}_0e^{5X}{}_0e^{5Z} & {}_0e^{5X}{}_0e^{5Y} \\ {}_0e^{6X}{}_0e^{6X} & {}_0e^{6Y}{}_0e^{6Y} & {}_0e^{6Z}{}_0e^{6Z} & {}_0e^{6Y}{}_0e^{6Z} & {}_0e^{6X}{}_0e^{6Z} & {}_0e^{6X}{}_0e^{6Y} \end{bmatrix} \begin{bmatrix} {}_0E_{XX} \\ {}_0E_{YY} \\ {}_0E_{ZZ} \\ 2{}_0E_{YZ} \\ 2{}_0E_{XZ} \\ 2{}_0E_{XY} \end{bmatrix} \tag{2.14}$$

2.4 Hyperelastic Hooke's law

The stresses need to be related to the strains through a constitutive relation, for instance through a hyperelastic material model. If there exist a strain energy per volume scalar function ψ fulfilling Equation 2.15, then the material model can be seen as hyperelastic ([7], p. 249).

$$\Delta\psi = \int_{\Delta\mathbf{E}} \mathbf{S}^T \delta\mathbf{E} = \int_{\Delta\mathbf{E}} \frac{\partial\psi}{\partial\mathbf{E}}\, \delta\mathbf{E} \tag{2.15}$$

The Hookean solid fulfills this criterion, assuming a linear relationship between the stress and strain tensor. For isotopic elasticity, the Hookean material model is described by two variables, the young's modulus (μ); and the Poisson ratio ratio (ν). This gives the constitutive relation for the 3-dimensional case in Equation 2.16 and the plane stress case in Equation 2.17.

$$\begin{bmatrix} {}_0S_{XX} \\ {}_0S_{YY} \\ {}_0S_{ZZ} \\ {}_0S_{YZ} \\ {}_0S_{XZ} \\ {}_0S_{XY} \end{bmatrix} = \frac{\mu}{(1-2\nu)(1+\nu)} \begin{bmatrix} 1-\nu & \nu & \nu & 0 & 0 & 0 \\ \nu & 1-\nu & \nu & 0 & 0 & 0 \\ \nu & \nu & 1-\nu & 0 & 0 & 0 \\ 0 & 0 & 0 & \frac{1-2\nu}{2} & 0 & 0 \\ 0 & 0 & 0 & 0 & \frac{1-2\nu}{2} & 0 \\ 0 & 0 & 0 & 0 & 0 & \frac{1-2\nu}{2} \end{bmatrix} \begin{bmatrix} {}_0E^{\mathrm{el}}_{XX} \\ {}_0E^{\mathrm{el}}_{YY} \\ {}_0E^{\mathrm{el}}_{ZZ} \\ 2{}_0E^{\mathrm{el}}_{YZ} \\ 2{}_0E^{\mathrm{el}}_{XZ} \\ 2{}_0E^{\mathrm{el}}_{XY} \end{bmatrix} \tag{2.16}$$

$${}_0\mathbf{S} = \begin{bmatrix} {}_0S_{XX} \\ {}_0S_{YY} \\ {}_0S_{XY} \end{bmatrix} = \mathbf{C}\ {}_0\mathbf{E}^{\mathrm{el}} = \frac{\mu}{(1-2\nu)(1+\nu)} \begin{bmatrix} 1-\nu & \nu & 0 \\ \nu & 1-\nu & 0 \\ 0 & 0 & \frac{1-2\nu}{2} \end{bmatrix} \begin{bmatrix} {}_0E^{\mathrm{el}}_{XX} \\ {}_0E^{\mathrm{el}}_{YY} \\ 2{}_0E^{\mathrm{el}}_{XY} \end{bmatrix} \tag{2.17}$$

2.5 Plasticity formulations

Multiplicative decomposition and additive decomposition are the two most popular choices for plasticity formulations. The multiplicative decomposition introduced by E. H. Lee et. al [9] and E. H Lee [10], assumes the total displacements to be a sum of an elastic displacement and a plastic displacement. Equation 2.18 shows the multiplicative decomposition of the displacement and velocity gradient. The multiplicative decomposition can also be written in terms of the deformation gradient in Equation 2.19.

$$G_{ij} = G_{ij}^{\mathrm{el}} + G_{ij}^{\mathrm{pl}}, \quad \delta G_{ij} = \delta G_{ij}^{\mathrm{el}} + \delta G_{ij}^{\mathrm{pl}} \tag{2.18}$$

$$F_{ij} = \frac{\partial_{\mathrm{t}} \mathbf{X}}{\partial_0 \mathbf{X}} = \frac{\partial_{\mathrm{t}} \mathbf{X}}{\partial \boldsymbol{\chi}} \frac{\partial \boldsymbol{\chi}}{\partial_0 \mathbf{X}} = {}_0F_{i\alpha}^{\mathrm{el}}\, {}_0F_{\alpha j}^{\mathrm{pl}} \tag{2.19}$$

Changing between different strain and stress tensors creates computational inefficient algorithms for practical purposes. An older and more efficient model is the additive decomposition, for instance seen in the paper from A. E. Green et al. [11]. Here the total strain tensor is assumed to be a sum of an elastic and plastic strain tensor, thus giving Equation 2.20.

$$\mathbf{E} = \mathbf{E}^{\mathrm{el}} + \mathbf{E}^{\mathrm{pl}} \tag{2.20}$$

Chapter 3

Method

3.1 The virtual work equation

The virtual work of a single element follows Equation 3.1. Here the strain tensor and traction forces have been differentiated in terms of the nodal displacements ($\mathbf{u}$) and integrated over the volume ($_0\Omega$) and area ($_0A$) of the element. Removing the incremental nodal displacements gives the internal and external force vectors in Equation 3.2. The distributed load, strain tensor, stress tensor, and volume, are all seen at time = 0, giving the Total Lagrangian description.

$$\delta\mathbf{u}^T \int_{_0A} {}_0\mathbf{q}\, d_0A = \delta\mathbf{u}^T \int_{_0\Omega} \frac{\partial_0\mathbf{E}^T}{\partial\mathbf{u}}\, {}_0\mathbf{S}\, d_0\Omega = \delta\mathbf{u}^T \int_{_0\Omega} \mathbf{B}^T {}_0\mathbf{S}\, d_0\Omega \tag{3.1}$$

$$\mathbf{f}^{\text{ext}} - \mathbf{f}^{\text{int}} = \int_{_0A} {}_0\mathbf{q}\, d_0A - \int_{_0\Omega} \mathbf{B}^T {}_0\mathbf{S}\, d_0\Omega = 0 \tag{3.2}$$

3.2 Solution methods

Newtons-Raphson methods are commonly used for solving systems of non-linear equations. The solution methods give fast and quadratic convergence close to the solution. Two sub choices of the Newtons-Raphson are the displacement and load control solvers. The displacement and load control solvers are two sides of the same coin and can be implemented into the same algorithm. Setting the load ($_0\mathbf{f}$) as a constant through the iterative solving procedure gives the load control solver. The same goes for the displacements control, but with constant displacements for selected nodes.

Obtaining a residual ($\mathbf{r}$) equal to zero as in Equation 3.3 is the objective of the solution process. Equation 3.4 shows the Taylor expansion of the internal and external force vector. Using the procedure in Table 3.1 and solving this system over and over creates convergence.

$$\mathbf{r} = \mathbf{f}^{\text{ext}} - \int_{_0\Omega} \mathbf{B}^T {}_0\mathbf{S}\, d_0\Omega = 0 \tag{3.3}$$

$$\mathbf{r}(\mathbf{u} + \delta\mathbf{u}, \lambda) \approx \mathbf{r}(\mathbf{u}, \lambda) + \frac{\partial\mathbf{r}}{\partial\mathbf{u}}\delta\mathbf{u} = \mathbf{r}(\mathbf{u}, \lambda) + \mathbf{K}\delta\mathbf{u} = 0 \tag{3.4}$$

Table 3.1: Load and displacement control procedure.

Initialize $\mathbf{u}$ and $\mathbf{f}$:
Iterations until $\mathbf{r}^T\mathbf{r}$ or $\lvert\mathbf{r}^T\delta\mathbf{u}\rvert <$ tol:
Solve for $\delta\mathbf{u}$:
$\mathbf{r}(\mathbf{u}) = \text{-}\mathbf{K}(\mathbf{u})\ \delta\mathbf{u}$
Set:
$\mathbf{u} = \mathbf{u} + \delta\mathbf{u}$

3.3 Conventional element formulations

Element formulations discretize the solid into points/nodes and create elements based on these points, while the shape functions assume a solution inside the element. Equation 3.5 shows the assumed solution for the three displacement components (u, v, w), with the nodal displacements (u_α, v_α, w_α) and the corresponding shape functions (N_α). The sub-indices follow dummy indices in Einstein's summation convention and sum up to the number of nodes in the element (n). An input position (X, Y) is inserted into a shape function. The output magnitude (N_α) then describes the influence of the nodal displacement components (u_α, v_α, w_α) at that position. Differentiating the assumed solution creates the displacement gradient components shown in Equation 3.6.

$$\begin{aligned} u &= N_\alpha u_\alpha \\ v &= N_\alpha v_\alpha \qquad\qquad \alpha = (1,\ \dots\ , n) \\ w &= N_\alpha w_\alpha \end{aligned} \tag{3.5}$$

$$\begin{aligned} \frac{\partial u}{\partial_0 X} &= \frac{\partial N_\alpha}{\partial_0 X} u_\alpha, \quad \frac{\partial u}{\partial_0 Y} = \frac{\partial N_\alpha}{\partial_0 Y} u_\alpha, \quad \frac{\partial u}{\partial_0 Z} = \frac{\partial N_\alpha}{\partial_0 Z} u_\alpha \\ \frac{\partial v}{\partial_0 X} &= \frac{\partial N_\alpha}{\partial_0 X} v_\alpha, \quad \frac{\partial v}{\partial_0 Y} = \frac{\partial N_\alpha}{\partial_0 Y} v_\alpha, \quad \frac{\partial v}{\partial_0 Z} = \frac{\partial N_\alpha}{\partial_0 Z} v_\alpha \\ \frac{\partial w}{\partial_0 X} &= \frac{\partial N_\alpha}{\partial_0 X} w_\alpha, \quad \frac{\partial w}{\partial_0 Y} = \frac{\partial N_\alpha}{\partial_0 Y} w_\alpha, \quad \frac{\partial w}{\partial_0 Z} = \frac{\partial N_\alpha}{\partial_0 Z} w_\alpha \end{aligned} \tag{3.6}$$

Shape functions for triangular and tetrahedron elements are best obtained through area and volume coordinates. Figure 3.1 shows the three areas defining the area coordinates for triangular elements. In this figure, node 1 relates to the area (A_1), node 2 to the area (A_2), and node 3 to the area (A_1). The area coordinate (ζ_1) can now be defined as the area ($_0A_1$) divided by the total area, following Equation 3.7. When inserting the nodal position of node 1 into the shape functions, area ($_0A_1$) is equal to the total area, while areas ($_0A_2$) and ($_0A_3$) are equal to zero. Meaning the nodal displacements correspond with the assumed solution. The tetrahedron volume coordinates follow the same logic but have four tetrahedral volumes instead.

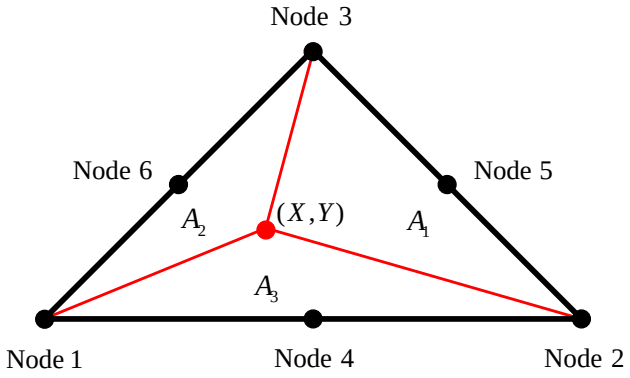

Figure 3.1: Node numbering and area coordinates for the 6-node triangle.

$$\zeta_i = \frac{{}_0A_i}{{}_0A} \tag{3.7}$$

Isoparametric element formulations use the same shape functions for positions as for the displacements, the positions can therefore be written as in Equation 3.8.

$$\begin{aligned} {}_0X &= N_\alpha \, {}_0X_\alpha \\ {}_0Y &= N_\alpha \, {}_0Y_\alpha \qquad\qquad \alpha = (1, \ \dots \ , n) \\ {}_0Z &= N_\alpha \, {}_0Z_\alpha \end{aligned} \tag{3.8}$$

Setting the $(m = 1)$ for the Seth-Hill strain tensor gives the Green-Lagrange strain tensor shown in Equation 3.9. Rewriting the deformation gradient in terms of the displacement gradient and adding the two shear strain components creates the strain tensor in Equation 3.10.

$${}_0E_{ij} = \frac{1}{2}({}_0F_{i\alpha} \, {}_0F_{\alpha j} - \delta_{ij}) = \frac{1}{2}\left({}_0G_{ij} + {}_0G_{ji} + {}_0G_{\alpha i} \, {}_0G_{\alpha j}\right), \qquad \alpha = (1,2,3) \tag{3.9}$$

$${}_0\mathbf{E}(m=1) = \begin{bmatrix} {}_0E_{XX} \\ {}_0E_{YY} \\ {}_0E_{ZZ} \\ 2 \, {}_0E_{YZ} \\ 2 \, {}_0E_{XZ} \\ 2 \, {}_0E_{XY} \end{bmatrix} = \begin{bmatrix} g_1 + \frac{1}{2}\left(g_1^2 + g_2^2 + g_3^2\right) \\ g_5 + \frac{1}{2}\left(g_4^2 + g_5^2 + g_6^2\right) \\ g_9 + \frac{1}{2}\left(g_7^2 + g_8^2 + g_9^2\right) \\ \frac{1}{2}(g_6 + g_8 + g_4 g_7 + g_5 g_8 + g_6 g_9) \\ \frac{1}{2}(g_3 + g_7 + g_1 g_7 + g_2 g_8 + g_3 g_9) \\ \frac{1}{2}(g_2 + g_4 + g_1 g_4 + g_2 g_5 + g_3 g_6) \end{bmatrix} \tag{3.10}$$

The internal force of the element can now be rewritten in terms of the chain rule, giving Equation 3.11.

$$\mathbf{f}^{\text{int}} = \int_{{}_0\Omega} \mathbf{B}^T \, {}_0\mathbf{S} \, d_0\Omega = \int_{{}_0\Omega} \frac{\partial \mathbf{g}}{\partial \mathbf{u}}^T \frac{\partial_0 \mathbf{E}}{\partial \mathbf{g}}^T \, {}_0\mathbf{S} \, d_0\Omega \tag{3.11}$$

3.3.1 Conventional constant strain triangle

The Cartesian coordinates and area coordinates are related through the Jacobi matrix in Equation 3.12. It is only necessary to use the (ζ_1 and ζ_2) coordinates as the (ζ_3) area coordinate can be seen as linearly dependent. The shape functions differentiated with respect to the global Cartesian coordinates are now given through the area coordinates and nodal positions in Equation 3.13.

$$\begin{bmatrix} \frac{\partial \mathbf{N}}{\partial \zeta_1} \\ \frac{\partial \mathbf{N}}{\partial \zeta_2} \end{bmatrix} = \begin{bmatrix} \frac{\partial_0 X}{\partial \zeta_1} & \frac{\partial_0 Y}{\partial \zeta_1} \\ \frac{\partial_0 X}{\partial \zeta_2} & \frac{\partial_0 Y}{\partial \zeta_2} \end{bmatrix} \begin{bmatrix} \frac{\partial \mathbf{N}}{\partial_0 X} \\ \frac{\partial \mathbf{N}}{\partial_0 Y} \end{bmatrix} = \mathbf{J} \frac{\partial \mathbf{N}}{\partial_0 \mathbf{X}} \tag{3.12}$$

$$\frac{\partial \mathbf{N}}{\partial_0 \mathbf{X}} = \mathbf{J}^{-1} \frac{\partial \mathbf{N}}{\partial \boldsymbol{\zeta}} \tag{3.13}$$

Figure 3.1 shows the node configuration of the 6-node triangle, but removing the mid-side nodes (4, 5, 6) gives the configuration of the 3-node constant strain triangle. The 3-node constant strain triangle assumes linear displacements with shape functions following Equation 3.14.

$$\begin{bmatrix} N_1 \\ N_2 \\ N_3 \end{bmatrix} = \begin{bmatrix} \zeta_1 \\ \zeta_2 \\ \zeta_3 \end{bmatrix} = \begin{bmatrix} \zeta_1 \\ \zeta_2 \\ 1 - \zeta_1 - \zeta_2 \end{bmatrix} \tag{3.14}$$

The shape functions can be differentiated in the area coordinates, giving the constant matrix in Equation 3.15. Using the constant matrix found in Equation 3.15 in collaboration with the nodal undeformed position gives the Jacobi matrix in Equation 3.16.

$$\frac{\partial \mathbf{N}}{\partial \boldsymbol{\zeta}} = \begin{bmatrix} \frac{\partial N_1}{\partial \zeta_1} & \frac{\partial N_2}{\partial \zeta_1} & \frac{\partial N_3}{\partial \zeta_1} \\ \frac{\partial N_1}{\partial \zeta_2} & \frac{\partial N_2}{\partial \zeta_2} & \frac{\partial N_3}{\partial \zeta_2} \end{bmatrix} = \begin{bmatrix} 1 & 0 & -1 \\ 0 & 1 & -1 \end{bmatrix} \tag{3.15}$$

$$\mathbf{J} = \begin{bmatrix} \frac{\partial_0 X}{\partial \zeta_1} & \frac{\partial_0 Y}{\partial \zeta_1} \\ \frac{\partial_0 X}{\partial \zeta_2} & \frac{\partial_0 Y}{\partial \zeta_2} \end{bmatrix} = \begin{bmatrix} \frac{\partial N_1}{\partial \zeta_1} & \frac{\partial N_2}{\partial \zeta_1} & \frac{\partial N_3}{\partial \zeta_1} \\ \frac{\partial N_1}{\partial \zeta_2} & \frac{\partial N_2}{\partial \zeta_2} & \frac{\partial N_3}{\partial \zeta_2} \end{bmatrix} \begin{bmatrix} {}_0X_1 & {}_0Y_1 \\ {}_0X_2 & {}_0Y_2 \\ {}_0X_3 & {}_0Y_3 \end{bmatrix} \tag{3.16}$$

Representing the displacement gradient increment (velocity gradient) through the element formulation gives Equation 3.17. The terms of the velocity gradient can be collected and rewritten into a matrix expression such that the shape function partials and the incremental displacements follow Equation 3.18. This gives the change of the displacement gradient in terms of the nodal displacements in the virtual work expression.

$$\begin{aligned} \delta g_1 &= \frac{\partial N_\alpha}{\partial_0 X} \delta u_\alpha, \qquad & \delta g_4 &= \frac{\partial N_\alpha}{\partial_0 Y} \delta u_\alpha \\ \delta g_2 &= \frac{\partial N_\alpha}{\partial_0 X} \delta v_\alpha, \qquad & \delta g_5 &= \frac{\partial N_\alpha}{\partial_0 Y} \delta v_\alpha \end{aligned} \qquad \alpha = (1, 2, 3) \tag{3.17}$$

$$\frac{\partial \mathbf{g}}{\partial \mathbf{u}} \delta \mathbf{u} = \mathbf{D} \delta \mathbf{u} = \begin{bmatrix} \frac{\partial N_1}{\partial_0 X} & 0 & \frac{\partial N_2}{\partial_0 X} & 0 & \frac{\partial N_3}{\partial_0 X} & 0 \\ 0 & \frac{\partial N_1}{\partial_0 X} & 0 & \frac{\partial N_2}{\partial_0 X} & 0 & \frac{\partial N_3}{\partial_0 X} \\ \frac{\partial N_1}{\partial_0 Y} & 0 & \frac{\partial N_2}{\partial_0 Y} & 0 & \frac{\partial N_3}{\partial_0 Y} & 0 \\ 0 & \frac{\partial N_1}{\partial_0 Y} & 0 & \frac{\partial N_2}{\partial_0 Y} & 0 & \frac{\partial N_3}{\partial_0 Y} \end{bmatrix} \begin{bmatrix} \delta u_1 \\ \delta v_1 \\ \delta u_2 \\ \delta v_2 \\ \delta u_3 \\ \delta v_3 \end{bmatrix} \tag{3.18}$$

Differentiation of the Green-Lagrange strain tensor in terms of the displacement gradient is needed for the virtual work. Using the interpolation/shape functions for expressing the displacement gradient gives Equation 3.19, with the dummy indices summing from 1 to 3. Equation 3.20 now shows the differentiated Green-Lagrange strain tensor with respect to displacement gradient.

$$\begin{aligned} g_1 &= \frac{\partial N_\alpha}{\partial_0 X} u_\alpha, \qquad g_4 = \frac{\partial N_\alpha}{\partial_0 Y} u_\alpha \\ g_2 &= \frac{\partial N_\alpha}{\partial_0 X} v_\alpha, \qquad g_5 = \frac{\partial N_\alpha}{\partial_0 Y} v_\alpha \end{aligned} \qquad \alpha = (1,2,3) \tag{3.19}$$

$$\frac{\partial_0 \mathbf{E}}{\partial \mathbf{g}} \delta\mathbf{g} = \begin{bmatrix} 1+g_1 & g_2 & 0 & 0 \\ 0 & 0 & g_4 & 1+g_5 \\ g_4 & 1+g_5 & 1+g_1 & g_2 \end{bmatrix} \begin{bmatrix} \delta g_1 \\ \delta g_2 \\ \delta g_4 \\ \delta g_5 \end{bmatrix} \tag{3.20}$$

Due to the constant integrand, the internal force vector in Equation 3.21 is found by multiplying with the volume (${}_0\Omega$). The same goes for the incremental internal force vector found in Equation 3.22.

$$\mathbf{f}^{\text{int}} = \mathbf{B}^T {}_0\mathbf{S}\ {}_0\Omega = \mathbf{B}^T {}_0\mathbf{S}\ {}_0A_0t \tag{3.21}$$

$$\delta\mathbf{f}^{\text{int}} = \delta\mathbf{B}^T\ {}_0\mathbf{S}\ {}_0A_0t + \mathbf{B}^T\delta_0\mathbf{S}\ {}_0A_0t = (\mathbf{K}_g + \mathbf{K}_m)\delta\mathbf{u} \tag{3.22}$$

Differentiation of the stresses in the incremental internal force vector gives the material stiffness. In plasticity, the stress increment can follow two approaches; the hyperelastic Hooke's law from Equation 2.16 or the tangent moduli shown in Equation 3.23. During the solution process, the stress increment switches between the tangent moduli and the hyperelastic model. An integration point or element subjected to yielding uses the tangent moduli, and the contrary uses the hyperelastic Hooke's law. It should be pointed out that the incremental form only appears in the material stiffness matrix. The residual in Equation 3.3 should only use the constitutive relations in elastic conditions to obtain stress work conjugates. In practice this means the constitutive relation related to plastic flow works purely as an assist for faster convergence. Inserting the tangent moduli obtained in Equation 3.23 into the stress increment, gives the material stiffness matrix shown in Equation 3.24.

$$\delta_0\mathbf{S} = \mathbf{C}^{\text{ep}}\ \delta_0\mathbf{E} \tag{3.23}$$

$$\mathbf{K}_m\delta\mathbf{u} = \mathbf{B}^T\mathbf{C}^{\text{ep}}\mathbf{B}^T\delta\mathbf{u}\ {}_0A_0t \tag{3.24}$$

The incremental differentiated strain tensor creates the geometric stiffness matrix for the conventional element formulation. Equation 3.25 is obtained by collecting and rewriting the stress tensor and the incremental differentiated strain tensor. Inserting Equation 3.25 into the incremental internal force vector gives the geometric stiffness matrix in Equation 3.26.

$$\delta\left(\frac{\partial_0 \mathbf{E}}{\partial \mathbf{g}}\right){}_0\mathbf{S} = \widehat{\mathbf{S}}\delta\mathbf{g} = \begin{bmatrix}\delta g_1 & 0 & \delta g_4\\ \delta g_2 & 0 & \delta g_5\\ 0 & \delta g_4 & \delta g_1\\ 0 & \delta g_5 & \delta g_2\end{bmatrix}\begin{bmatrix}{}_0S_{XX}\\ {}_0S_{YY}\\ {}_0S_{XY}\end{bmatrix} = \begin{bmatrix}{}_0S_{XX} & 0 & {}_0S_{XY} & 0\\ 0 & {}_0S_{XX} & 0 & {}_0S_{XY}\\ {}_0S_{XY} & 0 & {}_0S_{YY} & 0\\ 0 & {}_0S_{XY} & 0 & {}_0S_{YY}\end{bmatrix}\begin{bmatrix}\delta g_1\\ \delta g_2\\ \delta g_4\\ \delta g_5\end{bmatrix} \tag{3.25}$$

$$\mathbf{K}_g\delta\mathbf{u} = \delta\mathbf{B}^T{}_0\mathbf{S}\ {}_0\Omega = \mathbf{D}^T\ \widehat{\mathbf{S}}\ \mathbf{D}\delta\mathbf{u}\ {}_0A_0t \tag{3.26}$$

3.3.2 Conventional linear strain triangle

Assuming quadratic displacements inside the element gives the 6-node triangular element formulation, previously shown in Figure 3.1. This element is defined through the six shape functions in Equation 3.27.

$$\begin{bmatrix}N_1\\ N_2\\ N_3\\ N_4\\ N_5\\ N_6\end{bmatrix} = \begin{bmatrix}\zeta_1(2\zeta_1-1)\\ \zeta_2(2\zeta_2-1)\\ \zeta_3(2\zeta_3-1)\\ 4\zeta_1\zeta_2\\ 4\zeta_2\zeta_3\\ 4\zeta_1\zeta_3\end{bmatrix} = \begin{bmatrix}\zeta_1(2\zeta_1-1)\\ \zeta_2(2\zeta_2-1)\\ (1-\zeta_1-\zeta_2)(2(1-\zeta_1-\zeta_2)-1)\\ 4\zeta_1\zeta_2\\ 4\zeta_2(1-\zeta_1-\zeta_2)\\ 4\zeta_1(1-\zeta_1-\zeta_2)\end{bmatrix} \tag{3.27}$$

The differentiation of the six shape functions in area coordinates gives Equation 3.28, which can be used with the nodal undeformed positions to create the Jacobi matrix in Equation 3.29.

$$\frac{\partial \mathbf{N}}{\partial \boldsymbol{\zeta}} = \begin{bmatrix}(4\zeta_1-1) & 0 & (4\zeta_1+4\zeta_2-3) & (4\zeta_2) & (-4\zeta_2) & (4-8\zeta_1-4\zeta_2)\\ 0 & (4\zeta_2-1) & (4\zeta_1+4\zeta_2-3) & (4\zeta_1) & (4-4\zeta_1-8\zeta_2) & (-4\zeta_1)\end{bmatrix} \tag{3.28}$$

$$\mathbf{J} = \begin{bmatrix}\frac{\partial_0 X}{\partial \zeta_1} & \frac{\partial_0 Y}{\partial \zeta_1}\\ \frac{\partial_0 X}{\partial \zeta_2} & \frac{\partial_0 Y}{\partial \zeta_2}\end{bmatrix} = \begin{bmatrix}\frac{\partial N_1}{\partial \zeta_1} & \cdots & \frac{\partial N_6}{\partial \zeta_1}\\ \frac{\partial N_1}{\partial \zeta_2} & \cdots & \frac{\partial N_6}{\partial \zeta_2}\end{bmatrix}\begin{bmatrix}{}_0X_1 & {}_0Y_1\\ \vdots & \vdots\\ {}_0X_6 & {}_0Y_6\end{bmatrix} \tag{3.29}$$

The differentiated displacement gradient in global Cartesian coordinates gets a similar expression as the constant strain triangle. Using the six shape functions and the twelve nodal displacements gives Equation 3.30 for the incremental displacement gradient.

$$\frac{\partial \mathbf{g}}{\partial \mathbf{u}}\delta\mathbf{u} = \mathbf{D}\delta\mathbf{u} = \begin{bmatrix}\frac{\partial N_1}{\partial_0 X} & 0 & \cdots & \frac{\partial N_6}{\partial_0 X} & 0\\ 0 & \frac{\partial N_1}{\partial_0 X} & \cdots & 0 & \frac{\partial N_6}{\partial_0 X}\\ \frac{\partial N_1}{\partial_0 Y} & 0 & \cdots & \frac{\partial N_6}{\partial_0 Y} & 0\\ 0 & \frac{\partial N_1}{\partial_0 Y} & \cdots & 0 & \frac{\partial N_6}{\partial_0 Y}\end{bmatrix}\begin{bmatrix}\delta u_1\\ \delta v_1\\ \vdots\\ \delta u_6\\ \delta v_6\end{bmatrix} \tag{3.30}$$

Equation 3.31 shows the assumed solution for the displacement gradient. The differentiated strain tensor does not change when increasing the order of the shape functions and therefore follows Equation 3.32.

$$\begin{aligned} g_1 &= \frac{\partial N_\alpha}{\partial_0 X} u_\alpha, \qquad g_4 = \frac{\partial N_\alpha}{\partial_0 Y} u_\alpha \\ g_2 &= \frac{\partial N_\alpha}{\partial_0 X} v_\alpha, \qquad g_5 = \frac{\partial N_\alpha}{\partial_0 Y} v_\alpha \end{aligned} \qquad \alpha = (1, ..., 6) \tag{3.31}$$

$$\frac{\partial_0 \mathbf{E}}{\partial \mathbf{g}} \delta\mathbf{g} = \begin{bmatrix} 1+g_1 & g_2 & 0 & 0 \\ 0 & 0 & g_4 & 1+g_5 \\ g_4 & 1+g_5 & 1+g_1 & g_2 \end{bmatrix} \begin{bmatrix} \delta g_1 \\ \delta g_2 \\ \delta g_4 \\ \delta g_5 \end{bmatrix} \tag{3.32}$$

The integrand of the linear strain triangle varies across the element, thus creating a more comprehensive integration procedure than for the constant strain triangle. Numerical integration in area coordinates is beneficial when dealing with the internal force vector and the stiffness matrix, and changing the differential of the variable to area coordinates gives Equation 3.33. As the virtual work now is represented in the area coordinates, it can easily be numerically integrated through the Gauss point integration scheme presented in Equation 3.34.

$$\mathbf{f}^{\text{int}} = \int_{{}_0\Omega} \mathbf{B}^T \, {}_0\mathbf{S} \; d_0\Omega = \frac{{}_0t}{2} \int_0^1 \int_0^1 \mathbf{B}^T \, {}_0\mathbf{S} \; \text{Det}(\mathbf{J}) d\zeta_1 d\zeta_2 \tag{3.33}$$

$$\mathbf{f}^{\text{int}} \approx \frac{{}_0t}{2} \sum_{i=1}^{n} W(a_i) \mathbf{B}(a_i)^T {}_0\mathbf{S}(a_i) \; \text{Det}(\mathbf{J}(a_i)) \tag{3.34}$$

Table 3.2 shows a possible three-point Gauss scheme for area coordinates. Here (a_i) defines the three area coordinates $(\zeta_1, \zeta_2, \zeta_3)$. Each point also needs a corresponding weight, as seen in the right column in Table 3.2.

Table 3.2: Three-point Gauss integration for area coordinates.

n=3	ζ_1	ζ_2	ζ_3	Weight (W)
a_1	1/2	1/2	0	1/3
a_2	1/2	0	1/2	1/3
a_3	0	1/2	1/2	1/3

The undeformed volume $({}_0\Omega)$ does not change with nodal displacements, making the sequence of the derivative and integral irrelevant. Equation 3.35 now gives the internal force vector increment.

$$\delta\mathbf{f}^{\text{int}} = \frac{{}_0t}{2} \int_0^1 \int_0^1 \delta \left(\mathbf{B}^T {}_0\mathbf{S} \right) \text{Det}(\mathbf{J}) d\zeta_1 d\zeta_2 + \mathbf{B}^T {}_0\mathbf{S} \, \cancelto{0}{\delta \, {}_0\Omega} \tag{3.35}$$

The linear strain triangle follows the structure of the constant strain triangle material and geometric stiffness matrices. Using this structure with a three-point Gauss integration scheme generates Equations 3.36 and 3.37.

$$\mathbf{K}_m = \frac{{}_0t}{2} \sum_{i=1}^{3} W(a_i)\mathbf{B}(a_i)^T \mathbf{C}(a_i)^{\text{ep}}\mathbf{B}(a_i) \tag{3.36}$$

$$\mathbf{K}_g = \frac{{}_0t}{2} \sum_{i=1}^{3} W(a_i)\mathbf{D}(a_i)^T \, \widehat{\mathbf{S}}(a_i)\mathbf{D}(a_i) \tag{3.37}$$

3.3.3 Conventional constant strain tetrahedron

Four volumes (ζ_1, ζ_2, ζ_3, ζ_4) define the volume coordinates for a tetrahedron, where (ζ_4) can be seen as linearly dependent. Here a single-volume coordinate (ζ_i) follows the form shown in Equation 3.38, where (Ω) denotes the volume. Equation 3.39 shows the 3-dimensional Jacobi matrix for the volume coordinates (ζ_1, ζ_2, ζ_3), and inverting the Jacobi matrix gives the shape functions differentiated in global Cartesian coordinates shown in Equation 3.40.

$$\zeta_i = \frac{{}_0\Omega_i}{{}_0\Omega} \tag{3.38}$$

$$\begin{bmatrix} \frac{\partial \mathbf{N}}{\partial \zeta_1} \\ \frac{\partial \mathbf{N}}{\partial \zeta_2} \\ \frac{\partial \mathbf{N}}{\partial \zeta_3} \end{bmatrix} = \begin{bmatrix} \frac{\partial_0 X}{\partial \zeta_1} & \frac{\partial_0 Y}{\partial \zeta_1} & \frac{\partial_0 Z}{\partial \zeta_1} \\ \frac{\partial_0 X}{\partial \zeta_2} & \frac{\partial_0 Y}{\partial \zeta_2} & \frac{\partial_0 Z}{\partial \zeta_2} \\ \frac{\partial_0 X}{\partial \zeta_3} & \frac{\partial_0 Y}{\partial \zeta_3} & \frac{\partial_0 Z}{\partial \zeta_3} \end{bmatrix} \begin{bmatrix} \frac{\partial \mathbf{N}}{\partial_0 X} \\ \frac{\partial \mathbf{N}}{\partial_0 Y} \\ \frac{\partial \mathbf{N}}{\partial_0 Z} \end{bmatrix} = \mathbf{J} \frac{\partial \mathbf{N}}{\partial_0 \mathbf{X}} \tag{3.39}$$

$$\frac{\partial \mathbf{N}}{\partial_0 \mathbf{X}} = \mathbf{J}^{-1} \frac{\partial \mathbf{N}}{\partial \boldsymbol{\zeta}} \tag{3.40}$$

The shape function for a constant strain tetrahedron follows Equation 3.41, giving linear displacements and positions across the element.

$$\begin{bmatrix} N_1 \\ N_2 \\ N_3 \\ N_4 \end{bmatrix} = \begin{bmatrix} \zeta_1 \\ \zeta_2 \\ \zeta_3 \\ \zeta_4 \end{bmatrix} = \begin{bmatrix} \zeta_1 \\ \zeta_2 \\ \zeta_3 \\ 1 - \zeta_1 - \zeta_2 - \zeta_3 \end{bmatrix} \tag{3.41}$$

Differentiation of the shape functions in the volume coordinates now gives Equation 3.42. This gives a constant matrix and a constant virtual work integrand. Using Equation 3.42 in collaboration with the undeformed nodal positions creates the Jacobi matrix shown in Equation 3.43.

$$\frac{\partial \mathbf{N}}{\partial \boldsymbol{\zeta}} = \begin{bmatrix} \frac{\partial N_1}{\partial \zeta_1} & \frac{\partial N_2}{\partial \zeta_1} & \frac{\partial N_3}{\partial \zeta_1} & \frac{\partial N_4}{\partial \zeta_1} \\ \frac{\partial N_1}{\partial \zeta_2} & \frac{\partial N_2}{\partial \zeta_2} & \frac{\partial N_3}{\partial \zeta_2} & \frac{\partial N_4}{\partial \zeta_2} \\ \frac{\partial N_1}{\partial \zeta_3} & \frac{\partial N_2}{\partial \zeta_3} & \frac{\partial N_3}{\partial \zeta_3} & \frac{\partial N_4}{\partial \zeta_3} \end{bmatrix} = \begin{bmatrix} 1 & 0 & 0 & -1 \\ 0 & 1 & 0 & -1 \\ 0 & 0 & 1 & -1 \end{bmatrix} \tag{3.42}$$

$$\mathbf{J} = \begin{bmatrix} \frac{\partial N_1}{\partial \zeta_1} & \frac{\partial N_2}{\partial \zeta_1} & \frac{\partial N_3}{\partial \zeta_1} & \frac{\partial N_4}{\partial \zeta_1} \\ \frac{\partial N_1}{\partial \zeta_2} & \frac{\partial N_2}{\partial \zeta_2} & \frac{\partial N_3}{\partial \zeta_2} & \frac{\partial N_4}{\partial \zeta_2} \\ \frac{\partial N_1}{\partial \zeta_3} & \frac{\partial N_2}{\partial \zeta_3} & \frac{\partial N_3}{\partial \zeta_3} & \frac{\partial N_4}{\partial \zeta_3} \end{bmatrix} \begin{bmatrix} {}_0X_1 & {}_0Y_1 & {}_0Z_1 \\ \vdots & \vdots & \vdots \\ {}_0X_4 & {}_0Y_4 & {}_0Z_4 \end{bmatrix} \tag{3.43}$$

Using the inverse Jacobi relation creates the differentiated shape functions in Cartesian coordinates. Now the 3-dimensional differentiated displacement gradient is described through the incremental nodal displacements and differentiated shape functions shown in Equation 3.44.

$$\frac{\partial \mathbf{g}}{\partial \mathbf{u}} \delta\mathbf{u} = \mathbf{D}\delta\mathbf{u} = \begin{bmatrix} \frac{\partial N_1}{\partial_0 X} & 0 & 0 & \dots & \frac{\partial N_4}{\partial_0 X} & 0 & 0 \\ 0 & \frac{\partial N_1}{\partial_0 X} & 0 & \dots & 0 & \frac{\partial N_4}{\partial_0 X} & 0 \\ 0 & 0 & \frac{\partial N_1}{\partial_0 X} & \dots & 0 & 0 & \frac{\partial N_4}{\partial_0 X} \\ & \vdots & & \ddots & & \vdots & \\ \frac{\partial N_1}{\partial_0 Z} & 0 & 0 & \dots & \frac{\partial N_4}{\partial_0 Z} & 0 & 0 \\ 0 & \frac{\partial N_1}{\partial_0 Z} & 0 & \dots & 0 & \frac{\partial N_4}{\partial_0 Z} & 0 \\ 0 & 0 & \frac{\partial N_1}{\partial_0 Z} & \dots & 0 & 0 & \frac{\partial N_4}{\partial_0 Z} \end{bmatrix} \begin{bmatrix} \delta u_1 \\ \delta v_1 \\ \delta w_1 \\ \vdots \\ \delta u_4 \\ \delta v_4 \\ \delta w_4 \end{bmatrix} \tag{3.44}$$

The displacement gradient components are also defined through the shape functions, thus following Equation 3.45. Expressing the differentiated Green-Lagrange strain tensor in terms of the displacement gradient components gives the matrix expression shown in Equation 3.46.

$$\begin{aligned} g_1 &= \frac{\partial N_\alpha}{\partial_0 X} u_\alpha, \quad & g_4 &= \frac{\partial N_\alpha}{\partial_0 Y} v_\alpha, \quad & g_7 &= \frac{\partial N_\alpha}{\partial_0 Z} u_\alpha \\ g_2 &= \frac{\partial N_\alpha}{\partial_0 X} v_\alpha, \quad & g_5 &= \frac{\partial N_\alpha}{\partial_0 Y} v_\alpha, \quad & g_8 &= \frac{\partial N_\alpha}{\partial_0 Z} v_\alpha \qquad \alpha = (1, ..., 4) \\ g_3 &= \frac{\partial N_\alpha}{\partial_0 X} w_\alpha, \quad & g_6 &= \frac{\partial N_\alpha}{\partial_0 Y} w_\alpha, \quad & g_9 &= \frac{\partial N_\alpha}{\partial_0 Z} w_\alpha \end{aligned} \tag{3.45}$$

$$\frac{\partial_0 \mathbf{E}}{\partial \mathbf{g}} \delta\mathbf{g} = \begin{bmatrix} 1+g_1 & g_2 & g_3 & 0 & 0 & 0 & 0 & 0 & 0 \\ 0 & 0 & 0 & g_4 & 1+g_5 & g_6 & 0 & 0 & 0 \\ 0 & 0 & 0 & 0 & 0 & 0 & g_7 & g_8 & 1+g_9 \\ 0 & 0 & 0 & g_7 & g_8 & 1+g_9 & g_4 & 1+g_5 & g_6 \\ g_7 & g_8 & 1+g_9 & 0 & 0 & 0 & 1+g_1 & g_2 & g_3 \\ g_4 & 1+g_5 & g_6 & 1+g_1 & g_2 & g_3 & 0 & 0 & 0 \end{bmatrix} \begin{bmatrix} \delta g_1 \\ \vdots \\ \delta g_9 \end{bmatrix} \tag{3.46}$$

The constant integrand of the virtual work creates a simple integration procedure with a multiplication of the undeformed element volume, giving the internal force vector in Equation 3.47. Also, the incremental internal force vector in Equation 3.48 follows the same integration procedure.

$$\mathbf{f}^{\text{int}} = \int_{{}_0\Omega} \mathbf{B}^T {}_0\mathbf{S} \; d_0\Omega = \mathbf{B}^T {}_0\mathbf{S} \; {}_0\Omega \tag{3.47}$$

$$\delta\mathbf{f}^{\text{int}} = \delta\mathbf{B}^T {}_0\mathbf{S} \; {}_0\Omega + \mathbf{B}^T \delta_0\mathbf{S} \; {}_0\Omega \tag{3.48}$$

The differentiated stress tensor follows a similar form as the 2-dimensional elements. Using the tangent moduli and the differentiated Green-Lagrange strain tensor gives the material stiffness matrix shown in Equation 3.49.

$$\mathbf{K}_m = \mathbf{B}^T \mathbf{C}^{\text{ep}} \mathbf{B} \; {}_0\Omega \tag{3.49}$$

Also, the geometric stiffness gives a similar expression as the constant strain triangle. The main difference is the expanded ($\widehat{\mathbf{S}}$) matrix shown in Equation 3.50. Inserting this matrix into the incremental differentiated strain tensor gives the geometric stiffness matrix shown in Equation 3.51.

$$\widehat{\mathbf{S}} = \begin{bmatrix} {}_0S_{XX} & 0 & 0 & {}_0S_{XY} & 0 & 0 & {}_0S_{XZ} & 0 & 0 \\ 0 & {}_0S_{XX} & 0 & 0 & {}_0S_{XY} & 0 & 0 & {}_0S_{XZ} & 0 \\ 0 & 0 & {}_0S_{XX} & 0 & 0 & {}_0S_{XY} & 0 & 0 & {}_0S_{XZ} \\ {}_0S_{XY} & 0 & 0 & {}_0S_{YY} & 0 & 0 & {}_0S_{YZ} & 0 & 0 \\ 0 & {}_0S_{XY} & 0 & 0 & {}_0S_{YY} & 0 & 0 & {}_0S_{YZ} & 0 \\ 0 & 0 & {}_0S_{XY} & 0 & 0 & {}_0S_{YY} & 0 & 0 & {}_0S_{YZ} \\ {}_0S_{XZ} & 0 & 0 & {}_0S_{YZ} & 0 & 0 & {}_0S_{ZZ} & 0 & 0 \\ 0 & {}_0S_{XZ} & 0 & 0 & {}_0S_{YZ} & 0 & 0 & {}_0S_{ZZ} & 0 \\ 0 & 0 & {}_0S_{XZ} & 0 & 0 & {}_0S_{YZ} & 0 & 0 & {}_0S_{ZZ} \end{bmatrix} \tag{3.50}$$

$$\mathbf{K}_g = \mathbf{D}^T \widehat{\mathbf{S}} \mathbf{D} \; {}_0\Omega \tag{3.51}$$

3.3.4 Conventional linear strain tetrahedron

Figure 3.2 shows the 10-linear strain tetrahedron element. This node configuration follows the Abaqus softwares (C3D10) element definition and gives the shape functions in Equation 3.52 [12].

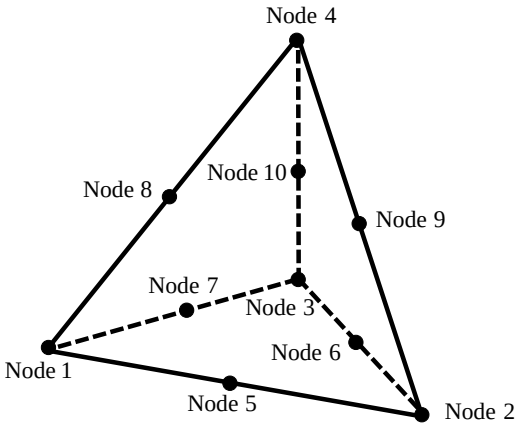

Figure 3.2: Node numbering of the 10-node tetrahedron.

$$\begin{bmatrix} N_1 \\ N_2 \\ N_3 \\ N_4 \\ N_5 \\ N_6 \\ N_7 \\ N_8 \\ N_9 \\ N_{10} \end{bmatrix} = \begin{bmatrix} \zeta_1(2\zeta_1-1) \\ \zeta_2(2\zeta_2-1) \\ \zeta_3(2\zeta_3-1) \\ \zeta_4(2\zeta_4-1) \\ 4\zeta_1\zeta_2 \\ 4\zeta_2\zeta_3 \\ 4\zeta_1\zeta_3 \\ 4\zeta_1\zeta_4 \\ 4\zeta_2\zeta_4 \\ 4\zeta_3\zeta_4 \end{bmatrix} = \begin{bmatrix} \zeta_1(2\zeta_1-1) \\ \zeta_2(2\zeta_2-1) \\ \zeta_3(2\zeta_3-1) \\ (1-\zeta_1-\zeta_2-\zeta_3)(2(1-\zeta_1-\zeta_2-\zeta_3)-1) \\ 4\zeta_1\zeta_2 \\ 4\zeta_2\zeta_3 \\ 4\zeta_1\zeta_3 \\ 4\zeta_1(1-\zeta_1-\zeta_2-\zeta_3) \\ 4\zeta_2(1-\zeta_1-\zeta_2-\zeta_3) \\ 4\zeta_3(1-\zeta_1-\zeta_2-\zeta_3) \end{bmatrix} \tag{3.52}$$

Differentiating the shape functions in volume coordinates provides Equation 3.53. These differentiated shape functions are further used with the undeformed nodal position to create the Jacobi matrix shown in Equation 3.54.

$$\frac{\partial \mathbf{N}}{\partial \boldsymbol{\zeta}}^T = \begin{bmatrix} (4\zeta_1 - 1) & 0 & 0 \\ 0 & (4\zeta_2 - 1) & 0 \\ 0 & 0 & (4\zeta_3 - 1) \\ (-3 + 4\zeta_1 + 4\zeta_2 + 4\zeta_3) & (-3 + 4\zeta_1 + 4\zeta_2 + 4\zeta_3) & (-3 + 4\zeta_1 + 4\zeta_2 + 4\zeta_3) \\ 4\zeta_2 & 4\zeta_1 & 0 \\ 0 & 4\zeta_3 & 4\zeta_2 \\ 4\zeta_3 & 0 & 4\zeta_1 \\ (4 - 8\zeta_1 - 4\zeta_2 - 4\zeta_3) & -4\zeta_1 & -4\zeta_1 \\ -4\zeta_2 & (4 - 4\zeta_1 - 8\zeta_2 - 4\zeta_3) & -4\zeta_2 \\ -4\zeta_3 & -4\zeta_3 & (4 - 4\zeta_1 - 4\zeta_2 - 8\zeta_3) \end{bmatrix} \tag{3.53}$$

$$\mathbf{J} = \begin{bmatrix} \frac{\partial N_1}{\partial \zeta_1} & \dots & \frac{\partial N_{10}}{\partial \zeta_1} \\ \frac{\partial N_1}{\partial \zeta_2} & \dots & \frac{\partial N_{10}}{\partial \zeta_2} \\ \frac{\partial N_1}{\partial \zeta_3} & \dots & \frac{\partial N_{10}}{\partial \zeta_3} \end{bmatrix} \begin{bmatrix} {}_0X_1 & {}_0Y_1 & {}_0Z_1 \\ \vdots & \vdots & \vdots \\ {}_0X_{10} & {}_0Y_{10} & {}_0Z_{10} \end{bmatrix} \tag{3.54}$$

The differentiated shape function found from the Jacobi matrix can be put into the differentiated displacement gradient, thus giving Equation 3.55.

$$\frac{\partial \mathbf{g}}{\partial \mathbf{u}} \delta\mathbf{u} = \mathbf{D}\delta\mathbf{u} = \begin{bmatrix} \frac{\partial N_1}{\partial_0 X} & 0 & 0 & \dots & \frac{\partial N_{10}}{\partial_0 X} & 0 & 0 \\ 0 & \frac{\partial N_1}{\partial_0 X} & 0 & \dots & 0 & \frac{\partial N_{10}}{\partial_0 X} & 0 \\ 0 & 0 & \frac{\partial N_1}{\partial_0 X} & \dots & 0 & 0 & \frac{\partial N_{10}}{\partial_0 X} \\ & \vdots & & \ddots & & \vdots & \\ \frac{\partial N_1}{\partial_0 Z} & 0 & 0 & \dots & \frac{\partial N_{10}}{\partial_0 Z} & 0 & 0 \\ 0 & \frac{\partial N_1}{\partial_0 Z} & 0 & \dots & 0 & \frac{\partial N_{10}}{\partial_0 Z} & 0 \\ 0 & 0 & \frac{\partial N_1}{\partial_0 Z} & \dots & 0 & 0 & \frac{\partial N_{10}}{\partial_0 Z} \end{bmatrix} \begin{bmatrix} \delta u_1 \\ \delta v_1 \\ \delta w_1 \\ \vdots \\ \delta u_{10} \\ \delta v_{10} \\ \delta w_{10} \end{bmatrix} \tag{3.55}$$

Similar expressions of the partial derivatives of the strain tensor are obtained for the constant and linear strain tetrahedron. Equation 3.56 shows the chain differentiated Green-Lagrange strain tensor with respect to the displacement gradient. In this expression, the displacement gradient follows the components shown in Equation 3.57.

$$\frac{\partial_0 \mathbf{E}}{\partial \mathbf{g}}\delta\mathbf{g} = \begin{bmatrix} 1+g_1 & g_2 & g_3 & 0 & 0 & 0 & 0 & 0 & 0 \\ 0 & 0 & 0 & g_4 & 1+g_5 & g_6 & 0 & 0 & 0 \\ 0 & 0 & 0 & 0 & 0 & 0 & g_7 & g_8 & 1+g_9 \\ 0 & 0 & 0 & g_7 & g_8 & 1+g_9 & g_4 & 1+g_5 & g_6 \\ g_7 & g_8 & 1+g_9 & 0 & 0 & 0 & 1+g_1 & g_2 & g_3 \\ g_4 & 1+g_5 & g_6 & 1+g_1 & g_2 & g_3 & 0 & 0 & 0 \end{bmatrix} \begin{bmatrix} \delta g_1 \\ \vdots \\ \delta g_9 \end{bmatrix} \tag{3.56}$$

$$\begin{aligned} g_1 &= \frac{\partial N_\alpha}{\partial_0 X} u_\alpha, \quad & g_4 &= \frac{\partial N_\alpha}{\partial_0 Y} v_\alpha, \quad & g_7 &= \frac{\partial N_\alpha}{\partial_0 Z} u_\alpha \\ g_2 &= \frac{\partial N_\alpha}{\partial_0 X} v_\alpha, \quad & g_5 &= \frac{\partial N_\alpha}{\partial_0 Y} v_\alpha, \quad & g_8 &= \frac{\partial N_\alpha}{\partial_0 Z} v_\alpha \qquad \alpha = (1, ..., 10) \\ g_3 &= \frac{\partial N_\alpha}{\partial_0 X} w_\alpha, \quad & g_6 &= \frac{\partial N_\alpha}{\partial_0 Y} w_\alpha, \quad & g_9 &= \frac{\partial N_\alpha}{\partial_0 Z} w_\alpha \end{aligned} \tag{3.57}$$

Collecting Equations 3.55 and 3.56 gives the differentiated strain tensor with respect to nodal displacements. The internal force vector is now given through Equation 3.58, where the integral is represented in both global Cartesian coordinates and volume coordinates. Volume coordinates are practical for numerical integration schemes, and using a Gauss point integration scheme gives the numerically integrated internal force vector in Equation 3.59.

$$\mathbf{f}^{\text{int}} = \int_{_0\Omega} \mathbf{B}^T{}_0\mathbf{S}\; d_0\Omega = \frac{1}{6}\int_0^1\int_0^1\int_0^1 \mathbf{B}^T{}_0\mathbf{S}\; \text{Det}(\mathbf{J}) d\zeta_1 d\zeta_2 d\zeta_3 \tag{3.58}$$

$$\mathbf{f}^{\text{int}} \approx \frac{1}{6}\sum_{i=1}^{n} W(a_i)\mathbf{B}(a_i)^T{}_0\mathbf{S}(a_i)\; \text{Det}(\mathbf{J}(a_i)) \tag{3.59}$$

Table 3.3 shows a four-point integration scheme calculated by FEBio [13]. The right column shows the weights of the numerical integration, while the four center columns show the volume coordinates.

Table 3.3: Four-point Gauss integration of volume coordinates.

n = 4	ζ_1	ζ_2	ζ_3	ζ_4	Weight (W)
a_1	0.58540	0.13820	0.13820	0.13820	0.25
a_2	0.13820	0.58540	0.13820	0.13820	0.25
a_3	0.13820	0.13820	0.58540	0.13820	0.25
a_4	0.13820	0.13820	0.13820	0.58540	0.25

Numerical integration of the two stiffness matrices with the Gauss point integration scheme from Table 3.3 yields Equations 3.60 and 3.61. With the geometric stiffness matrix written in terms of the $(\widehat{\mathbf{S}})$ matrix previously obtained in Equation 3.50.

$$\mathbf{K}_m = \frac{1}{6}\sum_{i=1}^{4} W(a_i)\mathbf{B}(a_i)^T\mathbf{C}(a_i)^{\text{ep}}\mathbf{B}(a_i) \tag{3.60}$$

$$\mathbf{K}_g = \frac{1}{6}\sum_{i=1}^{4} W(a_i)\mathbf{D}(a_i)^T\,\widehat{\mathbf{S}}(a_i)\mathbf{D}(a_i) \tag{3.61}$$

3.4 Assumed natural strain element formulations

3.4.1 Seth-Hill strain tensors for 1-dimensional rod

Assumed natural strain formulations predict strains or displacement gradients at specified locations in the element. One way of doing this is through 1-dimensional rods inside the element subjected to tensile or compression. Transforming between global Cartesian coordinates and the single local rod gives the transformation obtained in Equation 2.12. Assuming strains in three/six rods inside the element gives the invertible relations shown in Equations 2.13 and 2.14.

Figure 3.3 shows two nodes describing the linear displacements running from $(-L/2,$ $L/2)$ in the rod. Describing these linear displacements through deformed lengths gives Equation 3.62. While Equation 3.63 describes the undeformed positions using the undeformed rod lengths

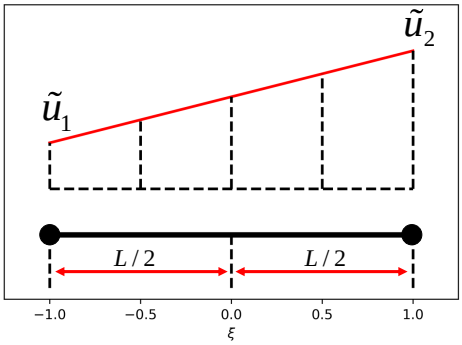

Figure 3.3: Assumed displacements for a single rod in local coordinates

$$\widetilde{u} = \frac{1}{2}\begin{bmatrix}-(\xi-1) & (\xi+1)\end{bmatrix}\left(\begin{bmatrix}-{}_{\text{t}}L/2\\ {}_{\text{t}}L/2\end{bmatrix} - \begin{bmatrix}-{}_{0}L/2\\ {}_{0}L/2\end{bmatrix}\right) \tag{3.62}$$

$${}_{0}\widetilde{X} = \frac{1}{2}\begin{bmatrix}-(\xi-1) & (\xi+1)\end{bmatrix}\begin{bmatrix}-{}_{0}L/2\\ {}_{0}L/2\end{bmatrix} \tag{3.63}$$

The local displacement gradient for a rod is obtained through the chain differentiating in Equation 3.64. This local displacement gradient can further be put into the Seth-Hill strain tensor previously shown in Equation 2.7, thus giving Equation 3.65.

$$\frac{d\widetilde{u}}{d\xi}\frac{d\xi}{d_0\widetilde{X}} = \frac{{}_tL}{{}_0L} - 1 = \widetilde{F} - 1 = \widetilde{G} \tag{3.64}$$

$${}_0\widetilde{E}_{\widetilde{X}\widetilde{X}} = \frac{1}{2m}\left(\left(\frac{{}_tL}{{}_0L}\right)^{2m} - 1\right) \tag{3.65}$$

A once and twice differentiating of the local Seth-Hill strain tensor gives Equations 3.66 and 3.67.

$$\frac{\partial_0\widetilde{E}_{\widetilde{X}\widetilde{X}}}{\partial_t L} = \left(\frac{({}_tL)^{2m-1}}{({}_0L)^{2m}}\right) \tag{3.66}$$

$$\frac{\partial_0^{(2)}\widetilde{E}_{\widetilde{X}\widetilde{X}}}{\partial_t L^{(2)}} = (2m-1)\left(\frac{({}_tL)^{2m-2}}{({}_0L)^{2m}}\right) \tag{3.67}$$

3.4.2 Assumed natural constant strain triangle

The 2-dimensional formulations use triangle configurations for creating the Seth-Hill strain tensors. Drawing a line/rod between the three nodes gives a set of undeformed and deformed lengths. Inserting the rod lengths into Equation 3.65 gives Seth-Hill strain tensors for each rod. The covariant transformation in Equation 2.13 is now applicable for relating the covariant basis and the global Cartesian strain tensor. Figure 3.4 shows the relation between the local rod basis displacement components and the nodes of the constant strain triangle. Rod 1 runs from node 1 to 2, with a basis following ($\mathbf{e}^1$); rod 2 runs from node 2 to 3, with a basis following ($\mathbf{e}^2$); and rod 3 runs from node 3 to 1, with a basis following ($\mathbf{e}^3$). Using this methodology gives the assumed natural strain formulation proposed by C. Felippa et al.[6] and unfolded by Eia et al. [4] and Østebø [5].

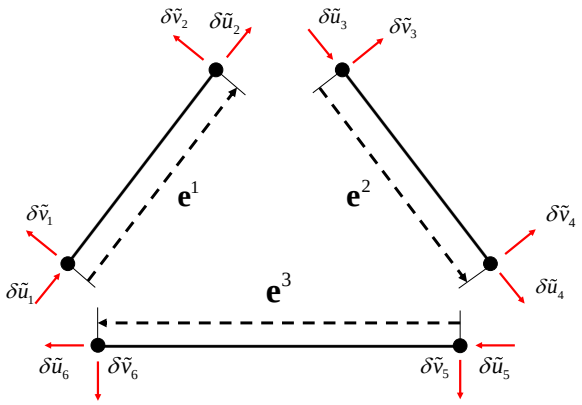

Figure 3.4: Local displacements components for the 2-dimensional assumed natural strain triangle configuration.

The local covariant CST strain tensor follows the form shown in Equation 3.68. This strain tensor can further be rewritten into global Cartesian strain tensors through the covariant transformation. Equation 3.68 also gives a similar expression for the differentiated strain tensors. Here the covariant strain tensor is defined by three rod lengths and can be chain differentiated through the three deformed rods/lengths.

$$ {}_0\widetilde{\mathbf{E}} = \widetilde{\mathbf{T}}\,{}_0\mathbf{E} = \frac{1}{2m}\begin{bmatrix} \left(\frac{{}_tL_1}{{}_0L_1}\right)^{2m} - 1 \\ \left(\frac{{}_tL_2}{{}_0L_2}\right)^{2m} - 1 \\ \left(\frac{{}_tL_3}{{}_0L_3}\right)^{2m} - 1 \end{bmatrix}, \quad \frac{\partial_0\widetilde{\mathbf{E}}}{\partial\mathbf{u}} = \frac{\partial_0\widetilde{\mathbf{E}}}{\partial_t\mathbf{L}}\frac{\partial_t\mathbf{L}}{\partial\mathbf{u}} = \widetilde{\mathbf{T}}\,\mathbf{B} \tag{3.68} $$

Nodal displacements can be represented either in the global Cartesian coordinates or in a local rod coordinate system, where the transformation follow Equation 3.69. Here ($\mathbf{e}$) is defined by the vector running in between two points, and ($\mathbf{n}$) is defined perpendicular to ($\mathbf{e}$). For instance, Equations 3.70 and 3.71 shows the local orthonormal rod coordinate system running in between nodes 1 to 2.

$$ \begin{bmatrix} \delta\widetilde{u} \\ \delta\widetilde{v} \end{bmatrix} = \begin{bmatrix} ({}_t\mathbf{e})^T \\ ({}_t\mathbf{n})^T \end{bmatrix} \begin{bmatrix} \delta u \\ \delta v \end{bmatrix} \tag{3.69} $$

$$ {}_t\mathbf{e}^1 = (({}_tX_2 - {}_tX_1)^2 + ({}_tY_2 - {}_tY_1)^2)^{-1/2} \begin{bmatrix} {}_tX_2 - {}_tX_1 \\ {}_tY_2 - {}_tY_1 \end{bmatrix} \tag{3.70} $$

$$ {}_t\mathbf{n}^1 = (({}_tX_2 - {}_tX_1)^2 + ({}_tY_2 - {}_tY_1)^2)^{-1/2} \begin{bmatrix} {}_tY_1 - {}_tY_2 \\ {}_tX_2 - {}_tX_1 \end{bmatrix} \tag{3.71} $$

Table 3.4 shows the system defining the ANS constant strain triangle. The rod numbering in the first column, the local orthonormal coordinate systems in the second and third columns, the node succession in the fourth column, the global Cartesian displacement components in the fifth column, and the local displacement components in the sixth column.

Table 3.4: Relation between rods, node succession, and displacement components for the ANS constant strain triangle.

Rod length	**Rod basis 1**	**Rod basis 2**	**Nodes**	**Displacements**	
L_1	$\mathbf{e}^1$	$\mathbf{n}^1$	$1 \to 2$	$\delta u_1, \delta v_1, \delta u_2, \delta v_2$	$\delta\widetilde{u}_1, \delta\widetilde{v}_1, \delta\widetilde{u}_2, \delta\widetilde{v}_2$
L_2	$\mathbf{e}^2$	$\mathbf{n}^2$	$2 \to 3$	$\delta u_2, \delta v_2, \delta u_3, \delta v_3$	$\delta\widetilde{u}_3, \delta\widetilde{v}_3, \delta\widetilde{u}_4, \delta\widetilde{v}_4$
L_3	$\mathbf{e}^3$	$\mathbf{n}^3$	$3 \to 1$	$\delta u_3, \delta v_3, \delta u_1, \delta v_1$	$\delta\widetilde{u}_5, \delta\widetilde{v}_5, \delta\widetilde{u}_6, \delta\widetilde{v}_6$

The change of deformed lengths shown in Equation 3.72 gives a simple expression in the local coordinates. As seen in Table 3.4, rod 1 correlates with the local displacement components ($\delta\widetilde{u}_1$ and $\delta\widetilde{u}_2$); rod 2 correlates with the local displacement components ($\delta\widetilde{u}_3$ and $\delta\widetilde{u}_4$); rod 3 correlates with the local displacement components ($\delta\widetilde{u}_5$ and $\delta\widetilde{u}_6$). A principal sketch of the local displacement components was previously shown in Figure 3.4.

$$\delta_{\mathrm{t}}\mathbf{L} = \begin{bmatrix} \delta_{\mathrm{t}}L_1 \\ \delta_{\mathrm{t}}L_2 \\ \delta_{\mathrm{t}}L_3 \end{bmatrix} = \begin{bmatrix} \delta\widetilde{u}_2 - \delta\widetilde{u}_1 \\ \delta\widetilde{u}_4 - \delta\widetilde{u}_3 \\ \delta\widetilde{u}_6 - \delta\widetilde{u}_5 \end{bmatrix} \tag{3.72}$$

The virtual work differentiated the strain tensor in terms of nodal displacements in Cartesian coordinates, a transformation between local and global coordinates is therefore needed. The local displacement components $\delta\widetilde{u}_1$ and $\delta\widetilde{u}_2$ follow rod 1, $\delta\widetilde{u}_3$ and $\delta\widetilde{u}_4$ follow rod 2, and $\delta\widetilde{u}_5$ and $\delta\widetilde{u}_6$ follow rod 3, thus giving the transformations ($\mathbf{e}^1$, $\mathbf{e}^2$, $\mathbf{e}^3$) for the six local displacement components. Also, the local displacement components ($\delta\widetilde{u}_1$ and $\delta\widetilde{u}_6$) follow node 1, ($\delta\widetilde{u}_2$ and $\delta\widetilde{u}_3$) follow node 2, and ($\delta\widetilde{u}_4$ and $\delta\widetilde{u}_5$) follow node 3. This system creates the pattern of the transformation shown in Equation 3.73.

$$\begin{bmatrix} \delta\widetilde{u}_1 \\ \delta\widetilde{u}_2 \\ \delta\widetilde{u}_3 \\ \delta\widetilde{u}_4 \\ \delta\widetilde{u}_5 \\ \delta\widetilde{u}_6 \end{bmatrix} = \begin{bmatrix} ({}_{\mathrm{t}}\mathbf{e}^1)^T & 0 & 0 \\ 0 & ({}_{\mathrm{t}}\mathbf{e}^1)^T & 0 \\ 0 & ({}_{\mathrm{t}}\mathbf{e}^2)^T & 0 \\ 0 & 0 & ({}_{\mathrm{t}}\mathbf{e}^2)^T \\ 0 & 0 & ({}_{\mathrm{t}}\mathbf{e}^3)^T \\ ({}_{\mathrm{t}}\mathbf{e}^3)^T & 0 & 0 \end{bmatrix} \begin{bmatrix} \delta u_1 \\ \delta v_1 \\ \delta u_2 \\ \delta v_2 \\ \delta u_3 \\ \delta v_3 \end{bmatrix} \tag{3.73}$$

Collecting Equations 3.72 and 3.73 gives the differentiated rod lengths shown in Equation 3.74. The first column relates the displacements of nodes 1 and 2 to the change in length of rod 1, the second column relates the displacements of nodes 2 and 3 to the change in length of rod 2, and the third column relates the displacements of node 3 and 1 to the change in length of rod 3.

$$\frac{\partial_{\mathrm{t}}\mathbf{L}^T}{\partial\mathbf{u}} = \mathbf{\Gamma}^T = \begin{bmatrix} -{}_{\mathrm{t}}\mathbf{e}^1 & 0 & {}_{\mathrm{t}}\mathbf{e}^3 \\ {}_{\mathrm{t}}\mathbf{e}^1 & -{}_{\mathrm{t}}\mathbf{e}^2 & 0 \\ 0 & {}_{\mathrm{t}}\mathbf{e}^2 & -{}_{\mathrm{t}}\mathbf{e}^3 \end{bmatrix} \tag{3.74}$$

Equation 3.75 shows the differentiated covariant strain tensor. The $({}_0\widetilde{E}_1)$ component with respect to $({}_{\mathrm{t}}L_1)$, $({}_0\widetilde{E}_2)$ component with respect to $({}_{\mathrm{t}}L_2)$, and $({}_0\widetilde{E}_3)$ component with respect to $({}_{\mathrm{t}}L_3)$.

$$\frac{\partial_0 \widetilde{\mathbf{E}}}{\partial_{\mathrm{t}} \mathbf{L}} = \begin{bmatrix} \frac{({}_{\mathrm{t}}L_1)^{2m-1}}{({}_0L_1)^{2m}} & 0 & 0 \\ 0 & \frac{({}_{\mathrm{t}}L_2)^{2m-1}}{({}_0L_2)^{2m}} & 0 \\ 0 & 0 & \frac{({}_{\mathrm{t}}L_3)^{2m-1}}{({}_0L_3)^{2m}} \end{bmatrix} \tag{3.75}$$

The 3-node ANS element gives a constant strain integrand for the virtual work. Using Equations 3.74 and 3.75 and with the covariant transformation gives the internal force vector shown in Equation 3.76.

$$\mathbf{f}^{\mathrm{int}} = \mathbf{B}^T {}_0\mathbf{S} \; {}_0\Omega = \frac{\partial_{\mathrm{t}} \mathbf{L}}{\partial \mathbf{u}}^T \frac{\partial_0 \widetilde{\mathbf{E}}}{\partial_{\mathrm{t}} \mathbf{L}}^T \widetilde{\mathbf{T}}^{-T} {}_0\mathbf{S} \; {}_0A_0 t \tag{3.76}$$

The integrand of the incremental internal force vector is also constant. Now differentiating in terms of the nodal displacements gives the three stiffness matrices shown in Equation 3.77, where each of the three stiffness matrices follows the increments from Equation 3.78.

$$\delta \mathbf{f}^{\mathrm{int}} = (\mathbf{K}_1 + \mathbf{K}_2 + \mathbf{K}_3) \delta \mathbf{u} \; {}_0\Omega \tag{3.77}$$

$$\begin{aligned} \mathbf{K}_1 \delta \mathbf{u} &= \delta \left(\frac{\partial_{\mathrm{t}} \mathbf{L}}{\partial \mathbf{u}}^T \right) \frac{\partial_0 \widetilde{\mathbf{E}}}{\partial_{\mathrm{t}} \mathbf{L}} \widetilde{\mathbf{T}}^{-T} {}_0\mathbf{S} \; {}_0A_0 t \\ \mathbf{K}_2 \delta \mathbf{u} &= \frac{\partial_{\mathrm{t}} \mathbf{L}}{\partial \mathbf{u}}^T \delta \left(\frac{\partial_0 \widetilde{\mathbf{E}}}{\partial_{\mathrm{t}} \mathbf{L}} \right) \widetilde{\mathbf{T}}^{-T} {}_0\mathbf{S} \; {}_0A_0 t \\ \mathbf{K}_3 \delta \mathbf{u} &= \frac{\partial_{\mathrm{t}} \mathbf{L}}{\partial \mathbf{u}}^T \frac{\partial_0 \widetilde{\mathbf{E}}}{\partial_{\mathrm{t}} \mathbf{L}} \widetilde{\mathbf{T}}^{-T} \delta \left({}_0\mathbf{S} \right) \; {}_0A_0 t \end{aligned} \tag{3.78}$$

$\mathbf{K}_1$ stiffness matrix, constant strain triangle

The ($\mathbf{K}_1$) stiffness matrix originates from the increment of the differentiated rod lengths. Taking the variation of the unit rod basis component ($_{\mathrm{t}}\mathbf{e}$) with respect to angular change gives the unit vector component ($_{\mathrm{t}}\mathbf{n}$) shown in Equation 3.79. Inserting this equation into the increment of the differentiated rod lengths now gives Equation 3.80.

$$\frac{\partial_{\mathrm{t}} \mathbf{e}}{\partial \theta} \delta\theta = {}_{\mathrm{t}}\mathbf{n} \; \delta\theta \tag{3.79}$$

$$\delta \left(\frac{\partial_{\mathrm{t}} \mathbf{L}}{\partial \mathbf{u}} \right)^T = \mathbf{P}^T \mathbf{M} = \begin{bmatrix} -\delta_{\mathrm{t}}\mathbf{e}^1 & 0 & \delta_{\mathrm{t}}\mathbf{e}^3 \\ \delta_{\mathrm{t}}\mathbf{e}^1 & -\delta_{\mathrm{t}}\mathbf{e}^2 & 0 \\ 0 & \delta_{\mathrm{t}}\mathbf{e}^2 & -\delta_{\mathrm{t}}\mathbf{e}^3 \end{bmatrix} = \begin{bmatrix} -{}_{\mathrm{t}}\mathbf{n}^1 & 0 & {}_{\mathrm{t}}\mathbf{n}^3 \\ {}_{\mathrm{t}}\mathbf{n}^1 & -{}_{\mathrm{t}}\mathbf{n}^2 & 0 \\ 0 & {}_{\mathrm{t}}\mathbf{n}^2 & -{}_{\mathrm{t}}\mathbf{n}^3 \end{bmatrix} \begin{bmatrix} \delta\theta_1 & 0 & 0 \\ 0 & \delta\theta_2 & 0 \\ 0 & 0 & \delta\theta_3 \end{bmatrix} \tag{3.80}$$

It is desired to get the incremental nodal displacements on the right-hand side, but some rewriting is needed for that to happen. Equation 3.81 shows a diagonalized matrix. Here the change of the strain tensor, the covariant transformation, and the stress tensor have been collected and inserted into the main diagonal. Swapping positions of the incremental angles ($\delta\theta$) and the collected term ($\mathbf{Q}$) gives Equation 3.82, where the increment of the angles ($\delta\theta$) now is on the right-hand side.

$$\mathbf{Q} = \left[\frac{\partial_0 \widetilde{\mathbf{E}}}{\partial_t \widetilde{\mathbf{L}}} \widetilde{\mathbf{T}}^{-T} {}_0\mathbf{S} \right] \tag{3.81}$$

$$\mathbf{K}_1 \delta\mathbf{u} = \mathbf{P}^T \mathbf{Q}\ \delta\boldsymbol{\theta}\ {}_0A_0 t \tag{3.82}$$

A principal sketch of a rod subjected to angular change is illustrated in Figure 3.5. Increasing the ($\delta\widetilde{v}_1$) displacement component turns the rod clockwise while increasing the ($\delta\widetilde{v}_2$) displacement component does the opposite. Now expressing the three incremental angles in terms of the local displacement components ($\delta\widetilde{v}$) gives Equation 3.83.

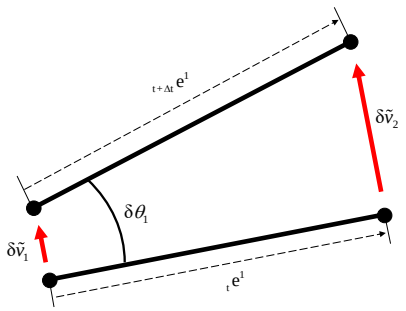

Figure 3.5: Angular change of a single rod.

$$\delta\boldsymbol{\theta} = \begin{bmatrix} \frac{1}{{}_tL_1}(\delta\widetilde{v}_2 - \delta\widetilde{v}_1) \\ \frac{1}{{}_tL_2}(\delta\widetilde{v}_4 - \delta\widetilde{v}_3) \\ \frac{1}{{}_tL_3}(\delta\widetilde{v}_6 - \delta\widetilde{v}_5) \end{bmatrix} \tag{3.83}$$

Equation 3.73 established a transformation between the local orthonormal rod basis and the global Cartesian basis for the ($\delta\widetilde{u}$) components. The same pattern is also applicable for the local displacement components ($\delta\widetilde{v}$) but with rod basis 2 from Table 3.4. Using the rod basis 2 ($_t\mathbf{n}$) in the transformation gives Equation 3.84.

$$\begin{bmatrix} \delta\widetilde{v}_1 \\ \delta\widetilde{v}_2 \\ \delta\widetilde{v}_3 \\ \delta\widetilde{v}_4 \\ \delta\widetilde{v}_5 \\ \delta\widetilde{v}_6 \end{bmatrix} = \begin{bmatrix} ({}_t\mathbf{n}^1)^T & 0 & 0 \\ 0 & ({}_t\mathbf{n}^1)^T & 0 \\ 0 & ({}_t\mathbf{n}^2)^T & 0 \\ 0 & 0 & ({}_t\mathbf{n}^2)^T \\ 0 & 0 & ({}_t\mathbf{n}^3)^T \\ ({}_t\mathbf{n}^3)^T & 0 & 0 \end{bmatrix} \begin{bmatrix} \delta u_1 \\ \delta v_1 \\ \delta u_2 \\ \delta v_2 \\ \delta u_3 \\ \delta v_3 \end{bmatrix} \tag{3.84}$$

Combing Equations 3.83 and 3.84 gives the rewritten version of the incremental angular change shown in Equation 3.85. Here the deformed lengths have been extracted into a separate diagonal matrix ($\mathbf{\Lambda}$).

$$\delta\boldsymbol{\theta} = \mathbf{\Lambda}\mathbf{P} = \begin{bmatrix} {}_{\mathrm{t}}L_1 & 0 & 0 \\ 0 & {}_{\mathrm{t}}L_2 & 0 \\ 0 & 0 & {}_{\mathrm{t}}L_3 \end{bmatrix} \begin{bmatrix} -({}_{\mathrm{t}}\mathbf{n}^1)^T & ({}_{\mathrm{t}}\mathbf{n}^1)^T & 0 \\ 0 & -({}_{\mathrm{t}}\mathbf{n}^2)^T & ({}_{\mathrm{t}}\mathbf{n}^2)^T \\ ({}_{\mathrm{t}}\mathbf{n}^3)^T & 0 & -({}_{\mathrm{t}}\mathbf{n}^3)^T \end{bmatrix} \tag{3.85}$$

The matrices ($\mathbf{Q}$ and $\mathbf{\Lambda}$) are now collected into a single term ($\mathbf{H}$) following Equation 3.86. Assembling Equations 3.82, 3.85 and 3.86 now gives the ($\mathbf{K}_1$) stiffness matrix shown in Equation 3.87.

$$\mathbf{H} = \mathbf{Q}\mathbf{\Lambda} = \mathbf{\Lambda}^T\mathbf{Q}^T \tag{3.86}$$

$$\mathbf{K}_1 = \mathbf{P}^T\mathbf{H}\mathbf{P}\ {}_0A_0t \tag{3.87}$$

$\mathbf{K}_2$ stiffness matrix, constant strain triangle

Double differentiating the covariant strain tensor derives the ($\mathbf{K}_2$) stiffness matrix, where the double derivative follows Equation 3.88. The twice differentiated strain tensor, covariant transformation, and stress tensor are now collected into the main diagonal of Equation 3.89. This form of rewriting creates length changes on the right-hand side of the expression.

$$\frac{\partial^{(2)}{}_0\widetilde{\mathbf{E}}}{\partial_{\mathrm{t}}\mathbf{L}^{(2)}}\delta_{\mathrm{t}}\mathbf{L} = (2m-1)\begin{bmatrix} \frac{({}_{\mathrm{t}}L_1)^{2m-2}}{({}_0L_1)^{2m}} & 0 & 0 \\ 0 & \frac{({}_{\mathrm{t}}L_2)^{2m-2}}{({}_0L_2)^{2m}} & 0 \\ 0 & 0 & \frac{({}_{\mathrm{t}}L_3)^{2m-2}}{({}_0L_3)^{2m}} \end{bmatrix} \begin{bmatrix} \delta_{\mathrm{t}}L_1 \\ \delta_{\mathrm{t}}L_2 \\ \delta_{\mathrm{t}}L_3 \end{bmatrix} \tag{3.88}$$

$$\mathbf{\Psi}\delta_{\mathrm{t}}\mathbf{L} = \left[\frac{\partial^{(2)}{}_0\widetilde{\mathbf{E}}}{\partial_{\mathrm{t}}\mathbf{L}^{(2)}}\widetilde{\mathbf{T}}^{-T}{}_0\mathbf{S}\right]\delta_{\mathrm{t}}\mathbf{L} \tag{3.89}$$

The length changes in Equation 3.89 are now rewritten in terms of the previously established relation in Equation 3.74. This rewriting gives the ($\mathbf{K}_2$) stiffness matrix shown in Equations 3.90 and 3.91.

$$\mathbf{K}_2\delta\mathbf{u} = \mathbf{\Gamma}^T\mathbf{\Psi}\delta_{\mathrm{t}}\mathbf{L}\ {}_0A_0t = \mathbf{\Gamma}^T\mathbf{\Psi}\mathbf{\Gamma}\delta\mathbf{u}\ {}_0A_0t \tag{3.90}$$

$$\mathbf{K}_2 = \mathbf{\Gamma}^T\mathbf{\Psi}\mathbf{\Gamma}\ {}_0A_0t \tag{3.91}$$

$\mathbf{K}_3$ stiffness matrix, constant strain triangle

The material matrix ($\mathbf{K}_3$) does not differ far from the one shown for the conventional shape functions. Rewriting the incremental stresses in terms of Hooke's law/tangent moduli gives the ($\mathbf{K}_3$) stiffness matrix in Equation 3.92.

$$\mathbf{K}_3 = \mathbf{B}^T\delta_0\mathbf{S}\ {}_0\Omega = \mathbf{B}^T\mathbf{C}^{\mathrm{ep}}\ \mathbf{B}\ {}_0A_0t \tag{3.92}$$

3.4.3 Assumed natural linear interpolated strain triangle

K. Y. Sze. et al. have previously used covariant small membrane strains for expressing the global Cartesian membrane strains at different sampling points [14]. The small strain tensor gave a practical explicit expression along the boundary for the six-node triangular element and could be implemented straight into the shape functions. The assumed natural interpolated strain 6-triangle derived below will follow a slightly different approach as the large strain tensor is not as easily derivable.

Figure 3.6 shows a principal sketch of the 6-node triangular ANS element. Dividing the element into four sub-elements gives one center triangle and three satellite triangles. Each satellite triangle can be used for creating covariant strain tensors. Interpolating the satellite triangles with their covariant transformations gives the global Cartesian strain tensor in Equation 3.93, and applying the Seth-Hill strain analogy of the constant strain triangle provides the three satellite strain tensors in Equation 3.94.

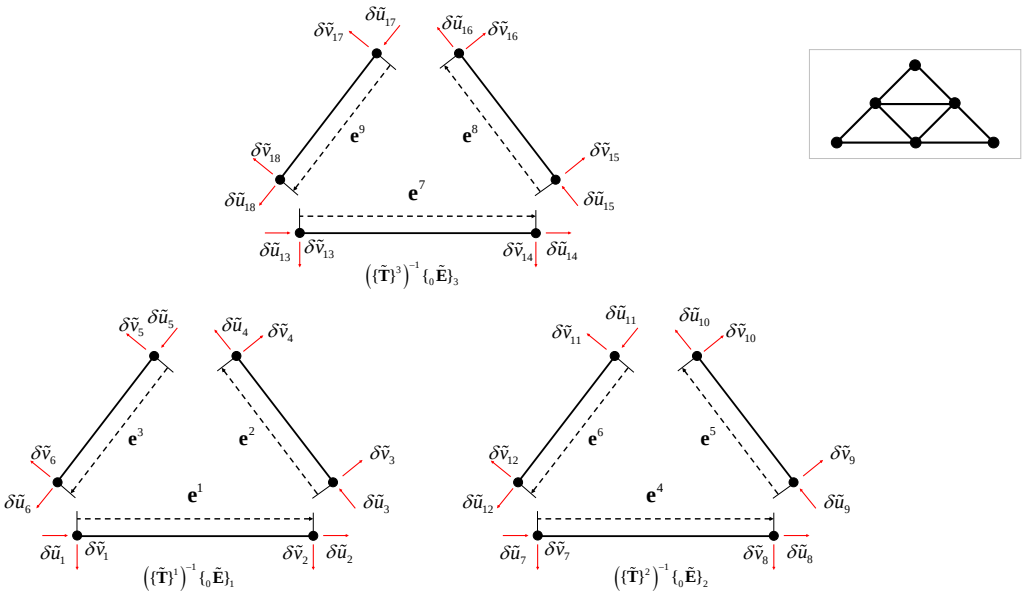

Figure 3.6: Principal sketch of the 6-node ANS triangle.

$$ {}_0\mathbf{E} = N_1 \left(\{\widetilde{\mathbf{T}}\}^1\right)^{-1} \{{}_0\widetilde{\mathbf{E}}\}_1 + N_2 \left(\{\widetilde{\mathbf{T}}\}^2\right)^{-1} \{{}_0\widetilde{\mathbf{E}}\}_2 + N_3 \left(\{\widetilde{\mathbf{T}}\}^3\right)^{-1} \{{}_0\widetilde{\mathbf{E}}\}_3 \tag{3.93} $$

$$ \{{}_0\widetilde{\mathbf{E}}\}_1 = \begin{bmatrix} {}_0\widetilde{E}_1 \\ {}_0\widetilde{E}_2 \\ {}_0\widetilde{E}_3 \end{bmatrix} = \frac{1}{2m} \begin{bmatrix} \left(\frac{{}_t L_1}{{}_0 L_1}\right)^{2m} - 1 \\ \left(\frac{{}_t L_2}{{}_0 L_2}\right)^{2m} - 1 \\ \left(\frac{{}_t L_3}{{}_0 L_3}\right)^{2m} - 1 \end{bmatrix} \quad \ldots \quad \{{}_0\widetilde{\mathbf{E}}\}_3 = \begin{bmatrix} {}_0\widetilde{E}_7 \\ {}_0\widetilde{E}_8 \\ {}_0\widetilde{E}_9 \end{bmatrix} = \frac{1}{2m} \begin{bmatrix} \left(\frac{{}_t L_7}{{}_0 L_7}\right)^{2m} - 1 \\ \left(\frac{{}_t L_8}{{}_0 L_8}\right)^{2m} - 1 \\ \left(\frac{{}_t L_9}{{}_0 L_9}\right)^{2m} - 1 \end{bmatrix} \tag{3.94} $$

Table A.1 in Appendix A and Figure 3.6 shows the relation between the rods, local displacement components, and global displacement components. Rod 1 is defined to run between nodes 1 and 4, rod 2 between nodes 4 and 6, rod 3 between nodes 6 and 1, rod 4 between nodes 4 and 2, and so forth.

Using the local displacements in Table A.1 for rewriting the increment of the rod lengths gives Equation 3.95. The change in length of the nine rods can now be written in terms of the global Cartesian displacements. Equation 3.96 shows the transformation between the local displacement and the global Cartesian displacements. This transformation follows the previously established Equation 3.69. The basis component $({}_{\mathrm{t}}\mathbf{e}^1)$ is placed in the first and fourth columns as it corresponds with the first and fourth nodes.

$$\delta_{\mathrm{t}}\mathbf{L} = \begin{bmatrix} \delta\widetilde{u}_2 - \delta\widetilde{u}_1 \\ \vdots \\ \delta\widetilde{u}_{18} - \delta\widetilde{u}_{17} \end{bmatrix} \tag{3.95}$$

$$\begin{bmatrix} \delta\widetilde{u}_1 \\ \delta\widetilde{u}_2 \\ \vdots \\ \delta\widetilde{u}_{17} \\ \delta\widetilde{u}_{18} \end{bmatrix} = \begin{bmatrix} ({}_{\mathrm{t}}\mathbf{e}^1)^T & 0 & 0 & 0 & 0 & 0 \\ 0 & 0 & 0 & ({}_{\mathrm{t}}\mathbf{e}^1)^T & 0 & 0 \\ & \vdots & & & \vdots & \\ 0 & 0 & ({}_{\mathrm{t}}\mathbf{e}^9)^T & 0 & 0 & 0 \\ 0 & 0 & 0 & 0 & 0 & ({}_{\mathrm{t}}\mathbf{e}^9)^T \end{bmatrix} \begin{bmatrix} \delta u_1 \\ \delta v_1 \\ \vdots \\ \delta u_6 \\ \delta v_6 \end{bmatrix} \tag{3.96}$$

Combining Equations 3.95 and 3.96 gives the differentiation of the nine rod lengths with respect to the global Cartesian nodal displacement, this is shown in Equation 3.97.

$$\frac{\partial_{\mathrm{t}}\mathbf{L}}{\partial\mathbf{u}}^T = \mathbf{\Gamma}^T = \begin{bmatrix} -{}_{\mathrm{t}}\mathbf{e}^1 & 0 & {}_{\mathrm{t}}\mathbf{e}^3 & 0 & 0 & 0 & 0 & 0 & 0 \\ 0 & 0 & 0 & {}_{\mathrm{t}}\mathbf{e}^4 & -{}_{\mathrm{t}}\mathbf{e}^5 & 0 & 0 & 0 & 0 \\ 0 & 0 & 0 & 0 & 0 & 0 & 0 & {}_{\mathrm{t}}\mathbf{e}^8 & -{}_{\mathrm{t}}\mathbf{e}^9 \\ {}_{\mathrm{t}}\mathbf{e}^1 & -{}_{\mathrm{t}}\mathbf{e}^2 & 0 & -{}_{\mathrm{t}}\mathbf{e}^4 & 0 & {}_{\mathrm{t}}\mathbf{e}^6 & 0 & 0 & 0 \\ 0 & 0 & 0 & 0 & {}_{\mathrm{t}}\mathbf{e}^5 & -{}_{\mathrm{t}}\mathbf{e}^6 & {}_{\mathrm{t}}\mathbf{e}^7 & -{}_{\mathrm{t}}\mathbf{e}^8 & 0 \\ 0 & {}_{\mathrm{t}}\mathbf{e}^2 & -{}_{\mathrm{t}}\mathbf{e}^3 & 0 & 0 & 0 & -{}_{\mathrm{t}}\mathbf{e}^7 & 0 & {}_{\mathrm{t}}\mathbf{e}^9 \end{bmatrix} \tag{3.97}$$

The virtual work also needs the differentiated global Cartesian strain tensor in Equation 3.98, with each satellite strain tensor following the differentiation in Equation 3.99. Satellite 1 with respect to rods 1 to 3, satellite 2 with respect to rods 4 to 6, and satellite 3 with respect to rods 7 to 9.

$$\frac{\partial_0\mathbf{E}}{\partial_{\mathrm{t}}\mathbf{L}}\delta_{\mathrm{t}}\mathbf{L} = \left[N_1 \left(\{\widetilde{\mathbf{T}}\}^1 \right)^{-1} \frac{\partial\{{}_0\widetilde{\mathbf{E}}\}_1}{\partial_{\mathrm{t}}\mathbf{L}} \quad N_2 \left(\{\widetilde{\mathbf{T}}\}^2 \right)^{-1} \frac{\partial\{{}_0\widetilde{\mathbf{E}}\}_2}{\partial_{\mathrm{t}}\mathbf{L}} \quad N_3 \left(\{\widetilde{\mathbf{T}}\}^3 \right)^{-1} \frac{\partial\{{}_0\widetilde{\mathbf{E}}\}_3}{\partial_{\mathrm{t}}\mathbf{L}} \right] \delta_{\mathrm{t}}\mathbf{L} \tag{3.98}$$

$$\begin{aligned}\frac{\partial\{{}_0\widetilde{\mathbf{E}}\}_1}{\partial_{\mathrm{t}}\mathbf{L}} &= \begin{bmatrix} \frac{\left({}_{\mathrm{t}}L^1\right)^{2m-1}}{\left({}_0L^1\right)^{2m}} & 0 & 0 \\ 0 & \frac{\left({}_{\mathrm{t}}L^2\right)^{2m-1}}{\left({}_0L^2\right)^{2m}} & 0 \\ 0 & 0 & \frac{\left({}_{\mathrm{t}}L^3\right)^{2m-1}}{\left({}_0L^3\right)^{2m}} \end{bmatrix} \ldots \\ \frac{\partial\{{}_0\widetilde{\mathbf{E}}\}_3}{\partial_{\mathrm{t}}\mathbf{L}} &= \begin{bmatrix} \frac{\left({}_{\mathrm{t}}L^7\right)^{2m-1}}{\left({}_0L^7\right)^{2m}} & 0 & 0 \\ 0 & \frac{\left({}_{\mathrm{t}}L^8\right)^{2m-1}}{\left({}_0L^8\right)^{2m}} & 0 \\ 0 & 0 & \frac{\left({}_{\mathrm{t}}L^9\right)^{2m-1}}{\left({}_0L^9\right)^{2m}} \end{bmatrix} \end{aligned} \tag{3.99}$$

Different configurations of shape functions are possible for the assumed natural interpolated strain elements, with area coordinates being practical for numerical integration. Setting the interpolation functions to give unit values in the center of the three satellite triangles gives Equation 3.100, thus corresponding with the three points $(2/3, 1/6, 1/6)$, $(1/6, 2/3, 1/6)$ and $(1/6, 1/6, 2/3)$

$$\begin{bmatrix} N_1 \\ N_2 \\ N_3 \end{bmatrix} = \begin{bmatrix} \frac{5}{3}\zeta_1 - \frac{1}{3}\zeta_2 - \frac{1}{3}\zeta_3 \\ \frac{5}{3}\zeta_2 - \frac{1}{3}\zeta_3 - \frac{1}{3}\zeta_1 \\ \frac{5}{3}\zeta_3 - \frac{1}{3}\zeta_1 - \frac{1}{3}\zeta_2 \end{bmatrix} \tag{3.100}$$

Equation 3.101 shows the internal force vector as a function of the global Cartesian coordinates and the area coordinates. The $(\mathrm{Det}(\mathbf{J}))$ term can be set to follow the shape functions of the conventional constant strain triangle or the linear strain triangle. Quadratic shape functions mimics the behavior of the conventional linear strain triangle, and now using the three-point Gauss integration scheme with quadratic shape functions gives Equation 3.102.

$$\mathbf{f}^{\mathrm{int}} = \int_{{}_0\Omega} \mathbf{B}^T {}_0\mathbf{S}\, d_0\Omega = \frac{{}_0t}{2} \int_0^1 \int_0^1 \mathbf{B}^T {}_0\mathbf{S}\, \mathrm{Det}(\mathbf{J}) d\zeta_1 d\zeta_2 \tag{3.101}$$

$$\mathbf{f}^{\mathrm{int}} \approx \frac{{}_0t}{2} \sum_{i=1}^{3} W(a_i) \mathbf{B}(a_i)^T {}_0\mathbf{S}(a_i)\, \mathrm{Det}(\mathbf{J}(a_i)) \tag{3.102}$$

$\mathbf{K}_1$ stiffness matrix, linear strain triangle

The $(\mathbf{K}_1)$ stiffness for the 6-node ANS element follows a similar approach as the 3-node ANS element. Equation 3.103 shows the increment of the differentiated rod lengths split into two parts; a matrix $(\mathbf{M})$ expressing the angular changes and a matrix $(\mathbf{P})$ expressing $({}_{\mathrm{t}}\mathbf{e})$ differentiated with respect to angular changes. The matrix $(\mathbf{P})$ is also shown in Equations 3.104.

$$\delta\left(\frac{\partial_{\mathrm{t}}\mathbf{L}}{\partial\mathbf{u}}\right)=\mathbf{P}^{T}\mathbf{M}=\begin{bmatrix}-{}_{\mathrm{t}}\mathbf{n}^{1} & 0 & {}_{\mathrm{t}}\mathbf{n}^{3} & \dots & 0 & 0 & 0\\ 0 & 0 & 0 & \dots & 0 & 0 & 0\\ 0 & 0 & 0 & \dots & 0 & {}_{\mathrm{t}}\mathbf{n}^{8} & -{}_{\mathrm{t}}\mathbf{n}^{9}\\ {}_{\mathrm{t}}\mathbf{n}^{1} & -{}_{\mathrm{t}}\mathbf{n}^{2} & 0 & \dots & 0 & 0 & 0\\ 0 & 0 & 0 & \dots & {}_{\mathrm{t}}\mathbf{n}^{7} & -{}_{\mathrm{t}}\mathbf{n}^{8} & 0\\ 0 & {}_{\mathrm{t}}\mathbf{n}^{2} & -{}_{\mathrm{t}}\mathbf{n}^{3} & \dots & -{}_{\mathrm{t}}\mathbf{n}^{7} & 0 & {}_{\mathrm{t}}\mathbf{n}^{9}\end{bmatrix}\begin{bmatrix}\delta\theta_{1} & \dots & 0\\ \vdots & \ddots & \vdots\\ 0 & \dots & \delta\theta_{9}\end{bmatrix} \tag{3.103}$$

$$\mathbf{P}^{T}=\begin{bmatrix}-{}_{\mathrm{t}}\mathbf{n}^{1} & 0 & {}_{\mathrm{t}}\mathbf{n}^{3} & 0 & 0 & 0 & 0 & 0 & 0\\ 0 & 0 & 0 & {}_{\mathrm{t}}\mathbf{n}^{4} & -{}_{\mathrm{t}}\mathbf{n}^{5} & 0 & 0 & 0 & 0\\ 0 & 0 & 0 & 0 & 0 & 0 & 0 & {}_{\mathrm{t}}\mathbf{n}^{8} & -{}_{\mathrm{t}}\mathbf{n}^{9}\\ {}_{\mathrm{t}}\mathbf{n}^{1} & -{}_{\mathrm{t}}\mathbf{n}^{2} & 0 & -{}_{\mathrm{t}}\mathbf{n}^{4} & 0 & {}_{\mathrm{t}}\mathbf{n}^{6} & 0 & 0 & 0\\ 0 & 0 & 0 & 0 & {}_{\mathrm{t}}\mathbf{n}^{5} & -{}_{\mathrm{t}}\mathbf{n}^{6} & {}_{\mathrm{t}}\mathbf{n}^{7} & -{}_{\mathrm{t}}\mathbf{n}^{8} & 0\\ 0 & {}_{\mathrm{t}}\mathbf{n}^{2} & -{}_{\mathrm{t}}\mathbf{n}^{3} & 0 & 0 & 0 & -{}_{\mathrm{t}}\mathbf{n}^{7} & 0 & {}_{\mathrm{t}}\mathbf{n}^{9}\end{bmatrix} \tag{3.104}$$

Collecting the differentiated strain tensor, the shape functions, the covariant transformations, and the stress tensor into the main diagonal gives Equation 3.105. Equations 3.103, 3.104 and 3.105 are now used for rewriting the integrand of the ($\mathbf{K}_1$) stiffness matrix in Equation 3.106.

$$\mathbf{Q}=\begin{bmatrix}N_1\frac{\partial\{{}_0\widetilde{\mathbf{E}}\}_1}{\partial_{\mathrm{t}}\mathbf{L}}^{T}\left(\{\widetilde{\mathbf{T}}\}^{1}\right)^{-T}{}_0\mathbf{S}\\ N_2\frac{\partial\{{}_0\widetilde{\mathbf{E}}\}_2}{\partial_{\mathrm{t}}\mathbf{L}}^{T}\left(\{\widetilde{\mathbf{T}}\}^{2}\right)^{-T}{}_0\mathbf{S}\\ N_3\frac{\partial\{{}_0\widetilde{\mathbf{E}}\}_3}{\partial_{\mathrm{t}}\mathbf{L}}^{T}\left(\{\widetilde{\mathbf{T}}\}^{3}\right)^{-T}{}_0\mathbf{S}\end{bmatrix} \tag{3.105}$$

$$\delta\left(\frac{\partial_{\mathrm{t}}\mathbf{L}}{\partial\mathbf{u}}^{T}\right)\frac{\partial_0\mathbf{E}}{\partial_{\mathrm{t}}\mathbf{L}}{}_0\mathbf{S}=\mathbf{P}^{T}\mathbf{Q}\;\delta\boldsymbol{\theta} \tag{3.106}$$

Equation 3.107 gives the angular change as a function of the local displacement components ($\delta\widetilde{v}$). Relating the local displacement components and the global Cartesian displacement components through ($\mathbf{P}$) gives Equation 3.108. Here ($_{\mathrm{t}}\mathbf{n}$) follows the same pattern as in Equation 3.96.

$$\delta\boldsymbol{\theta}=\begin{bmatrix}\delta\theta_{1}\\ \vdots\\ \delta\theta_{9}\end{bmatrix}=\begin{bmatrix}\frac{\delta\widetilde{v}_2-\delta\widetilde{v}_1}{{}_{\mathrm{t}}L_1}\\ \vdots\\ \frac{\delta\widetilde{v}_{18}-\delta\widetilde{v}_{17}}{{}_{\mathrm{t}}L_9}\end{bmatrix} \tag{3.107}$$

$$\begin{bmatrix} \delta\widetilde{v}_1 \\ \delta\widetilde{v}_2 \\ \vdots \\ \delta\widetilde{v}_{17} \\ \delta\widetilde{v}_{18} \end{bmatrix} = \begin{bmatrix} ({}_{\mathrm{t}}\mathbf{n}^1)^T & 0 & 0 & 0 & 0 & 0 \\ 0 & 0 & 0 & ({}_{\mathrm{t}}\mathbf{n}^1)^T & 0 & 0 \\ & \vdots & & & \vdots & \\ 0 & 0 & ({}_{\mathrm{t}}\mathbf{n}^9)^T & 0 & 0 & 0 \\ 0 & 0 & 0 & 0 & 0 & ({}_{\mathrm{t}}\mathbf{n}^9)^T \end{bmatrix} \begin{bmatrix} \delta u_1 \\ \delta v_1 \\ \vdots \\ \delta u_6 \\ \delta v_6 \end{bmatrix} \tag{3.108}$$

The deformed lengths from Equation 3.107 can be extracted into the main diagonal matrix ($\mathbf{\Lambda}$) in Equation 3.109. The ($\mathbf{\Lambda}$) matrix and the collect term ($\mathbf{Q}$) are further collected into the matrix ($\mathbf{H}$) seen in Equation 3.110.

$$\mathbf{\Lambda} = \begin{bmatrix} {}_{\mathrm{t}}L_1 & \dots & 0 \\ \vdots & \ddots & \vdots \\ 0 & \dots & {}_{\mathrm{t}}L_9 \end{bmatrix} \tag{3.109}$$

$$\mathbf{H} = \mathbf{\Lambda}\mathbf{Q} = \mathbf{Q}^T\mathbf{\Lambda}^T \tag{3.110}$$

Equations 3.103 and 3.110 are now used to form the integrand of the ($\mathbf{K}_1$) stiffness matrix in Equation 3.111, and applying a three-point Gauss integration scheme to the integral gives the ($\mathbf{K}_1$) stiffness matrix in Equation 3.112.

$$\mathbf{K}_1 = \frac{{}_0t}{2}\int_0^1\int_0^1 \mathbf{P}^T\mathbf{H}\mathbf{P}\mathrm{Det}(\mathbf{J})d\zeta_1 d\zeta_2 \tag{3.111}$$

$$\mathbf{K}_1 = \frac{{}_0t}{2}\sum_{i=1}^{3} W(a_i)\mathbf{P}^T(a_i)\mathbf{H}(a_i)\mathbf{P}(a_i)\mathrm{Det}(\mathbf{J}(a_i)) \tag{3.112}$$

$\mathbf{K}_2$ stiffness matrix, linear strain triangle

The two times differentiation of the satellite strain tensors in Equation 3.113 develops the ($\mathbf{K}_2$) stiffness matrix. Combing the shape functions, double differentiated satellite strain tensors, covariant transformations, and the stress tensor create the diagonalized matrix in Equation 3.114. This diagonalization arranges for writing the length changes on the right-hand side of the expression.

$$\begin{aligned} \frac{\partial^{(2)}\{{}_0\widetilde{\mathbf{E}}\}_1}{\partial_{\mathrm{t}}\mathbf{L}^{(2)}} &= (2m-1)\begin{bmatrix} \frac{({}_{\mathrm{t}}L_1)^{2m-2}}{({}_0L_1)^{2m}} & 0 & 0 \\ 0 & \frac{({}_{\mathrm{t}}L_2)^{2m-2}}{({}_0L_2)^{2m}} & 0 \\ 0 & 0 & \frac{({}_{\mathrm{t}}L_3)^{2m-2}}{({}_0L_3)^{2m}} \end{bmatrix} \dots \\ \frac{\partial^{(2)}\{{}_0\widetilde{\mathbf{E}}\}_3}{\partial_{\mathrm{t}}\mathbf{L}^{(2)}} &= (2m-1)\begin{bmatrix} \frac{({}_{\mathrm{t}}L_7)^{2m-1}}{({}_0L_7)^{2m}} & 0 & 0 \\ 0 & \frac{({}_{\mathrm{t}}L_8)^{2m-1}}{({}_0L_8)^{2m}} & 0 \\ 0 & 0 & \frac{({}_{\mathrm{t}}L_9)^{2m-1}}{({}_0L_9)^{2m}} \end{bmatrix} \end{aligned} \tag{3.113}$$

$$\boldsymbol{\Psi}\delta_{\mathrm{t}}\mathbf{L} = \begin{bmatrix} N_1 \left(\frac{\partial^{(2)}\{{}_0\widetilde{\mathbf{E}}\}_1}{\partial_{\mathrm{t}}\mathbf{L}^{(2)}}\right)^T \left(\{\widetilde{\mathbf{T}}\}^1\right)^{-T} {}_0\mathbf{S} \\ N_2 \left(\frac{\partial^{(2)}\{{}_0\widetilde{\mathbf{E}}\}_2}{\partial_{\mathrm{t}}\mathbf{L}^{(2)}}\right)^T \left(\{\widetilde{\mathbf{T}}\}^2\right)^{-T} {}_0\mathbf{S} \\ N_3 \left(\frac{\partial^{(2)}\{{}_0\widetilde{\mathbf{E}}\}_3}{\partial_{\mathrm{t}}\mathbf{L}^{(2)}}\right)^T \left(\{\widetilde{\mathbf{T}}\}^3\right)^{-T} {}_0\mathbf{S} \end{bmatrix} \delta_{\mathrm{t}}\mathbf{L} \tag{3.114}$$

Equation 3.115 now shows the integrand of the ($\mathbf{K}_2$) stiffness matrix assembled by Equations 3.95, 3.97, and 3.114.

$$\frac{\partial_{\mathrm{t}}\mathbf{L}}{\partial\mathbf{u}}^T \delta \left(\frac{\partial_0\mathbf{E}}{\partial_{\mathrm{t}}\mathbf{L}}^T\right) {}_0\mathbf{S} = \boldsymbol{\Gamma}^T\boldsymbol{\Psi}\delta_{\mathrm{t}}\mathbf{L} = \boldsymbol{\Gamma}^T\boldsymbol{\Psi}\boldsymbol{\Gamma}\delta\mathbf{u} \tag{3.115}$$

Inserting the integrand from Equation 3.115 into the virtual work integral gives the ($\mathbf{K}_2$) stiffness matrix in Equation 3.116, with the stiffness matrix integrated with three Gauss points in Equation 3.117.

$$\mathbf{K}_2 = \frac{{}_0t}{2}\int_0^1\int_0^1 \boldsymbol{\Gamma}^T\boldsymbol{\Psi}\boldsymbol{\Gamma}\mathrm{Det}(\mathbf{J})d\zeta_1 d\zeta_2 \tag{3.116}$$

$$\mathbf{K}_2 = \frac{{}_0t}{2}\sum_{i=1}^{3} W(a_i)\boldsymbol{\Gamma}^T(a_i)\boldsymbol{\Psi}(a_i)\boldsymbol{\Gamma}(a_i)\mathrm{Det}(\mathbf{J}(a_i)) \tag{3.117}$$

$\mathbf{K}_3$ stiffness matrix, linear strain triangle

The material stiffness ($\mathbf{K}_3$) matrix follows a similar form as the 3-node ANS element, with the main difference being a non-constant integrand. Equation 3.118 gives the material stiffness matrix ($\mathbf{K}_3$) in global Cartesian coordinates and area coordinates, which is further rewritten with Gauss point integration in Equation 3.119.

$$\mathbf{K}_3 = \frac{{}_0t}{2}\int_0^1\int_0^1 \mathbf{B}^T\delta\mathbf{S}d\zeta_1 d\zeta_2 = \frac{{}_0t}{2}\int_0^1\int_0^1 \mathbf{B}^T\mathbf{C}^{\mathrm{ep}}\mathbf{B}d\zeta_1 d\zeta_2 \tag{3.118}$$

$$\mathbf{K}_3 \approx \frac{{}_0t}{2}\sum_{i=1}^{3} W(a_i)\mathbf{B}(a_i)^T\mathbf{C}(a_i)^{\mathrm{ep}}\mathbf{B}(a_i)\ \mathrm{Det}(\mathbf{J}(a_i)) \tag{3.119}$$

3.4.4 Assumed natural constant strain tetrahedron

Figure 3.7 shows a principal sketch of the 4-node ANS element. Drawing a line between the four nodes creates six rods. The six rods create six Seth-Hill strain tensors following Equation 3.120. The global Cartesian strain tensor is now related to the covariant strain tensor through the covariant transformation in Equation 2.14.

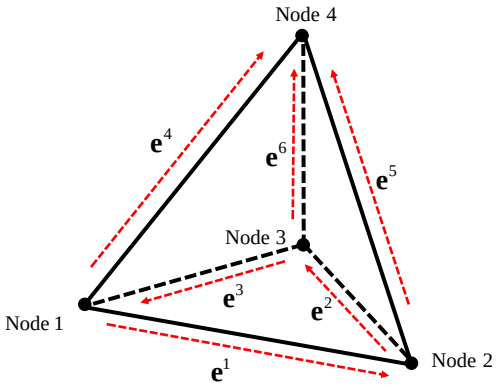

Figure 3.7: Node configuration and rod definitions of the 4-node constant strain tetrahedron.

$$\widetilde{\mathbf{T}}\,{}_0\mathbf{E} = {}_0\widetilde{\mathbf{E}} = \frac{1}{2m}\begin{bmatrix} \left(\frac{{}_tL_1}{{}_0L_1}\right)^{2m} - 1 \\ \vdots \\ \left(\frac{{}_tL_6}{{}_0L_6}\right)^{2m} - 1 \end{bmatrix} \tag{3.120}$$

A deformed orthonormal unit basis is practical when working with deformed rod lengths. Equation 3.121 shows the transformation between the local coordinate system for a single rod and the global Cartesian coordinate system. Here the $({}_t\mathbf{e})$ basis vector follows the rod direction, while $({}_t\mathbf{n}$ and ${}_t\boldsymbol{\eta})$ create the two other basis vectors for the unit orthonormal local coordinate system. A single rod denoted 1 running from node 1 to 2 then gives the transformation shown in Equation 3.122. Setting $({}_t\mathbf{n})$ to follow Equation 3.123 and $({}_t\boldsymbol{\eta})$ to follow Equation 3.124 now creates a local orthonormal unit basis.

$$\begin{bmatrix} \delta\widetilde{u} \\ \delta\widetilde{v} \\ \delta\widetilde{w} \end{bmatrix} = \begin{bmatrix} ({}_t\mathbf{e})^T \\ ({}_t\mathbf{n})^T \\ ({}_t\boldsymbol{\eta})^T \end{bmatrix} \begin{bmatrix} \delta u \\ \delta v \\ \delta w \end{bmatrix} \tag{3.121}$$

$${}_t\mathbf{e}^1 = (({}_tX_2 - {}_tX_1)^2 + ({}_tY_2 - {}_tY_1)^2 + ({}_tZ_2 - {}_tZ_1)^2)^{-1/2} \begin{bmatrix} {}_tX_2 - {}_tX_1 \\ {}_tY_2 - {}_tY_1 \\ {}_tZ_2 - {}_tZ_1 \end{bmatrix} \tag{3.122}$$

$${}_t\mathbf{n}^1 = (({}_tX_2 - {}_tX_1)^2 + ({}_tY_2 - {}_tY_1)^2)^{-1/2} \begin{bmatrix} {}_tY_1 - {}_tY_2 \\ {}_tX_2 - {}_tX_1 \\ 0 \end{bmatrix} \tag{3.123}$$

$${}_t\boldsymbol{\eta}^1 = {}_t\mathbf{e}^1 \times {}_t\mathbf{n}^1 \tag{3.124}$$

Figure 3.7 and Table A.2 in Appendix A shows the definition of rod bases. Rod 1 runs from nodes 1 to 2, rod 2 from nodes 2 to 3, rod 3 from nodes 3 to 1, rod 4 runs from nodes 1 to 4, and so forth. While the right column in Table A.2 shows the local displacement components, and the second to the right column shows the global Cartesian displacement components.

The incremental rod lengths shown in Equation 3.125 can now be represented through the local displacement components ($\delta\widetilde{u}$), following the system presented in Appendix A and Table A.2.

$$\delta_{\mathrm{t}}\mathbf{L} = \begin{bmatrix} \delta_{\mathrm{t}}L_1 \\ \delta_{\mathrm{t}}L_2 \\ \vdots \\ \delta_{\mathrm{t}}L_5 \\ \delta_{\mathrm{t}}L_6 \end{bmatrix} = \begin{bmatrix} \delta\widetilde{u}_2 - \delta\widetilde{u}_1 \\ \delta\widetilde{u}_4 - \delta\widetilde{u}_3 \\ \vdots \\ \delta\widetilde{u}_{10} - \delta\widetilde{u}_9 \\ \delta\widetilde{u}_{12} - \delta\widetilde{u}_{11} \end{bmatrix} \tag{3.125}$$

The virtual work uses global Cartesian nodal displacements for expressing the internal force vector. A transformation of the local nodal displacements is therefore needed. Equation 3.126 expresses the local ($\delta\widetilde{u}$) displacement components through the global Cartesian displacements. Rod 1 runs between nodes 1 and 2, and rod 2 runs between nodes 2 and 3, consequently placing (${}_{\mathrm{t}}\mathbf{e}^1$) in the first and second column and (${}_{\mathrm{t}}\mathbf{e}^2$) in the second and third column.

$$\begin{bmatrix} \delta\widetilde{u}_1 \\ \delta\widetilde{u}_2 \\ \delta\widetilde{u}_3 \\ \delta\widetilde{u}_4 \\ \delta\widetilde{u}_5 \\ \delta\widetilde{u}_6 \\ \delta\widetilde{u}_7 \\ \delta\widetilde{u}_8 \\ \delta\widetilde{u}_9 \\ \delta\widetilde{u}_{10} \\ \delta\widetilde{u}_{11} \\ \delta\widetilde{u}_{12} \end{bmatrix} = \begin{bmatrix} \left({}_{\mathrm{t}}\mathbf{e}^1\right)^T & 0 & 0 & 0 \\ 0 & \left({}_{\mathrm{t}}\mathbf{e}^1\right)^T & 0 & 0 \\ 0 & \left({}_{\mathrm{t}}\mathbf{e}^2\right)^T & 0 & 0 \\ 0 & 0 & \left({}_{\mathrm{t}}\mathbf{e}^2\right)^T & 0 \\ 0 & 0 & \left({}_{\mathrm{t}}\mathbf{e}^3\right)^T & 0 \\ \left({}_{\mathrm{t}}\mathbf{e}^3\right)^T & 0 & 0 & 0 \\ \left({}_{\mathrm{t}}\mathbf{e}^4\right)^T & 0 & 0 & 0 \\ 0 & 0 & 0 & \left({}_{\mathrm{t}}\mathbf{e}^4\right)^T \\ 0 & \left({}_{\mathrm{t}}\mathbf{e}^5\right)^T & 0 & 0 \\ 0 & 0 & 0 & \left({}_{\mathrm{t}}\mathbf{e}^5\right)^T \\ 0 & 0 & \left({}_{\mathrm{t}}\mathbf{e}^6\right)^T & 0 \\ 0 & 0 & 0 & \left({}_{\mathrm{t}}\mathbf{e}^6\right)^T \end{bmatrix} \begin{bmatrix} \delta u_1 \\ \delta v_1 \\ \delta w_1 \\ \delta u_2 \\ \delta v_2 \\ \delta w_2 \\ \delta u_3 \\ \delta v_3 \\ \delta w_3 \\ \delta u_4 \\ \delta v_4 \\ \delta w_4 \end{bmatrix} \tag{3.126}$$

Gathering Equations 3.125 and 3.126 creates the differentiated rod lengths with respect to Cartesian nodal displacement in Equation 3.127, which further can be inserted into the virtual work expression.

$$\frac{\partial_{\mathrm{t}}\mathbf{L}}{\partial\mathbf{u}}^{T} = \mathbf{\Gamma}^{T} = \begin{bmatrix} -{}_{\mathrm{t}}\mathbf{e}^{1} & 0 & {}_{\mathrm{t}}\mathbf{e}^{3} & -{}_{\mathrm{t}}\mathbf{e}^{4} & 0 & 0 \\ {}_{\mathrm{t}}\mathbf{e}^{1} & -{}_{\mathrm{t}}\mathbf{e}^{2} & 0 & 0 & -{}_{\mathrm{t}}\mathbf{e}^{5} & 0 \\ 0 & {}_{\mathrm{t}}\mathbf{e}^{2} & -{}_{\mathrm{t}}\mathbf{e}^{3} & 0 & 0 & -{}_{\mathrm{t}}\mathbf{e}^{6} \\ 0 & 0 & 0 & {}_{\mathrm{t}}\mathbf{e}^{4} & {}_{\mathrm{t}}\mathbf{e}^{5} & {}_{\mathrm{t}}\mathbf{e}^{6} \end{bmatrix} \tag{3.127}$$

The internal force vector also needs the covariant strain tensor differentiated through rod lengths, and this is given by Equation 3.128.

$$\frac{\partial_0\widetilde{\mathbf{E}}}{\partial_{\mathrm{t}}\mathbf{L}} = \begin{bmatrix} \frac{({}_{\mathrm{t}}L_1)^{2m-1}}{({}_0L_1)^{2m}} & \dots & 0 \\ \vdots & \ddots & \vdots \\ 0 & \dots & \frac{({}_{\mathrm{t}}L_6)^{2m-1}}{({}_0L_6)^{2m}} \end{bmatrix} \tag{3.128}$$

Inserting Equations 3.127 and 3.128 into the virtual work creates the internal force vector shown in Equation 3.129. The constant strain tensor gives a constant integrand and a simple integration procedure.

$$\mathbf{f}^{\mathrm{int}} = \int_{{}_0\Omega} \mathbf{B}^{T}{}_0\mathbf{S}\; d_0\Omega = \mathbf{B}^{T}{}_0\mathbf{S}_0\Omega = \frac{\partial_{\mathrm{t}}\mathbf{L}}{\partial\mathbf{u}}^{T} \frac{\partial_0\widetilde{\mathbf{E}}}{\partial_{\mathrm{t}}\mathbf{L}}^{T} \widetilde{\mathbf{T}}^{-T}{}_0\mathbf{S}_0\Omega \tag{3.129}$$

$\mathbf{K}_1$ stiffness matrix, constant strain tetrahedron

The increment of the differentiated rod lengths from Equation 3.127 changes with two angular changes, unlike the 2-dimensional formulation changing through one angular change. Equation 3.130 shows a single basis $({}_{\mathrm{t}}\mathbf{e})$ chain differentiated through two angular changes, a change in the $({}_{\mathrm{t}}\mathbf{n})$ direction and a change in the $({}_{\mathrm{t}}\boldsymbol{\eta})$ direction. The obtained result from Equation 3.130 is now inserted into the increment of the differentiated rod lengths, thus giving Equation 3.131. Here Equation 3.131 follows a similar pattern to Equation 3.127.

$$\delta_{\mathrm{t}}\mathbf{e} = \frac{\partial_{\mathrm{t}}\mathbf{e}}{\partial\theta}\delta\theta + \frac{\partial_{\mathrm{t}}\mathbf{e}}{\partial\vartheta}\delta\vartheta = {}_{\mathrm{t}}\mathbf{n}\;\delta\theta + {}_{\mathrm{t}}\boldsymbol{\eta}\;\delta\vartheta \tag{3.130}$$

$$\delta\left(\frac{\partial_{\mathrm{t}}\mathbf{L}}{\partial\mathbf{u}}^{T}\right) = \begin{bmatrix} -({}_{\mathrm{t}}\mathbf{n}^1\delta\theta_1 + {}_{\mathrm{t}}\boldsymbol{\eta}^1\delta\vartheta_1) & 0 & \dots & 0 \\ ({}_{\mathrm{t}}\mathbf{n}^1\delta\theta_1 + {}_{\mathrm{t}}\boldsymbol{\eta}^1\delta\vartheta_1) & -({}_{\mathrm{t}}\mathbf{n}^2\delta\theta_2 + {}_{\mathrm{t}}\boldsymbol{\eta}^2\delta\vartheta_2) & \dots & 0 \\ 0 & ({}_{\mathrm{t}}\mathbf{n}^2\delta\theta_2 + {}_{\mathrm{t}}\boldsymbol{\eta}^2\delta\vartheta_2) & \dots & -({}_{\mathrm{t}}\mathbf{n}^6\delta\theta_6 + {}_{\mathrm{t}}\boldsymbol{\eta}^6\delta\vartheta_6) \\ 0 & 0 & \dots & ({}_{\mathrm{t}}\mathbf{n}^6\delta\theta_6 + {}_{\mathrm{t}}\boldsymbol{\eta}^6\delta\vartheta_6) \end{bmatrix} \tag{3.131}$$

Rewriting the increment of the differentiated rod lengths gives Equation 3.132. This gives a matrix $(\mathbf{M})$ containing the angular changes and a matrix $(\mathbf{P})$ containing $({}_{\mathrm{t}}\mathbf{e})$ differentiated with respect to angular changes. The matrix $(\mathbf{M})$ in Equation 3.133 has six columns, one per rod. Each rod also has two angular changes, creating 12 rows. For instance, the first column shows the angular changes of rod 1. The angles (θ_1 and ϑ_1) change rod 1, thus giving the position in column 1 and rows 1 and 2. This pattern continues downwards, with (θ_2 and ϑ_2) in the second column and the third and fourth row.

$$\delta\left(\frac{\partial_{\mathrm{t}}\mathbf{L}^{T}}{\partial\mathbf{u}}\right)=\mathbf{P}^{T}\mathbf{M} \tag{3.132}$$

$$\mathbf{M}=\begin{bmatrix}\delta\theta_1 & 0 & \dots & 0\\ \delta\vartheta_1 & 0 & \dots & 0\\ 0 & \delta\theta_2 & \dots & 0\\ 0 & \delta\vartheta_2 & \dots & 0\\ \vdots & \vdots & \ddots & \vdots\\ 0 & 0 & \dots & \delta\theta_6\\ 0 & 0 & \dots & \delta\vartheta_6\end{bmatrix} \tag{3.133}$$

The matrix ($\mathbf{P}$) in Equation 3.134 is an expanded version of the differentiated lengths and has 12 rows (4 nodes x 3 degrees of freedom) and 12 columns (12 angular changes). Each of the twelve columns relates to the twelve angular changes, while each row relates to the four nodal displacements. For instance, rod 1 gets angular changes with (θ_1, ϑ_1) and runs between nodes 1 to 2.

$$\mathbf{P}^{T}=\begin{bmatrix}-({}_{\mathrm{t}}\mathbf{n}^1) & -({}_{\mathrm{t}}\boldsymbol{\eta}^1) & 0 & 0 & \dots & 0 & 0\\ ({}_{\mathrm{t}}\mathbf{n}^1) & ({}_{\mathrm{t}}\boldsymbol{\eta}^1) & -({}_{\mathrm{t}}\mathbf{n}^2) & -({}_{\mathrm{t}}\boldsymbol{\eta}^2) & \dots & 0 & 0\\ 0 & 0 & ({}_{\mathrm{t}}\mathbf{n}^2) & ({}_{\mathrm{t}}\boldsymbol{\eta}^2) & \dots & -({}_{\mathrm{t}}\mathbf{n}^6) & -({}_{\mathrm{t}}\boldsymbol{\eta}^6)\\ 0 & 0 & 0 & 0 & \dots & ({}_{\mathrm{t}}\mathbf{n}^6) & ({}_{\mathrm{t}}\boldsymbol{\eta}^6)\end{bmatrix} \tag{3.134}$$

Equation 3.135 shows a collected vector of the differentiated strain tensor, the stress tensor, and the covariant transformation. This way of rewriting allows for writing the angular changes on the right-hand side of the ($\mathbf{K}_1$) stiffness matrix integrand. Equation 3.136 is now provided by swapping the collected term in Equation 3.135 and the angular changes. Here the diagonalized matrix in Equation 3.136 follows the pattern, Q_1 in the first row and column; Q_1 in the second row and column; Q_2 in the third row and column; Q_2 in the fourth row and column; and so on.

$$\mathbf{Q}=\frac{\partial_0\widetilde{\mathbf{E}}}{\partial_{\mathrm{t}}\mathbf{L}}\widetilde{\mathbf{T}}^{-T}{}_0\mathbf{S} \tag{3.135}$$

$$\mathbf{MQ}=\begin{bmatrix}\delta\theta_1 & 0 & \dots & 0\\ \delta\vartheta_1 & 0 & \dots & 0\\ 0 & \delta\theta_2 & \dots & 0\\ 0 & \delta\vartheta_2 & \dots & 0\\ \vdots & \vdots & \ddots & \vdots\\ 0 & 0 & \dots & \delta\theta_6\\ 0 & 0 & \dots & \delta\vartheta_6\end{bmatrix}\begin{bmatrix}Q_1\\ \vdots\\ Q_6\end{bmatrix}=\begin{bmatrix}Q_1 & 0 & \dots & 0 & 0\\ 0 & Q_1 & \dots & 0 & 0\\ \vdots & \vdots & \ddots & \vdots & \vdots\\ 0 & 0 & \dots & Q_6 & 0\\ 0 & 0 & \dots & 0 & Q_6\end{bmatrix}\begin{bmatrix}\delta\theta_1\\ \delta\vartheta_1\\ \vdots\\ \delta\theta_6\\ \delta\vartheta_6\end{bmatrix} \tag{3.136}$$

Now writing the angular change as a function of the local displacement components ($\delta\widetilde{v}$ and $\delta\widetilde{w}$) gives Equation 3.137. These local displacements can further be transformed into global Cartesian coordinates.

$$\delta\boldsymbol{\theta} = \begin{bmatrix} \delta\theta_1 \\ \delta\vartheta_1 \\ \vdots \\ \delta\theta_6 \\ \delta\vartheta_6 \end{bmatrix} = \begin{bmatrix} \frac{\delta\widetilde{v}_2 - \delta\widetilde{v}_1}{{}_{\mathrm{t}}L_1} \\ \frac{\delta\widetilde{w}_2 - \delta\widetilde{w}_1}{{}_{\mathrm{t}}L_1} \\ \vdots \\ \frac{\delta\widetilde{v}_{12} - \delta\widetilde{v}_{11}}{{}_{\mathrm{t}}L_6} \\ \frac{\delta\widetilde{w}_{12} - \delta\widetilde{w}_{11}}{{}_{\mathrm{t}}L_6} \end{bmatrix} \tag{3.137}$$

Equation 3.138 shows the transformation between the local displacements ($\delta\widetilde{v}$ and $\delta\widetilde{w}$) and the global displacements ($\delta\mathbf{u}$), following a similar arrangement as Equation 3.126. ($\delta\widetilde{v}_1$ and $\delta\widetilde{w}_1$) related to the first node (column 1) and the first rod (superindex 1), ($\delta\widetilde{v}_2$ and $\delta\widetilde{w}_2$) related to the second node and the first rod, ($\delta\widetilde{v}_3$ and $\delta\widetilde{w}_3$) related to the second node and the second rod (superindex 2), ($\delta\widetilde{v}_4$ and $\delta\widetilde{w}_4$) related to the third node and the second rod.

$$\begin{bmatrix} \delta\widetilde{v}_1 \\ \delta\widetilde{w}_1 \\ \delta\widetilde{v}_2 \\ \delta\widetilde{w}_2 \\ \delta\widetilde{v}_3 \\ \delta\widetilde{w}_3 \\ \vdots \\ \delta\widetilde{v}_{12} \\ \delta\widetilde{w}_{12} \end{bmatrix} = \begin{bmatrix} \left({}_{\mathrm{t}}\mathbf{n}^1\right)^T & 0 & 0 & 0 \\ \left({}_{\mathrm{t}}\boldsymbol{\eta}^1\right)^T & 0 & 0 & 0 \\ 0 & \left({}_{\mathrm{t}}\mathbf{n}^1\right)^T & 0 & 0 \\ 0 & \left({}_{\mathrm{t}}\boldsymbol{\eta}^1\right)^T & 0 & 0 \\ 0 & \left({}_{\mathrm{t}}\mathbf{n}^2\right)^T & 0 & 0 \\ 0 & \left({}_{\mathrm{t}}\boldsymbol{\eta}^2\right)^T & 0 & 0 \\ \vdots & \vdots & \vdots & \vdots \\ 0 & 0 & 0 & \left({}_{\mathrm{t}}\mathbf{n}^6\right)^T \\ 0 & 0 & 0 & \left({}_{\mathrm{t}}\boldsymbol{\eta}^6\right)^T \end{bmatrix} \begin{bmatrix} \delta u_1 \\ \delta v_1 \\ \delta w_1 \\ \vdots \\ \delta u_4 \\ \delta v_4 \\ \delta w_4 \end{bmatrix} \tag{3.138}$$

The lengths from the angular changes are further extracted and combined with the diagonalized matrix ($\mathbf{Q}$) to form the ($\mathbf{H}$) matrix in Equation 3.139.

$$\mathbf{H} = \begin{bmatrix} Q_1 & 0 & \dots & 0 & 0 \\ 0 & Q_1 & \dots & 0 & 0 \\ \vdots & \vdots & \ddots & \vdots & \vdots \\ 0 & 0 & \dots & Q_6 & 0 \\ 0 & 0 & \dots & 0 & Q_6 \end{bmatrix} \begin{bmatrix} \frac{1}{{}_{\mathrm{t}}L_1} & 0 & \dots & 0 & 0 \\ 0 & \frac{1}{{}_{\mathrm{t}}L_1} & \dots & 0 & 0 \\ \vdots & \vdots & \ddots & \vdots & \vdots \\ 0 & 0 & \dots & \frac{1}{{}_{\mathrm{t}}L_6} & 0 \\ 0 & 0 & \dots & 0 & \frac{1}{{}_{\mathrm{t}}L_6} \end{bmatrix} \tag{3.139}$$

Now combining Equations 3.134, 3.137, 3.139, and 3.138 gives the ($\mathbf{K}_1$) stiffness matrix for the constant strain 4-node tetrahedron in Equation 3.140.

$$\mathbf{K}_1 = \mathbf{P}^T\mathbf{H}\mathbf{P}_0\Omega \tag{3.140}$$

$\mathbf{K}_2$ stiffness matrix, constant strain tetrahedron

The ($\mathbf{K}_2$) stiffness matrix follows the double differentiated strain tensor shown in Equation 3.141.

$$\mathbf{K}_2\delta\mathbf{u} = \frac{\partial_{\mathrm{t}}\mathbf{L}}{\partial\mathbf{u}}^T \delta\left(\frac{\partial_0\widetilde{\mathbf{E}}}{\partial_{\mathrm{t}}\mathbf{L}}\right)\widetilde{\mathbf{T}}^{-T}{}_0\mathbf{S}_0\Omega \tag{3.141}$$

The double differentiated strain tensor, the covariant strain tensor and the stress tensor can be collected and inserted into the main diagonal following Equation 3.142, giving length changes on the right-hand side of the expression. Bringing together Equations 3.141 and 3.142 gives the integrand of the ($\mathbf{K}_2$) stiffness matrix in Equation 3.143 differentiated with respect to length changes of the rods.

$$\mathbf{\Psi}\delta_{\mathrm{t}}\mathbf{L} = \left\lceil \frac{\partial^{(2)}{}_0\widetilde{\mathbf{E}}}{\partial_{\mathrm{t}}\mathbf{L}^{(2)}}\widetilde{\mathbf{T}}^{-T}{}_0\mathbf{S}\right\rfloor \delta_{\mathrm{t}}\mathbf{L} \tag{3.142}$$

$$\frac{\partial_{\mathrm{t}}\mathbf{L}}{\partial\mathbf{u}}^T \delta\left(\frac{\partial_0\widetilde{\mathbf{E}}}{\partial_{\mathrm{t}}\mathbf{L}}\right)\widetilde{\mathbf{T}}^{-T}{}_0\mathbf{S} = \mathbf{\Gamma}^T\mathbf{\Psi}\delta_{\mathrm{t}}\mathbf{L} \tag{3.143}$$

Inserting Equation 3.127 into the incremental rod lengths fully defines the ($\mathbf{K}_2$) stiffness matrix's integrand, and thus gives the ($\mathbf{K}_2$) stiffness matrix in Equation 3.144.

$$\mathbf{K}_2 = \mathbf{\Gamma}^T\mathbf{\Psi}\mathbf{\Gamma}\ {}_0\Omega \tag{3.144}$$

$\mathbf{K}_3$ stiffness matrix, constant strain tetrahedron

The constant integrand also gives a simple expression for the ($\mathbf{K}_3$) material stiffness matrix. Inserting Hooke's law or the elastic-plastic tangent moduli now defines the stiffness matrix in Equation 3.145.

$$\mathbf{K}_3 = \mathbf{B}^T\delta_0\mathbf{S}\ {}_0\Omega = \mathbf{B}^T\mathbf{C}^{\mathrm{ep}}\ \mathbf{B}\ {}_0\Omega \tag{3.145}$$

3.4.5 Assumed natural linear interpolated strain tetrahedron

Splitting the 10-node tetrahedron into four satellite tetrahedrons gives the ANS interpolated strain tetrahedron. Figure 3.8 shows a principal sketch of the node configuration and rod definitions of satellite number 4. A single satellite tetrahedron consists of 6 line segments, giving (4x6=24) independent rods. Assuming each rod follows the 1-dimensional Seth-Hill strain tensor gives the four satellite covariant strain tensors in Equation 3.146. Interpolating and transforming the four covariant satellite strain tensors now gives the global Cartesian strain tensor in Equation 3.147.

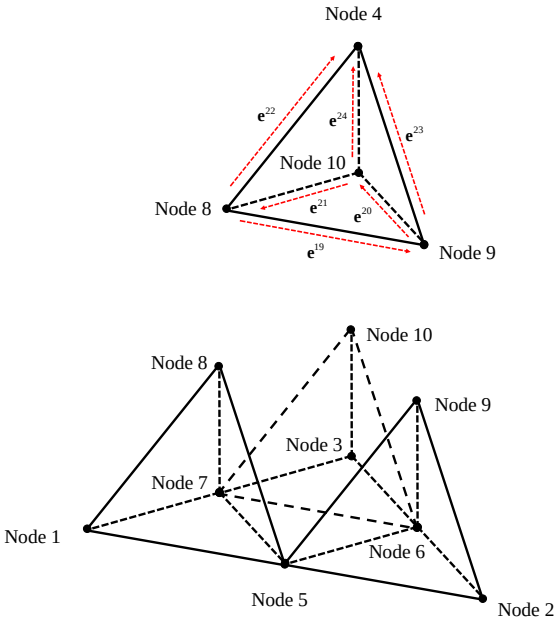

Figure 3.8: Node configuration of the ANS 10-node linear strain tetrahedron.

$$\{{}_0\widetilde{\mathbf{E}}\}_1 = \begin{bmatrix} {}_0\widetilde{E}_1 \\ \vdots \\ {}_0\widetilde{E}_6 \end{bmatrix} = \frac{1}{2m} \begin{bmatrix} (\frac{{}_tL_1}{{}_0L_1})^{2m} - 1 \\ \vdots \\ (\frac{{}_tL_6}{{}_0L_6})^{2m} - 1 \end{bmatrix} \ldots \{{}_0\widetilde{\mathbf{E}}\}_4 = \begin{bmatrix} {}_0\widetilde{E}_{19} \\ \vdots \\ {}_0\widetilde{E}_{24} \end{bmatrix} = \frac{1}{2m} \begin{bmatrix} (\frac{{}_tL_{19}}{{}_0L_{19}})^{2m} - 1 \\ \vdots \\ (\frac{{}_tL_{24}}{{}_0L_{24}})^{2m} - 1 \end{bmatrix} \tag{3.146}$$

$${}_0\mathbf{E} = N_1 \left(\{\widetilde{\mathbf{T}}\}^1 \right)^{-1} \{{}_0\widetilde{\mathbf{E}}\}_1 + \ \ldots \ + N_4 \left(\{\widetilde{\mathbf{T}}\}^4 \right)^{-1} \{{}_0\widetilde{\mathbf{E}}\}_4 \tag{3.147}$$

The system relating the rods, the local and global displacement components are shown in Appendix A, table A.3 to A.6. The four satellites are also visible in Figure 3.8. Satellite 1 defined by nodes (1, 5, 7, 8), Satellite 2 defined by nodes (2, 5, 6, 9), Satellite 3 defined by nodes (3, 6, 7, 10), and Satellite 4 defined by nodes (4, 8, 9, 10).

The virtual work is defined through chain differentiation of the strain tensor in terms of rod lengths, and differentiation of the global Cartesian strain tensor with respect to the 24 rods gives Equation 3.148. With each of the differentiated sub/satellite tetrahedron following Equation 3.149.

$$\frac{\partial_0 \mathbf{E}}{\partial_t \mathbf{L}} \delta_t \mathbf{L} = \left[N_1 \left(\{\widetilde{\mathbf{T}}\}^1 \right)^{-1} \frac{\partial \{{}_0\widetilde{\mathbf{E}}\}_1}{\partial_t \mathbf{L}} \quad \ldots \quad N_4 \left(\{\widetilde{\mathbf{T}}\}^4 \right)^{-1} \frac{\partial \{{}_0\widetilde{\mathbf{E}}\}_4}{\partial_t \mathbf{L}} \right] \delta_t \mathbf{L} \tag{3.148}$$

$$\frac{\partial\{{}_0\widetilde{\mathbf{E}}\}_1}{\partial_{\mathrm{t}}\mathbf{L}} = \begin{bmatrix} \frac{({}_{\mathrm{t}}L_1)^{2m-1}}{({}_0L_1)^{2m}} & \dots & 0 \\ \vdots & \ddots & \vdots \\ 0 & \dots & \frac{({}_{\mathrm{t}}L_6)^{2m-1}}{({}_0L_6)^{2m}} \end{bmatrix} \dots$$
$$\frac{\partial\{{}_0\widetilde{\mathbf{E}}\}_4}{\partial_{\mathrm{t}}\mathbf{L}} = \begin{bmatrix} \frac{({}_{\mathrm{t}}L_{19})^{2m-1}}{({}_0L_{19})^{2m}} & \dots & 0 \\ \vdots & \ddots & \vdots \\ 0 & \dots & \frac{({}_{\mathrm{t}}L_{24})^{2m-1}}{({}_0L_{24})^{2m}} \end{bmatrix} \tag{3.149}$$

The differentiated lengths in Equation 3.150 are now represented through the 48 local displacement components ($\delta\widetilde{u}$). Transforming the components of the local displacement into the global Cartesian displacements gives Equation 3.151. ($\delta\widetilde{u}_1$) is the transformed global Cartesian displacements of node 5 in the direction of rod 1, thus setting (${}_{\mathrm{t}}\mathbf{e}^1$) into the fifth column. ($\delta\widetilde{u}_2$) relates to rod 1 and node 7 setting (${}_{\mathrm{t}}\mathbf{e}^1$) in column 7. The pattern continues through the 24 rods with the system from Table A.3 to A.6.

$$\delta_{\mathrm{t}}\mathbf{L} = \begin{bmatrix} \delta_{\mathrm{t}}L_1 \\ \vdots \\ \delta_{\mathrm{t}}L_{24} \end{bmatrix} = \begin{bmatrix} \delta\widetilde{u}_2 - \delta\widetilde{u}_1 \\ \vdots \\ \delta\widetilde{u}_{48} - \delta\widetilde{u}_{47} \end{bmatrix} \tag{3.150}$$

$$\begin{bmatrix} \delta\widetilde{u}_1 \\ \delta\widetilde{u}_2 \\ \delta\widetilde{u}_3 \\ \delta\widetilde{u}_4 \\ \vdots \\ \delta\widetilde{u}_{45} \\ \delta\widetilde{u}_{46} \\ \delta\widetilde{u}_{47} \\ \delta\widetilde{u}_{48} \end{bmatrix} = \begin{bmatrix} 0 & 0 & 0 & 0 & \left({}_{\mathrm{t}}\mathbf{e}^1\right)^T & 0 & 0 & 0 & 0 & 0 \\ 0 & 0 & 0 & 0 & 0 & 0 & \left({}_{\mathrm{t}}\mathbf{e}^1\right)^T & 0 & 0 & 0 \\ 0 & 0 & 0 & 0 & 0 & 0 & \left({}_{\mathrm{t}}\mathbf{e}^2\right)^T & 0 & 0 & 0 \\ 0 & 0 & 0 & 0 & 0 & 0 & 0 & \left({}_{\mathrm{t}}\mathbf{e}^2\right)^T & 0 & 0 \\ & \vdots & & \vdots & & & \vdots & & \vdots & \\ 0 & 0 & 0 & 0 & 0 & 0 & 0 & 0 & \left({}_{\mathrm{t}}\mathbf{e}^{23}\right)^T & 0 \\ 0 & 0 & 0 & \left({}_{\mathrm{t}}\mathbf{e}^{23}\right)^T & 0 & 0 & 0 & 0 & 0 & 0 \\ 0 & 0 & 0 & 0 & 0 & 0 & 0 & 0 & 0 & \left({}_{\mathrm{t}}\mathbf{e}^{24}\right)^T \\ 0 & 0 & 0 & \left({}_{\mathrm{t}}\mathbf{e}^{24}\right)^T & 0 & 0 & 0 & 0 & 0 & 0 \end{bmatrix} \begin{bmatrix} \delta u_1 \\ \delta v_1 \\ \delta w_1 \\ \vdots \\ \delta u_{10} \\ \delta v_{10} \\ \delta w_{10} \end{bmatrix} \tag{3.151}$$

Collecting Equations 3.150 and 3.151 gives the change in rod lengths in terms of nodal displacements. This is shown in Equation 3.152 with rod 1 running from node 5 (row 5) towards node 7 (row 7) and rod 24 running from node 10 (row 10) towards node 4 (row 4).

$$\frac{\partial_{\mathrm{t}}\mathbf{L}}{\partial\mathbf{u}}^T = \mathbf{\Gamma}^T = \begin{bmatrix} 0 & 0 & & 0 & 0 \\ 0 & 0 & & 0 & 0 \\ 0 & 0 & & 0 & 0 \\ 0 & 0 & \dots & {}_{\mathrm{t}}\mathbf{e}^{23} & {}_{\mathrm{t}}\mathbf{e}^{24} \\ -{}_{\mathrm{t}}\mathbf{e}^{1} & 0 & & 0 & 0 \\ 0 & 0 & & 0 & 0 \\ {}_{\mathrm{t}}\mathbf{e}^{1} & -{}_{\mathrm{t}}\mathbf{e}^{2} & \dots & 0 & 0 \\ 0 & {}_{\mathrm{t}}\mathbf{e}^{2} & & 0 & 0 \\ 0 & 0 & & -{}_{\mathrm{t}}\mathbf{e}^{23} & 0 \\ 0 & 0 & & 0 & -{}_{\mathrm{t}}\mathbf{e}^{24} \end{bmatrix} \tag{3.152}$$

The center of mass of a tetrahedron follows (1/4) of the height. Each satellite tetrahedron then has a center of mass at (5/8) of the volume coordinate, shown in Equation 3.153. Equation 3.154 now gives interpolation functions with unit value in the center of each satellite.

$$\text{Center of mass} = \left(\frac{1}{2} + \frac{1}{2}\cdot\frac{1}{4}\right)\zeta_i = \frac{5}{8}\zeta_i \tag{3.153}$$

$$\begin{bmatrix} N_1 \\ N_2 \\ N_3 \\ N_4 \end{bmatrix} = \begin{bmatrix} \frac{7}{4}\zeta_1 - \frac{1}{4}\zeta_2 - \frac{1}{4}\zeta_3 - \frac{1}{4}\zeta_4 \\ \frac{7}{4}\zeta_2 - \frac{1}{4}\zeta_3 - \frac{1}{4}\zeta_4 - \frac{1}{3}\zeta_1 \\ \frac{7}{4}\zeta_3 - \frac{1}{4}\zeta_4 - \frac{1}{4}\zeta_1 - \frac{1}{3}\zeta_2 \\ \frac{7}{4}\zeta_4 - \frac{1}{4}\zeta_1 - \frac{1}{4}\zeta_2 - \frac{1}{4}\zeta_3 \end{bmatrix} \tag{3.154}$$

The shape functions, differentiated rod lengths, and the global Cartesian strain tensor can be collected to form the internal force vector shown in Equation 3.155. The expression can also be numerically integrated, thus following Equation 3.156. Different options relating the volume coordinates of the shape functions and positions of the elements are possible. Now choosing the conventional 10-node tetrahedron's Jacobi matrix preserves the internal force vector during constant strains.

$$\mathbf{f}^{\text{int}} = \int_{{}_0\Omega} \mathbf{B}^T {}_0\mathbf{S}\; d_0\Omega = \frac{1}{6}\int_0^1\int_0^1\int_0^1 \frac{\partial_{\mathrm{t}}\mathbf{L}}{\partial\mathbf{u}}^T \frac{\partial_0\mathbf{E}}{\partial_{\mathrm{t}}\mathbf{L}}^T {}_0\mathbf{S}\;\mathrm{Det}(\mathbf{J}) d\zeta_1 d\zeta_2 d\zeta_3 \tag{3.155}$$

$$\mathbf{f}^{\text{int}} \approx \frac{1}{6}\sum_{i=1}^{4} W(a_i)\mathbf{B}(a_i)^T {}_0\mathbf{S}(a_i)\;\mathrm{Det}(\mathbf{J}(a_i)) \tag{3.156}$$

$\mathbf{K}_1$ stiffness matrix, linear strain tetrahedron

The ($\mathbf{K}_1$) stiffness matrix integrand is assembled from the increment of Equation 3.152, and rewriting the increment in terms of angular changes gives Equation 3.157.

$$\delta\left(\frac{\partial_t \mathbf{L}^T}{\partial \mathbf{u}}\right)=\begin{bmatrix} 0 & 0 & \dots & 0 \\ 0 & 0 & \dots & 0 \\ 0 & 0 & \dots & 0 \\ 0 & 0 & \dots & ({}_t\mathbf{n}^{24}\delta\theta_{24} + {}_t\boldsymbol{\eta}^{24}\delta\vartheta_{24}) \\ -({}_t\mathbf{n}^{1}\delta\theta_{1} + {}_t\boldsymbol{\eta}^{1}\delta\vartheta_{1}) & 0 & \dots & 0 \\ 0 & 0 & \dots & 0 \\ ({}_t\mathbf{n}^{1}\delta\theta_{1} + {}_t\boldsymbol{\eta}^{1}\delta\vartheta_{1}) & -({}_t\mathbf{n}^{2}\delta\theta_{2} + {}_t\boldsymbol{\eta}^{2}\delta\vartheta_{2}) & \dots & 0 \\ 0 & ({}_t\mathbf{n}^{2}\delta\theta_{2} + {}_t\boldsymbol{\eta}^{2}\delta\vartheta_{2}) & \dots & 0 \\ 0 & 0 & \dots & 0 \\ 0 & 0 & \dots & -({}_t\mathbf{n}^{24}\delta\theta_{24} + {}_t\boldsymbol{\eta}^{24}\delta\vartheta_{24}) \end{bmatrix} \tag{3.157}$$

Separating the angular changes and the rod bases (${}_t\mathbf{n}$ and ${}_t\boldsymbol{\eta}$) gives the two matrices ($\mathbf{M}$) and ($\mathbf{P}$) in Equation 3.158, where ($\mathbf{P}$) and ($\mathbf{M}$) follow Equations 3.159 and 3.160. The ($\mathbf{M}$) matrix now has 24 columns and 48 rows. Column 1 relates the angular changes to rod 1, column 2 relates the angular changes to rod 2, and so forth. Equation 3.160 shows the ($\mathbf{P}$) matrix relating nodal displacements and angular changes. Row 5 and columns 1 and 2 relates the nodal displacements of node 5 to the angular changes of rod 1. This system continues through the 24 rods.

$$\delta\left(\frac{\partial_t \mathbf{L}^T}{\partial \mathbf{u}}\right) = \mathbf{P}^T\mathbf{M} \tag{3.158}$$

$$\mathbf{M} = \begin{bmatrix} \delta\theta_1 & 0 & \dots & 0 \\ \delta\vartheta_1 & 0 & \dots & 0 \\ 0 & \delta\theta_2 & \dots & 0 \\ 0 & \delta\vartheta_2 & \dots & 0 \\ \vdots & \vdots & \ddots & \vdots \\ 0 & 0 & \dots & \delta\theta_{24} \\ 0 & 0 & \dots & \delta\vartheta_{24} \end{bmatrix} \tag{3.159}$$

$$\mathbf{P}^T = \begin{bmatrix} 0 & 0 & 0 & 0 & \dots & 0 & 0 & 0 & 0 \\ 0 & 0 & 0 & 0 & \dots & 0 & 0 & 0 & 0 \\ 0 & 0 & 0 & 0 & \dots & 0 & 0 & 0 & 0 \\ 0 & 0 & 0 & 0 & \dots & {}_{\mathrm{t}}\mathbf{n}^{23} & {}_{\mathrm{t}}\boldsymbol{\eta}^{23} & {}_{\mathrm{t}}\mathbf{n}^{24} & {}_{\mathrm{t}}\boldsymbol{\eta}^{24} \\ -{}_{\mathrm{t}}\mathbf{n}^{1} & -{}_{\mathrm{t}}\boldsymbol{\eta}^{1} & 0 & 0 & \dots & 0 & 0 & 0 & 0 \\ 0 & 0 & 0 & 0 & \dots & 0 & 0 & 0 & 0 \\ {}_{\mathrm{t}}\mathbf{n}^{1} & {}_{\mathrm{t}}\boldsymbol{\eta}^{1} & -{}_{\mathrm{t}}\mathbf{n}^{2} & -{}_{\mathrm{t}}\boldsymbol{\eta}^{2} & \dots & 0 & 0 & 0 & 0 \\ 0 & 0 & {}_{\mathrm{t}}\mathbf{n}^{2} & {}_{\mathrm{t}}\boldsymbol{\eta}^{2} & \dots & 0 & 0 & 0 & 0 \\ 0 & 0 & 0 & 0 & \dots & -{}_{\mathrm{t}}\mathbf{n}^{23} & -{}_{\mathrm{t}}\boldsymbol{\eta}^{23} & 0 & 0 \\ 0 & 0 & 0 & 0 & \dots & 0 & 0 & -{}_{\mathrm{t}}\mathbf{n}^{24} & -{}_{\mathrm{t}}\mathbf{n}^{24} \end{bmatrix} \tag{3.160}$$

The shape functions, differentiated strain tensor, and stress tensor are now collected into the vector in Equation 3.161. This way of arranging the ($\mathbf{Q}$) vector allows the incremental angles to be written on the right-hand side in Equation 3.162.

$$\mathbf{Q} = \begin{bmatrix} N_1 \frac{\partial \{{}_0\widetilde{\mathbf{E}}\}_1}{\partial {}_{\mathrm{t}}\mathbf{L}}^T \left(\{\widetilde{\mathbf{T}}\}^1 \right)^{-T} {}_0\mathbf{S} \\ N_2 \frac{\partial \{{}_0\widetilde{\mathbf{E}}\}_2}{\partial {}_{\mathrm{t}}\mathbf{L}}^T \left(\{\widetilde{\mathbf{T}}\}^2 \right)^{-T} {}_0\mathbf{S} \\ N_3 \frac{\partial \{{}_0\widetilde{\mathbf{E}}\}_3}{\partial {}_{\mathrm{t}}\mathbf{L}}^T \left(\{\widetilde{\mathbf{T}}\}^3 \right)^{-T} {}_0\mathbf{S} \\ N_4 \frac{\partial \{{}_0\widetilde{\mathbf{E}}\}_4}{\partial {}_{\mathrm{t}}\mathbf{L}}^T \left(\{\widetilde{\mathbf{T}}\}^4 \right)^{-T} {}_0\mathbf{S} \end{bmatrix} \tag{3.161}$$

$$\mathbf{MQ} = \begin{bmatrix} \delta\theta_1 & 0 & \dots & 0 \\ \delta\vartheta_1 & 0 & \dots & 0 \\ 0 & \delta\theta_2 & \dots & 0 \\ 0 & \delta\vartheta_2 & \dots & 0 \\ \vdots & \vdots & \ddots & \vdots \\ 0 & 0 & \dots & \delta\theta_{24} \\ 0 & 0 & \dots & \delta\vartheta_{24} \end{bmatrix} \begin{bmatrix} Q_1 \\ \vdots \\ Q_{24} \end{bmatrix} = \begin{bmatrix} Q_1 & 0 & \dots & 0 & 0 \\ 0 & Q_1 & \dots & 0 & 0 \\ \vdots & \vdots & \ddots & \vdots & \vdots \\ 0 & 0 & \dots & Q_{24} & 0 \\ 0 & 0 & \dots & 0 & Q_{24} \end{bmatrix} \begin{bmatrix} \delta\theta_1 \\ \delta\vartheta_1 \\ \vdots \\ \delta\theta_{24} \\ \delta\vartheta_{24} \end{bmatrix} \tag{3.162}$$

Rewriting the angular changes as a function of the local displacement ($\delta\widetilde{v}$, $\delta\widetilde{w}$) gives Equation 3.163. Rod 1 in rows 1 and 2; rod 2 in rows 3 and 4; and so on. The local displacements can be further expressed as the global Cartesian displacements through the transformation shown in Equation 3.164. Here ($\delta\widetilde{v}_1$, $\delta\widetilde{w}_1$) correlates with the fifth node and rod 1 and is consequently put in the fifth column, with basis vectors following superindex 1.

$$\delta\boldsymbol{\theta} = \begin{bmatrix} \delta\theta_1 \\ \delta\vartheta_1 \\ \vdots \\ \delta\theta_{24} \\ \delta\vartheta_{24} \end{bmatrix} = \begin{bmatrix} \frac{\delta\widetilde{v}_2 - \delta\widetilde{v}_1}{{}_{\mathrm{t}}L_1} \\ \frac{\delta\widetilde{w}_2 - \delta\widetilde{w}_1}{{}_{\mathrm{t}}L_1} \\ \vdots \\ \frac{\delta\widetilde{v}_{48} - \delta\widetilde{v}_{47}}{{}_{\mathrm{t}}L_{24}} \\ \frac{\delta\widetilde{w}_{48} - \delta\widetilde{w}_{47}}{{}_{\mathrm{t}}L_{24}} \end{bmatrix} \tag{3.163}$$

$$\begin{bmatrix} \delta\widetilde{v}_1 \\ \delta\widetilde{w}_1 \\ \delta\widetilde{v}_2 \\ \delta\widetilde{w}_2 \\ \vdots \\ \delta\widetilde{v}_{48} \\ \delta\widetilde{w}_{48} \end{bmatrix} = \begin{bmatrix} 0 & 0 & 0 & 0 & \left({}_{\mathrm{t}}\mathbf{n}^1\right)^T & 0 & 0 & 0 & 0 & 0 \\ 0 & 0 & 0 & 0 & \left({}_{\mathrm{t}}\boldsymbol{\eta}^1\right)^T & 0 & 0 & 0 & 0 & 0 \\ 0 & 0 & 0 & 0 & 0 & 0 & \left({}_{\mathrm{t}}\mathbf{n}^1\right)^T & 0 & 0 & 0 \\ 0 & 0 & 0 & 0 & 0 & 0 & \left({}_{\mathrm{t}}\boldsymbol{\eta}^1\right)^T & 0 & 0 & 0 \\ & \vdots & & \vdots & & & \vdots & & \vdots & \\ 0 & 0 & 0 & 0 & 0 & 0 & 0 & 0 & 0 & \left({}_{\mathrm{t}}\mathbf{n}^{24}\right)^T \\ 0 & 0 & 0 & \left({}_{\mathrm{t}}\boldsymbol{\eta}^{24}\right)^T & 0 & 0 & 0 & 0 & 0 & 0 \end{bmatrix} \begin{bmatrix} \delta u_1 \\ \delta v_1 \\ \delta w_1 \\ \vdots \\ \delta u_{10} \\ \delta v_{10} \\ \delta w_{10} \end{bmatrix} \tag{3.164}$$

Now combining the lengths with the diagonalized matrix from Equation 3.162 gives the ($\mathbf{H}$) matrix in Equation 3.165. Here (Q_1 and L_1) is found in the first column and row, and the second column and row; (Q_2 and L_2) found in the third column and row, and the fourth column and row; and so on.

$$\mathbf{H} = \begin{bmatrix} Q_1 & 0 & \dots & 0 & 0 \\ 0 & Q_1 & \dots & 0 & 0 \\ \vdots & \vdots & \ddots & \vdots & \vdots \\ 0 & 0 & \dots & Q_{24} & 0 \\ 0 & 0 & \dots & 0 & Q_{24} \end{bmatrix} \begin{bmatrix} \frac{1}{{}_{\mathrm{t}}L_1} & 0 & \dots & 0 & 0 \\ 0 & \frac{1}{{}_{\mathrm{t}}L_1} & \dots & 0 & 0 \\ \vdots & \vdots & \ddots & \vdots & \vdots \\ 0 & 0 & \dots & \frac{1}{{}_{\mathrm{t}}L_{24}} & 0 \\ 0 & 0 & \dots & 0 & \frac{1}{{}_{\mathrm{t}}L_{24}} \end{bmatrix} \tag{3.165}$$

Collecting Equations 3.160, 3.163, 3.165 and 3.164 gives the integrand of the ($\mathbf{K}_1$) stiffness matrix in Equation 3.166, which can be numerically integrated following Equation 3.167.

$$\mathbf{K}_1 = \frac{1}{6}\int_0^1\int_0^1\int_0^1 \mathbf{P}^T\mathbf{H}\mathbf{P}\mathrm{Det}(\mathbf{J})d\zeta_1 d\zeta_2 d\zeta_3 \tag{3.166}$$

$$\mathbf{K}_1 = \frac{1}{6}\sum_{i=1}^{4} W(a_i)\mathbf{P}^T(a_i)\mathbf{H}(a_i)\mathbf{P}(a_i)\mathrm{Det}(\mathbf{J}(a_i)) \tag{3.167}$$

$\mathbf{K}_2$ stiffness matrix, linear strain tetrahedron

The integrand of the ($\mathbf{K}_2$) stiffness matrix is derived from the double differentiated strain tensor in Equation 3.168. Equation 3.169 shows a matrix where the twice differentiated strain tensor, stress tensor, shape functions, and covariant transformation have been collected into the main diagonal. This form of rewriting gives length changes on the right-hand side of the expression.

$$\begin{aligned}
\frac{\partial^{(2)}\{{}_0\widetilde{\mathbf{E}}\}_1}{\partial_{\mathrm{t}}\mathbf{L}^{(2)}} &= (2m-1)\begin{bmatrix} \frac{({}_{\mathrm{t}}L_1)^{2m-2}}{({}_0L_1)^{2m}} & \dots & 0 \\ \vdots & \ddots & \vdots \\ 0 & \dots & \frac{({}_{\mathrm{t}}L_6)^{2m-2}}{({}_0L_6)^{2m}} \end{bmatrix} \dots \\
\frac{\partial^{(2)}\{{}_0\widetilde{\mathbf{E}}\}_4}{\partial_{\mathrm{t}}\mathbf{L}^{(2)}} &= (2m-1)\begin{bmatrix} \frac{({}_{\mathrm{t}}L_{19})^{2m-2}}{({}_0L_{19})^{2m}} & \dots & 0 \\ \vdots & \ddots & \vdots \\ 0 & \dots & \frac{({}_{\mathrm{t}}L_{24})^{2m-2}}{({}_0L_{24})^{2m}} \end{bmatrix}
\end{aligned} \tag{3.168}$$

$$\boldsymbol{\Psi}\delta_{\mathrm{t}}\mathbf{L} = \begin{bmatrix} N_1\left(\frac{\partial^{(2)}\{{}_0\widetilde{\mathbf{E}}\}_1}{\partial_{\mathrm{t}}\mathbf{L}^{(2)}}\right)^T\left(\{\widetilde{\mathbf{T}}\}^1\right)^{-T}{}_0\mathbf{S} \\ N_2\left(\frac{\partial^{(2)}\{{}_0\widetilde{\mathbf{E}}\}_2}{\partial_{\mathrm{t}}\mathbf{L}^{(2)}}\right)^T\left(\{\widetilde{\mathbf{T}}\}^2\right)^{-T}{}_0\mathbf{S} \\ N_3\left(\frac{\partial^{(2)}\{{}_0\widetilde{\mathbf{E}}\}_3}{\partial_{\mathrm{t}}\mathbf{L}^{(2)}}\right)^T\left(\{\widetilde{\mathbf{T}}\}^3\right)^{-T}{}_0\mathbf{S} \\ N_4\left(\frac{\partial^{(2)}\{{}_0\widetilde{\mathbf{E}}\}_4}{\partial_{\mathrm{t}}\mathbf{L}^{(2)}}\right)^T\left(\{\widetilde{\mathbf{T}}\}^4\right)^{-T}{}_0\mathbf{S} \end{bmatrix}\delta_{\mathrm{t}}\mathbf{L} \tag{3.169}$$

The length changes are now rewritten in terms of the previously established Equation 3.152. This gives the ($\mathbf{K}_2$) stiffness matrix integrand in Equation 3.170, which is used for creating the ($\mathbf{K}_2$) stiffness matrix in Equations 3.171 and 3.172.

$$\frac{\partial_{\mathrm{t}}\mathbf{L}}{\partial\mathbf{u}}^T\delta\left(\frac{\partial_0\mathbf{E}}{\partial_{\mathrm{t}}\mathbf{L}}^T\right){}_0\mathbf{S} = \boldsymbol{\Gamma}^T\boldsymbol{\Psi}\delta_{\mathrm{t}}\mathbf{L} = \boldsymbol{\Gamma}^T\boldsymbol{\Psi}\boldsymbol{\Gamma}\delta\mathbf{u} \tag{3.170}$$

$$\mathbf{K}_2 = \frac{1}{6}\int_0^1\int_0^1\int_0^1 \boldsymbol{\Gamma}^T\boldsymbol{\Psi}\boldsymbol{\Gamma}\mathrm{Det}(\mathbf{J})d\zeta_1 d\zeta_2 d\zeta_3 \tag{3.171}$$

$$\mathbf{K}_2 \approx \frac{1}{6}\sum_{i=1}^{4} W(a_i)\boldsymbol{\Gamma}^T(a_i)\boldsymbol{\Psi}(a_i)\boldsymbol{\Gamma}(a_i)\mathrm{Det}(\mathbf{J}(a_i)) \tag{3.172}$$

$\mathbf{K}_3$ stiffness matrix, linear strain tetrahedron

Writing the incremental stresses in terms of the tangent moduli or Hooke's law creates the ($\mathbf{K}_3$) stiffness matrix shown in Equation 3.173, which further can be integrated through the four-point Gauss integration in Equation 3.174.

$$\mathbf{K}_3 = \frac{1}{6}\int_0^1\int_0^1\int_0^1 \mathbf{B}^T\delta\mathbf{S}d\zeta_1 d\zeta_2 d\zeta_3 = \frac{1}{6}\int_0^1\int_0^1\int_0^1 \mathbf{B}^T\mathbf{C}^{\mathrm{ep}}\mathbf{B}d\zeta_1 d\zeta_2 d\zeta_3 \tag{3.173}$$

$$\mathbf{K}_3 \approx \frac{1}{6}\sum_{i=1}^{4} W(a_i)\mathbf{B}(a_i)^T\mathbf{C}(a_i)^{\mathrm{ep}}\mathbf{B}(a_i)\ \mathrm{Det}(\mathbf{J}(a_i)) \tag{3.174}$$

3.5 Plasticity formulation

3.5.1 The yield function

The von Mises yield Criteria is one of the most commonly used yield criteria for metals, with the theory basing itself upon the second invariant of the deviatoric stress tensor. Plane stress conditions assume neglectable out-of-plane stress components, giving the von Mises yield criteria in the first row in Table 3.5. The second row in Table 3.5 shows the generalized version for the 3-dimensional stress state.

Table 3.5: The Von-Mises yield criterion for different 2- and 3-dimensional cases.

Plane stress	$\mathscr{F} = \sqrt{S_{XX}^2 + S_{YY}^2 - S_{XX}S_{YY} + 3S_{XY}^2}$
Generalized	$\mathscr{F} = \sqrt{\frac{1}{2}((S_{XX}-S_{YY})^2+(S_{YY}-S_{ZZ})^2+(S_{ZZ}-S_{XX})^2+6(S_{YZ}^2+S_{XZ}^2+S_{XY}^2))}$

An elastic-plastic material model needs three ingredients, a yield criteria, an hardening law, and elastic constants. The hardening law and elastic constants describe the stress-strain curve, while the yield criteria connect multiaxial stress states to the stress-strain curve. A commonly used assumption is the isotropic hardening, giving a uniform expansion of the yield surface during plastic flow. The uniform expansion of the yield surface is described with a single parameter, the equivalent plastic strain. The second row in Table 3.6 shows two commonly used hardening models, the perfect elastic-plastic and Johnson-Cook material models. The perfect-elastic-plastic material model assumes a constant equivalent yield stress, while the Johnson-Cook model expands after the relation in the right column in Table 3.6.

Table 3.6: Isotropic hardening models used for the yield function.

	Perfect-Plastic	Johnson-Cook
$\mathscr{R}(p)$	S_{ys}	$b_1 + b_2 p^{b_3}$
$h(p)$	0	$b_3 b_2 p^{b_3-1}$

Subtracting the isotropic hardening model from the yield criteria gives the yield surface shown in Equation 3.175. This function explains whether or not a material behaves plastically. Either the material experiences plastic flow at the yield surface or elastic deformations inside the yield surface, while stress-states outside the yield surface are inadmissible for static conditions.

$$\phi = \mathscr{F}(\mathbf{S}) - \mathscr{R}(p) \leq 0 \tag{3.175}$$

Equation 3.176 shows the plastic flow rule for associated plasticity. The associated plastic flow assumes plastic flow in the direction of the gradient of the yield surface. Here the Seth-Hill work conjugate stress tensor has been inserted into the yield criteria. Differentiation of the von Mises yield criterion now gives Equation 3.177 for the generalized 3-dimensional case and plane stress conditions.

$$\delta_0 \mathbf{E}^{\mathrm{pl}} = \frac{\partial \phi}{\partial_0 \mathbf{S}} \delta p \tag{3.176}$$

$$\frac{\partial \phi}{\partial_0 \mathbf{S}} = \frac{1}{2\mathscr{F}} \begin{bmatrix} 2\,{}_0S_{XX} - {}_0S_{YY} - {}_0S_{ZZ} \\ 2\,{}_0S_{YY} - {}_0S_{XX} - {}_0S_{ZZ} \\ 2\,{}_0S_{ZZ} - {}_0S_{XX} - {}_0S_{YY} \\ 6\,{}_0S_{YZ} \\ 6\,{}_0S_{XZ} \\ 6\,{}_0S_{XY} \end{bmatrix}, \quad \frac{\partial \phi}{\partial_0 \mathbf{S}} = \frac{1}{2\mathscr{F}} \begin{bmatrix} 2\,{}_0S_{XX} - {}_0S_{YY} \\ 2\,{}_0S_{YY} - {}_0S_{XX} \\ 6\,{}_0S_{XY} \end{bmatrix} \tag{3.177}$$

3.5.2 The return mapping algorithm

The Kuhn-Tucker conditions in Equation 3.178 explain the plastic behavior of a material. A stress state is either found inside or at the yield surface. If the stress state is inside the yield surface no plastic flow occurs. If the material is at the yield surface, the yield function is by definition set to zero.

$$\mathscr{F} \leq 0,\ \delta p \geq 0,\ \mathscr{F}\delta p = 0 \tag{3.178}$$

No changes in the yield function occur during plastic flow. This can be explained through the consistency conditions in Equation 3.179, stating the increment of the yield criteria must be equal to the increment of the plastic flow.

$$\delta\phi = \frac{\partial \phi}{\partial_0 \mathbf{S}} \delta_0 \mathbf{S} - h\delta p = 0 \tag{3.179}$$

The transition between the elastic behavior and plastic flow can be difficult to model for multidimensional geometries. Instead of always fulfilling the Kuhn-Tucker and consistency conditions, trial stresses corrected by mapping algorithms are practical for element formulations. Return mapping algorithms follow this logic, and the full Newton backward Euler return mapping algorithm presented here will follow the work of K. Krabbenhoft [15].

The first step of the return mapping algorithm is finding elastic trial stresses through Hooke's law presented in Equations 2.16 and 2.17. The stress state is accepted if the trial stress state gives a value inside the yield surface. Contrary, a corrector algorithm is applied if the trial stress is outside the yield surface. The corrector algorithm must finish with a stress state at the yield surface, and thus follow Equation 3.180.

$$\phi({}_0\mathbf{S}, p) = 0 \tag{3.180}$$

Hooke's law in Equations 2.16 and 2.17 follows the elastic parts of the strain tensor. The same relation is also valid for incremental stresses and strains. Assuming small finite stresses and strains gives Equation 3.181 through the additive decomposition plasticity presented in Equation 2.20.

$$\Delta_0\mathbf{S} = \mathbf{C}\Delta_0\mathbf{E}^{\mathrm{el}} = \mathbf{C}\left(\Delta_0\mathbf{E} - \Delta_0\mathbf{E}^{\mathrm{pl}}\right) \tag{3.181}$$

Equation 3.182 shows a rewritten version of the incremental Hooke's law. Here the plastic flow rule in Equation 3.176 is used for replacing the incremental plastic strain tensor. The total incremental strains and the incremental stresses can be collected and rewritten in terms of trial stresses and stresses at the yield surface. Figure 3.9 shows a trial stress state outside the yield surface (non-dotted quarter ellipse). Since the trial stresses give yielding, the trial stress tensor is mapped back to the yield surface. During the mapping, the yield surface gets an expansion (dotted quarter ellipse), and the yield surface gives a value of zero at the stress state ($_0\mathbf{S}$).

$$-\Delta_0\mathbf{S} + \mathbf{C}\Delta_0\mathbf{E} - \mathbf{C}\Delta_0\mathbf{E}^{\mathrm{pl}} = {}_0\mathbf{S} - {}_0\mathbf{S}^{\mathrm{trial}} + \mathbf{C}\frac{\partial\phi}{\partial_0\mathbf{S}}\Delta p = 0 \tag{3.182}$$

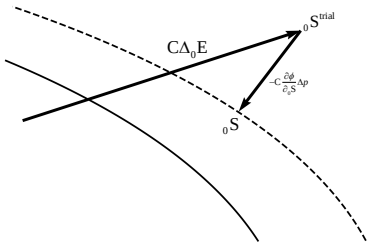

Figure 3.9: Principal sketch of the return mapping algorithm.

Equations 3.180 and 3.182 are now collected and inserted into the residual expression in Equation 3.183. This procedure gives the robust backward Euler return mapping scheme. Newton-Raphson methods are now applied to the system of non-linear equations, giving the derivative in Equation 3.184 and solving procedure in Table 3.7.

$$\mathbf{r} = \begin{bmatrix} {}_0\mathbf{S} - {}_0\mathbf{S}^{\mathrm{trial}} + \mathbf{C}\frac{\partial\phi}{\partial\mathbf{S}}\Delta p \\ \phi({}_0\mathbf{S}, p) \end{bmatrix} = 0 \tag{3.183}$$

$$\boldsymbol{\kappa}\delta\mathbf{r} = \begin{bmatrix} \mathbf{I} + \mathbf{C}\frac{\partial^{(2)}\phi}{\partial_0\mathbf{S}^{(2)}}\Delta p & \mathbf{C}\frac{\partial\phi}{\partial_0\mathbf{S}} \\ \frac{\partial\phi^T}{\partial_0\mathbf{S}} & h \end{bmatrix} \begin{bmatrix} \delta_0\mathbf{S} \\ \delta p \end{bmatrix} = -\mathbf{r} \tag{3.184}$$

Table 3.7: Procedure for the backward Euler return mapping algorithm.

Input: ${}_0\mathbf{S}^{\text{trial}}, p$

If $\phi({}_0\mathbf{S}^{\text{trial}}, p) < 0$:
accept trial stresses and set:
${}_0\mathbf{S} = {}_0\mathbf{S}^{\text{trial}}$

Or iterations until $\mathbf{r}^T\mathbf{r} < tol$:
Solve:
$\mathbf{r} = -\boldsymbol{\kappa}\delta\mathbf{r}$:

Set:
${}_0\mathbf{S} = {}_0\mathbf{S} + \delta_0\mathbf{S}$
$\Delta p = \Delta p + \delta p$
$p = p + \delta p$

Add plastic flow to plastic strains:
${}_0\mathbf{E}^{\text{pl}} = {}_0\mathbf{E}^{\text{pl}} + \frac{\partial\phi}{\partial_0\mathbf{S}}\Delta p$

3.5.3 Elastic-plastic tangent moduli

The stress increment in the material stiffness matrix can follow two approaches. Either the material is in elastic conditions and follows Hooke's law, or plastic flow occurs and the material follows the elastic-plastic tangent moduli, an idea first addressed by J. Nagtegaal [16] and further expanded by J. Simo et al. [17]. Rewriting the consistency conditions in Equation 3.179 in terms of incremental stresses, strains, and the plastic flow rule gives Equation 3.185. Now solving this equation in terms of the plastic multiplier gives Equation 3.186.

$$\frac{\partial\phi^T}{\partial_0\mathbf{S}}\mathbf{C}\left(\delta_0\mathbf{E} - \frac{\partial\phi}{\partial_0\mathbf{S}}\delta p\right) - h\delta p = 0 \tag{3.185}$$

$$\delta p = \frac{\frac{\partial\phi^T}{\partial_0\mathbf{S}}\,\mathbf{C}\,\delta_0\mathbf{E}}{h + \frac{\partial\phi^T}{\partial_0\mathbf{S}}\mathbf{C}\frac{\partial\phi}{\partial_0\mathbf{S}}} \tag{3.186}$$

Equation 3.187 shows the constitutive relation/incremental Hooke's law written in terms of the plastic flow rule, and inserting the plastic multiplier from Equation 3.186 into the constitutive relation gives the elastic-plastic tangent moduli in Equation 3.188.

$$\delta_0\mathbf{S} = \mathbf{C}\left(\delta_0\mathbf{E} - \delta_0\mathbf{E}^{\text{pl}}\right) = \mathbf{C}\left(\delta_0\mathbf{E} - \frac{\partial\phi}{\partial_0\mathbf{S}}\delta p\right) \tag{3.187}$$

$$\delta_0\mathbf{S} = \mathbf{C}^{\text{ep}}\,\delta_0\mathbf{E} = \left(\mathbf{C} - \frac{\mathbf{C}\frac{\partial\phi}{\partial_0\mathbf{S}}\frac{\partial\phi^T}{\partial_0\mathbf{S}}\mathbf{C}}{h + \frac{\partial\phi^T}{\partial_0\mathbf{S}}\mathbf{C}\frac{\partial\phi}{\partial_0\mathbf{S}}}\right)\delta_0\mathbf{E} \tag{3.188}$$

Chapter 4

Results and Discussion

4.1 Eigenvalues of triangular element

The element stiffness matrix needs to be able to preserve properties regarding rigid body motions. A way of checking this is through the eigenvalues of the stiffness matrix. The eigenvalue formulation of the stiffness matrix follows the form in Equation 4.1. Non-zero rigid body motion produces zero changes in the internal energy of the element and has a corresponding eigenvalue equal to zero. A 2-dimensional geometry needs to be able to preserve two translational degrees of freedom. For small strain assumptions, a rotational non-zero rigid body motion shall also be apparent in the stiffness matrix.

$$\mathbf{K}\delta\mathbf{u} = \omega\delta\mathbf{u} \tag{4.1}$$

Table 4.1 represents the geometry for the 3-node and 6-node triangular elements used for investigating the stiffness matrix, while Figure 4.1 shows the step-by-step process. The step-by-step process started with a stretch into a constant strain state, with the next and last step sending the geometry into a rigid body rotation of 45 degrees. Material constants ($\mu = 210 \cdot 10^3, \nu = 0.3$) were applied to the four formulations, 3-node conventional; 6-node conventional; 3-node ANS; 6-node ANS, all with the Green-Lagrange strain tensor.

Table 4.1: Coordinates for the triangular elements.

Node number:	1	2	3	4	5	6
3-node triangular element ($_0X$, $_0Y$)	(0,0)	(1,0)	(0,1)			
6-node triangular element ($_0X$, $_0Y$)	(0,0)	(1,0)	(0,1)	$\left(\frac{1}{2}, 0\right)$	$\left(\frac{1}{2}, \frac{1}{2}\right)$	$\left(0, \frac{1}{2}\right)$

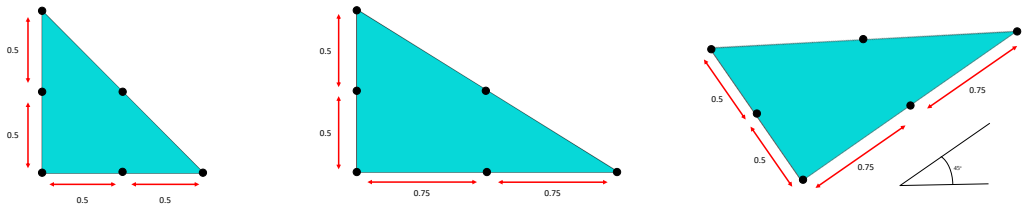

Figure 4.1: Mesh and geometry for a single element subjected to stretches and rigid body rotations.

Figure 4.2, 4.3, 4.4, and 4.5 shows the eigenvalues plotted against time for the four different formulations. The 3-node element formulations in Figures 4.2 and 4.3 shows the same eigenvalues. Having six nodal degrees of freedom, the 3-node element formulations create six eigenvalues. Counting downwards, four lines increases through the process while two stay constant at a value of zero. Midway through, the elements are sent into a rigid body rotation, giving constant eigenvalues for the rest of the simulations. Figures 4.4 and 4.5 show similar patterns, but with twelve degrees of freedom. The eigenvalues are continuously differentiable and two zero eigenvalues are always existing. The ratio of the largest to lowest non-zero eigenvalue in Figures 4.2, 4.3, 4.4, and 4.5 give values of around 10 and 20. Indicating well-conditioned stiffness matrices of the four element formulations.

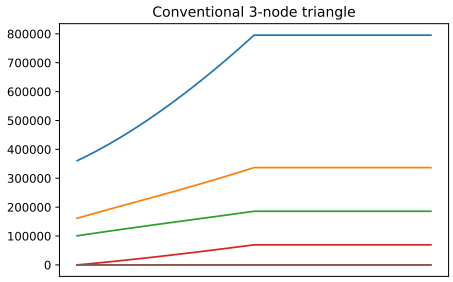

Figure 4.2: Eigenvalues plotted against time for the 2-dimensional 3-node conventional formulation.

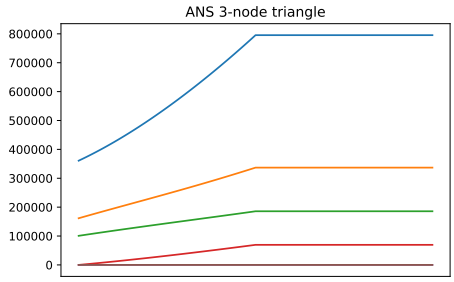

Figure 4.3: Eigenvalues plotted against time for the 2-dimensional ANS 3-node triangle.

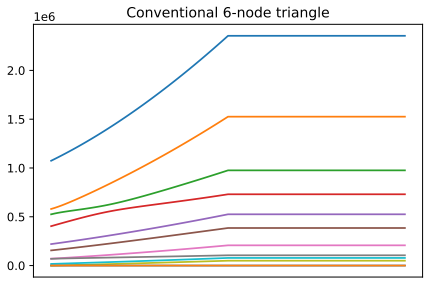

Figure 4.4: Eigenvalues plotted against time for the 2-dimensional 6-node conventional formulation.

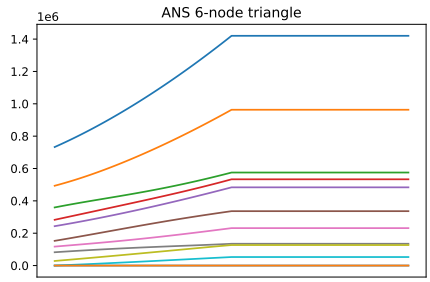

Figure 4.5: Eigenvalues plotted against time for the 2-dimensional ANS 6-node triangle.

4.2 Rod in 1-dimensional stress state

A simple way of testing the plasticity model in the element formulation is by making a tensile specimen in a uniaxial constant stress state. Pulling the tensile specimen in the elastic regime should give an effective Poisson ratio ($\nu_{XZ} = -\mathbf{E}_{XX}/\mathbf{E}_{ZZ}$) equal to the inserted value in the hyperelastic Hooke's law. Increasing plastic deformation makes the effective Poisson ratio deviate from the value inserted into the hyperelastic Hooke's law. The von Mises yield criterion with associated plastic flow assumes a constant sum of plastic normal strains and therefore should give an effective Poisson ratio of 0.5 for large plastic strains.

Figure 4.6 shows the rod geometry and mesh used for investigating the plasticity model. Conventional 4-node elements with a mesh size of ∼7mm were assigned to the rod with a length of 100 mm and a radius of 10 mm. The top surface applied with a displacement of 15 mm and two additional point constraints for avoiding rigid body motions. The red arrow at the bottom points toward the bottom surface of the rod, fixing the z-direction on this surface. Elastic material constant of ($\mu = 210 \cdot 10^3$[MPa], $\nu = 0.3$) were provided to the model with von Mises yield criteria and the perfect elastic-plastic hardening model ($_0S_{ys} = 700$[MPa]).

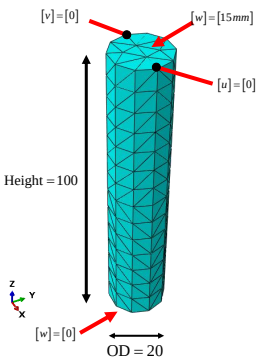

Figure 4.6: Mesh and geometry of tensile specimen in uniaxial stress state.

Figures 4.7 and 4.8 show the effective Poisson ratio and the stress-strain curve. The effective Poisson ratio starts at 0.3, and with a ramping plastic strain, the effective Poisson ratio goes towards a value of 0.5, thus following the desired behavior.

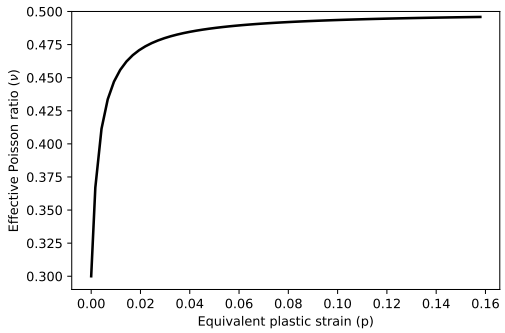

Figure 4.7: Effective Poisson ratio plotted against the equivalent plastic strain.

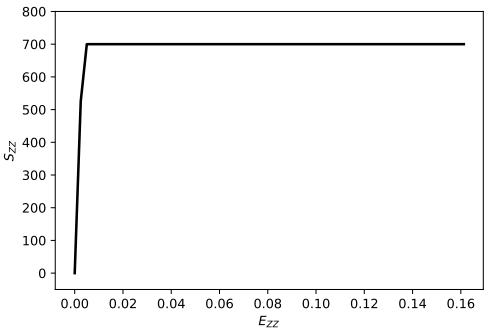

Figure 4.8: Stress strain curve for the rod subjected to uniaxial loading.

4.3 Beam subjected to plastic strains

A beam subjected to bending stresses gives tensile stresses on one side of the cross-section and compressive stresses on the other, while the relationship in between behaves close to linearly for the elastic regime. The equivalent stresses are at their largest at the top and bottom of the beam, creating two starting points for the plastic flow. With increasing load, the plastic flow increases in the two starting points and moves progressively towards the center cross-section. Unloading the beam creates a spring-back behavior. The stresses close to the top and bottom reduce in magnitude and changes sign. Closer to the center, the stresses reduce in magnitude. This gives a stress state going from tensile to compression to tensile to compression.

Figure 4.9 shows a beam with dimensions 1000 mm x 100 mm x 10 mm tested in plane stress conditions. The red arrow in Figure 4.9 indicates a load of -19 kN ramping linearly through 40 steps. A fully constrained fixture to the left of the beam is also visible in this figure. The 3-node ANS formulation, 6-node ANS formulation, 3-node conventional formulation, and 6-node conventional formulation were tested with the Green-Lagrange strain tensor. All with the Johnson-Cook model with constants ($b_1 = 700[\text{MPa}], b_2 = 300[\text{MPa}], b_3 = 0.6$) provided to the material, while the elastic parameters were set to follow ($\mu = 210 \cdot 10^3[\text{MPa}], \nu = 0.3$).

Figure 4.9: Geometry and mesh investigated of the beam subjected to plastic strains.

The applied force plotted against the right-hand side displacements (v) is visible in Figure 4.10. This figure shows the stiff nature of the 3-node constant strain elements, while the 6-node element formulations gave significantly larger displacements and strains. The 6-node ANS element gave a somewhat more stiff element formulation than the conventional formulation, but the two force-displacement curves follow each other closely throughout most of the simulation.

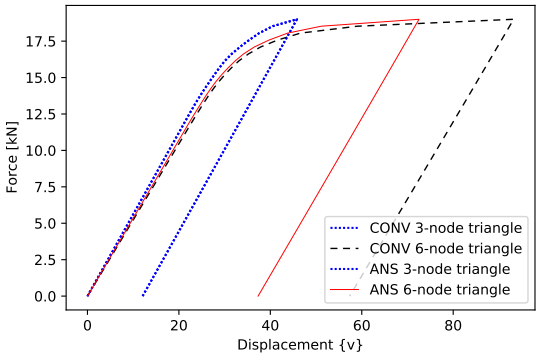

Figure 4.10: Applied force plotted against the v-displacement component of the bottom node on the right side in Figure 4.9

Figures 4.11 and 4.12 show the stress state at the left-hand side of the beam at -19 kN load and after the unloading process. Here the stresses have been linearly extrapolated from the three Gauss-points. Again the stiff nature of the constant strain elements is shown. At -19 kN load, the Stress-position curves can be divided into two parts; a linearly elastic part, where no plastic flow has occurred (center); and two parts influenced by the plastic flow (non-linear regime to the left and right of the center). This is best visible on the curve of the 6-node ANS formulation. The non-linear regime of the 6-node elements is much greater than for the 3-node element formulations, thus creating larger residual stresses in Figure 4.12. This figure follows the desired tensile to compression to tensile to compression stress behavior. Figure 4.13 shows the conventional 6-node element's normal stresses plotted at different load steps. Normal stresses (${}_0\mathbf{S}_{XX}$) around 700 [MPa] move toward the center of the beam. After the unloading, residual stresses occur in the tensile, compression, tensile, compression pattern.

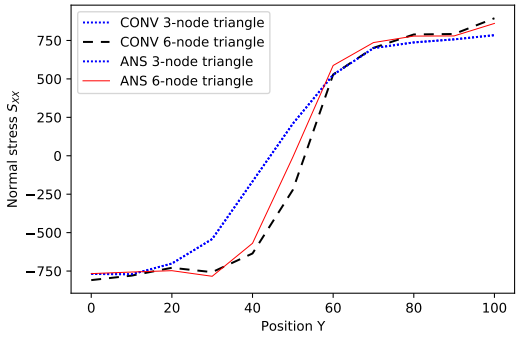

Figure 4.11: Normal stresses at a global load of 19.0 kN.

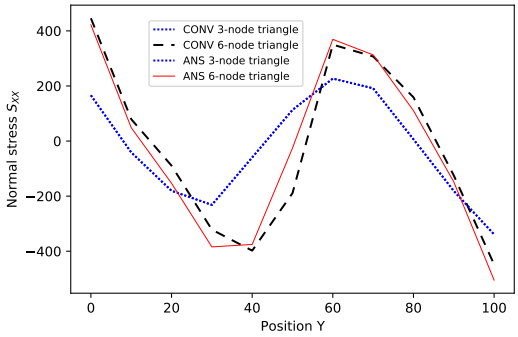

Figure 4.12: Normal stresses after the unloading process.

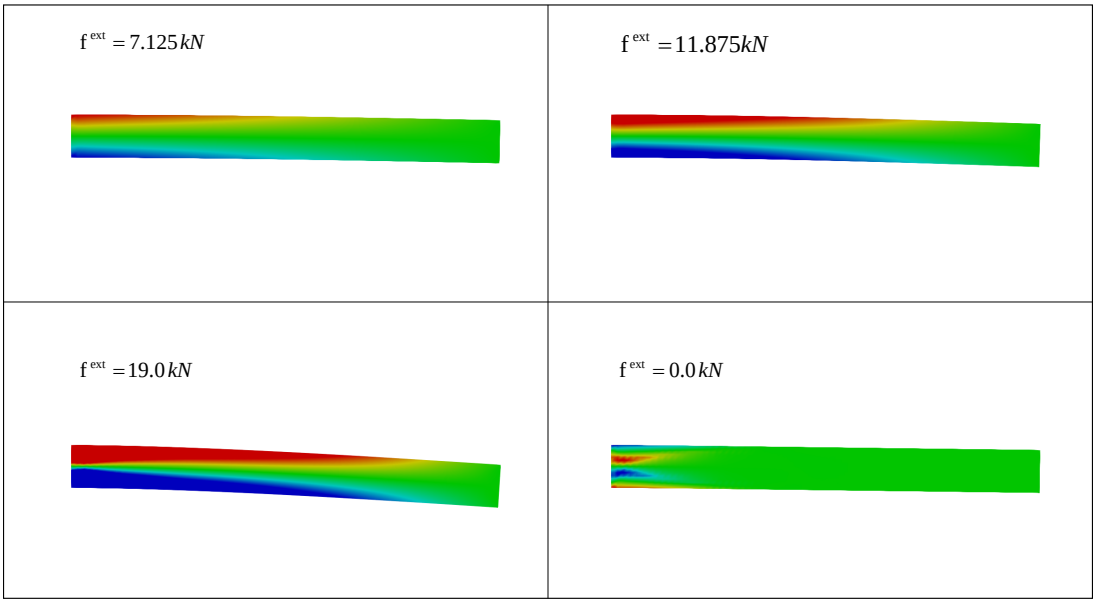

Figure 4.13: Normal stresses ${}_0\mathbf{S}_{XX}$ viewed at different load steps for the 6-node conventional element formulation.

4.4 Incompressible cube

The constant strain triangles and tetrahedrons are known for their poor convergence rate and stiff behavior. One way of measuring the performance of an element is through the incompressible cube. J. Schröder et al. [18] have previously discussed the incompressible cube, and a similar approach will be used here.

The cube investigated was set to follow the same geometry as J. Schröder et al. [18], giving a cube with 100 mm width, 100 mm length and 50 mm height. The geometry is also viewed in Figure 4.14. Since the cube contains two symmetry planes, the geometry could be split up into 1/4 of the actual geometry, giving dimensions of 50 mm length, 50 mm width, and 50 mm height. The smallest quadrilateral on the top surface was applied with a load of - 50 kN. The grey area in Figure 4.14, symbolizes a "floor" fixing the bottom surface in the y-direction. Along the yellow line in Figure 4.14, a shear stress singularity is occurring as a consequence of the applied loads and boundary conditions. Faster converging elements approach the displacement values faster, while the shear stress singularity diverge faster.

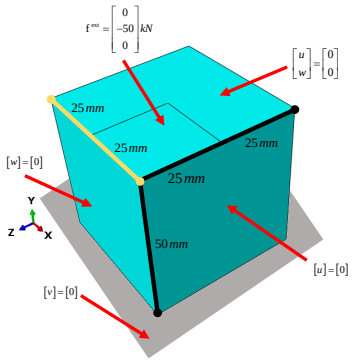

Figure 4.14: Geometry used for investigating the incompressible cube.

Figure 4.15 shows the maximum (v) displacement on the top surfaces plotted against degrees of freedom of the reduced model. The two 10-node tetrahedron formulations are superior in convergence pace for a smaller number of nodes, while the 4-node elements seems to lock for coarse mesh sizes. At around 7000 degrees of freedom, the differences in displacements can be seen as neglectable. In the general, the assumed natural interpolated strain formulation seems a bit stiffer than the higher-order conventional element formulation.

On the top surface, a shear stress singularity is occurring. Figure 4.16 shows the displacements plotted against the ${}_0X$-position along the yellow line at 34359 degrees of freedom. Both 10-node tetrahedral formulations follow each other closely, but some small discrepancies appear for stresses in Figure 4.17, where the conventional element formulations reduce the stresses quicker than the ANS formulations.

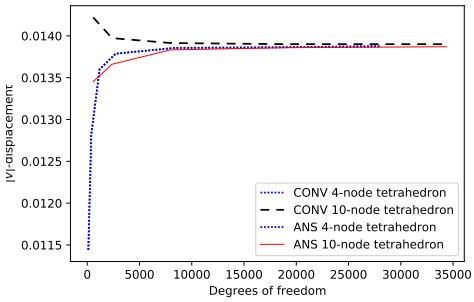

Figure 4.15: Displacements plotted against degrees of freedom for the incompressible cube.

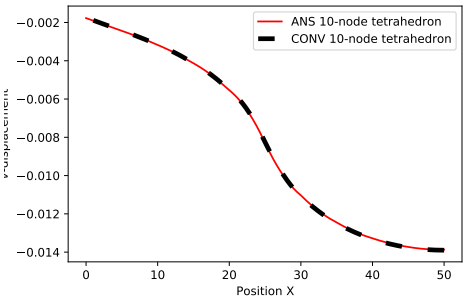

Figure 4.16: Displacements plotted against positions along the yellow line.

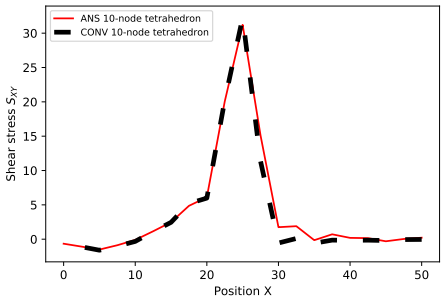

Figure 4.17: Shear stresses plotted against positions along the yellow line.

4.5 The Poynting effect of a cylinder subjected to torsion

John Henry Poynting investigated thin steel wires subjected to torsion [19]. His experiment gave elongation of the wires with an increasing twist. The Seth-Hill strain tensors are known for their shear-strain behavior, and choosing low values of (m) gives elongating behavior in combination with shear strains.

For investigating the Poynting effect and Seth-Hill strain tensors, a cylinder with a length of 100 mm and a diameter of 40 mm was subjected to torsion. Figure 4.18 illustrates the mesh and geometry of the cylinder. This model was applied with ANS 4-node and 10-node tetrahedral element geometries with a mesh size of ∼8mm. A twist of (0.5 radians) was subjected to the close side while being fixed in the radial direction. On the far side, all degrees of freedom was set to zero. Each element was further assigned with elastic material constants ($\mu = 210 \cdot 10^3, \nu = 0.3$).

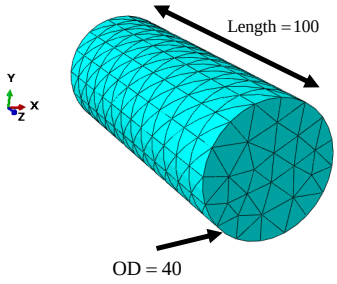

Figure 4.18: Mesh and geometry used for investigating the shortening/lengthening behaviour of a cylinder in torsion.

Figure 4.18 and 4.19 shows the average change of length with increasing twist of the cylinder. Figure 4.18 for the 4-node ANS tetrahedron and Figure 4.19 for the 10-node ANS tetrahedron. Both graphs explain a similar behavior: lower values of m give the lengthening behavior of rods/cylinders in elastic conditions, and visa versa. Both the 4-node and 10-node tetrahedron element formulation predicts similar elongation behaviors, but the 10-node tetrahedron elements seem more conservative with the length change. This is especially apparent in regimes with low m-values.

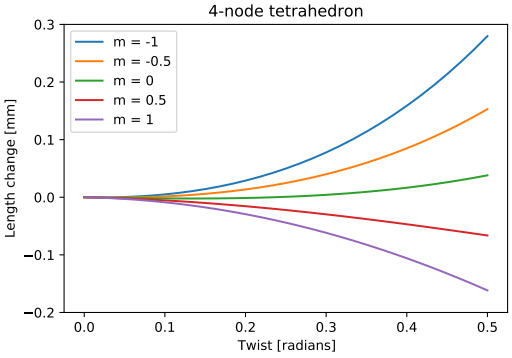

Figure 4.19: Change in length plotted against twist for a cylinder in elastic conditions with 4-node ANS elements.

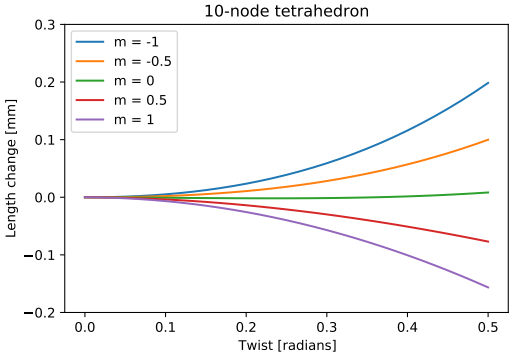

Figure 4.20: Change in length plotted against twist for a cylinder in elastic conditions with 10-node ANS elements.

Figure 4.21 shows how the twist affects the Almansi and Green-Lagrange strain tensors. In this figure, the displacements along the (w)-direction are scaled 50 times. At the outer rim, the elongation is at its largest. Moving towards the center of the rod reduces the magnitude of the elongation. A rod subjected to twist gives close to linearly shear strain in the radial directions, thus giving a bulge for the Green-Lagrange strain tensor and a crater for the Almansi strain tensor.

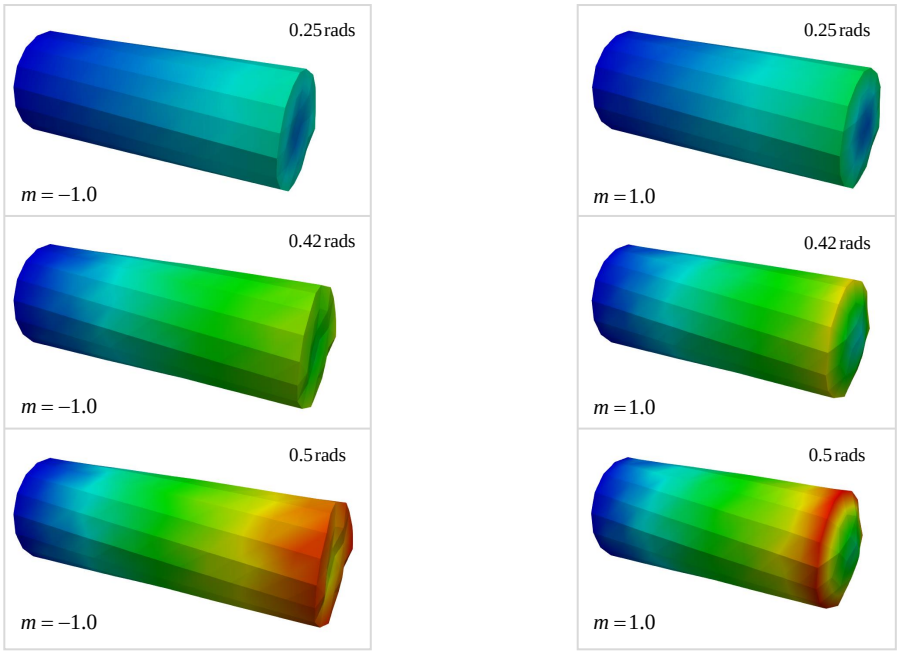

Figure 4.21: Length change rod subjected to twist with the 4-node tetrahedron formulation. Almansi strain to the left, Green-Lagrange strain to the right.

4.6 Considerations on shape functions and meshing

The results presented with the linear strain ANS triangle and tetrahedron used shape functions for relating three/four satellite covariant strain tensors, both formulations with shape functions having unit values in the center of the satellite strain tensors. This assumption is not derived from any mathematical standpoint and different unit value configurations would probably affect the results for simulations with large Taylor polynomial solutions. By changing the positions of the unit values, the element can probably be simulated as both softer and stiffer, depending on whether the unit values are placed closer or further away from the center.

An undesired effect of the ANS elements is a somewhat strange shear strain behavior. The mesh and applied boundary conditions of the "The Poynting effect of a cylinder subjected to torsion" is a great example of this behavior. This type of mesh in combination with boundary conditions does not necessarily give a symmetrical behavior with different signs of the twist, thus creating a somewhat strange unsymmetrical behavior for some mesh geometries. Care therefore needs to be taken into consideration when applying meshes with shear strains.

Chapter 5

Conclusion

The main objective of this thesis was to investigate higher-order ANS finite element formulations with Seth-Hill strain tensor properties. Elements interpolating covariant satellite Seth-Hill strain tensors were successfully derived and implemented into a Python FEA solver. The higher-order ANS elements were further compared with the lower-order ANS elements previously established by C. Felippa et al. [6], M. Eia et al. [4] and A. Østebø [5], and the conventional triangle and tetrahedral formulations.

A beam subjected to loading in the plastic regime was investigated for comparing different 2-dimensional element formulations. The 3-node conventional and ANS constant strain triangles showed a significantly stiffer behavior than the 6-node conventional and ANS linear strain triangles, both in the elastic and plastic regimes. The four tetrahedral elements were compared through the incompressible cube. Here the 10-node conventional element formulation overshoot the displacements for small mesh sizes, while the 4-node conventional, 4-node ANS and 10-node ANS underestimated the vertical displacements for small mesh sizes. The 4-node elements with more locking than the promising results of the 10-node ANS formulation.

At last, the Seth-Hill strain tenors were tested in elastic shear conditions and were found to give the desired properties such that the shortening in the Poynting effect could be simulated through the ANS formulations.

5.1 Further work

The dense nature of the tetrahedral elements creates large numbers of degrees of freedom packed in small regions. The ANS methodology is not bound to any particular element shapes, and an 8-node brick element could create better geometric arrangements. A 4-node quadrilateral element should also be of interest when expanding the element library of the ANS methodology.

The higher-order ANS elements created in this thesis interpolated the covariant strain tensor of three/four satellite strain tensors. Another approach is through interpolation of three/four satellite deformation gradients. Future studies should compare ANS interpolated deformation gradient elements with ANS interpolated strain element formulations, both for the element geometries represented in this thesis and the futuristic 4-node quadrilateral and 8-node brick elements.

References

[1] Seth BR. Generalized strain measure with applications to physical problems. Madison, Wisconsin: University of Wisconsin; 1961.

[2] Hill R. On constitutive inequalities for simple materials—I. *Journal of the Mechanics and Physics of Solids*, 16(4):229–242, 1968.

[3] Willam K. Finite element analysis of cellular structures [PhD thesis]. Berkeley, California: University of California; 1969.

[4] Jacobsen HI, Eia, ME. 2d triangular finite elements based on assumed natural coordinate strains and the seth-hill family of finite strains [M.Sc thesis]. Trondheim: Norwegian University of Science and Technology; 2021.

[5] Østebø A. Triangle and tetrahedron finite elements based on assumed natural coordinate strains and the seth-hill family of finite strains [M.Sc thesis]. Trondheim: Norwegian University of Science and Technology; 2021.

[6] Felippa C, Melo, C. Unification of geometrically nonlinear finite element analysis of solids and structures. 13th World Congress on Computational Mechanics (WCCM XIII). New York, New York; 2018.

[7] Irgens F. Continuum mechanics. 1st ed. Berlin Heidelberg: Springer-Verlag; 2008.

[8] Wikipedia contributors. Finite strain theory. Wikipedia, The Free Encyclopedia; 11.07.2005; [21.03.2022; 23.03.2022] URL: `https://en.wikipedia.org/wiki/Finite_strain_theory`.

[9] Lee EH, Liu DT. Finite-strain elastic—plastic theory with application to plane-wave analysis. *Journal of Applied Physics*, 38(1):19–27, 1967.

[10] Lee EH. Elastic-Plastic Deformation at Finite Strains. *Journal of Applied Mechanics*, 36(1):1–6, 03 1969.

[11] Green AE, Naghdi PM. A general theory of an elastic-plastic continuum. *Archive for Rational Mechanics and Analysis*, 18:251–281, 1965.

[12] Dhondt G. Ten-node tetrahedral element (C3D10 and F3D10). Cambridge, Massachusetts: Massachusetts Institute of Technology; [06.06.2022] URL: `https://web.mit.edu/calculix_v2.7/CalculiX/ccx_2.7/doc/ccx/node33.html`.

[13] FEBio. Quadratic tetrahedral elements. Salt Lake City, Utah: University of Utah; [15.05.2022] URL: `https://help.febio.org/FEBio/FEBio_tm_2_7/FEBio_tm_2-7-Subsection-4.1.4.html`.

[14] Sze KY, Zhu D. A quadratic assumed natural strain curved triangular shell element. *Computer Methods in Applied Mechanics and Engineering*, 174(1):57–71, 1999.

[15] Krabbenhoft K. Basic computational plasticity. Lyngby: Technical University of Denmark; 2002 [28.10.2021] URL: `http://homes.civil.aau.dk/lda/continuum/plast.pdf`.

[16] Nagtegaal J. On the implementation of inelastic constitutive equations with special reference to large deformation problems. *Computer Methods in Applied Mechanics and Engineering*, 33(1):469–484, 1982.

[17] Simo JC, Taylor RL. Consistent tangent operators for rate-independent elastoplasticity. *Computer Methods in Applied Mechanics and Engineering*, 48(1):101–118, 1985.

[18] Schröder J, Wick T et al. A selection of benchmark problems in solid mechanics and applied mathematics. *Archives of Computational Methods in Engineering*, 28:1–39, 09 2020.

[19] Poynting JH. On pressure perpendicular to the shear planes in finite pure shears , and on the lengthening of loaded wires when twisted. *Proceedings of the Royal Society of London. Series A, Containing Papers of a Mathematical and Physical Character*, 82(557):546–559, 1909.

Appendix A

Tables

Table A.1: Relation between basis vectors and nodal displacement components for the 6-node ANS triangle.

Rod length	**Rod basis 1**	**Rod basis 2**	**Nodes**	**Displacements**	
L_1	$\mathbf{e}^1$	$\mathbf{n}^1$	$1 \to 4$	$\delta u_1, \delta v_1, \delta u_4, \delta v_4$	$\delta\widetilde{u}_1, \delta\widetilde{v}_1, \delta\widetilde{u}_2, \delta\widetilde{v}_2$
L_2	$\mathbf{e}^2$	$\mathbf{n}^2$	$4 \to 6$	$\delta u_4, \delta v_4, \delta u_6, \delta v_6$	$\delta\widetilde{u}_3, \delta\widetilde{v}_3, \delta\widetilde{u}_4, \delta\widetilde{v}_4$
L_3	$\mathbf{e}^3$	$\mathbf{n}^3$	$6 \to 1$	$\delta u_6, \delta v_6, \delta u_1, \delta v_1$	$\delta\widetilde{u}_5, \delta\widetilde{v}_5, \delta\widetilde{u}_6, \delta\widetilde{v}_6$
L_4	$\mathbf{e}^4$	$\mathbf{n}^4$	$4 \to 2$	$\delta u_4, \delta v_4, \delta u_2, \delta v_2$	$\delta\widetilde{u}_7, \delta\widetilde{v}_7, \delta\widetilde{u}_8, \delta\widetilde{v}_8$
L_5	$\mathbf{e}^5$	$\mathbf{n}^5$	$2 \to 5$	$\delta u_2, \delta v_2, \delta u_5, \delta v_5$	$\delta\widetilde{u}_9, \delta\widetilde{v}_9, \delta\widetilde{u}_{10}, \delta\widetilde{v}_{10}$
L_6	$\mathbf{e}^6$	$\mathbf{n}^6$	$5 \to 4$	$\delta u_5, \delta v_5, \delta u_4, \delta v_1$	$\delta\widetilde{u}_{11}, \delta\widetilde{v}_{11}, \delta\widetilde{u}_{12}, \delta\widetilde{v}_{12}$
L_7	$\mathbf{e}^7$	$\mathbf{n}^7$	$6 \to 5$	$\delta u_6, \delta v_6, \delta u_5, \delta v_5$	$\delta\widetilde{u}_{13}, \delta\widetilde{v}_{13}, \delta\widetilde{u}_{14}, \delta\widetilde{v}_{14}$
L_8	$\mathbf{e}^8$	$\mathbf{n}^8$	$5 \to 3$	$\delta u_5, \delta v_5, \delta u_3, \delta v_3$	$\delta\widetilde{u}_{15}, \delta\widetilde{v}_{15}, \delta\widetilde{u}_{16}, \delta\widetilde{v}_{16}$
L_9	$\mathbf{e}^9$	$\mathbf{n}^9$	$3 \to 6$	$\delta u_3, \delta v_3, \delta u_6, \delta v_6$	$\delta\widetilde{u}_{17}, \delta\widetilde{v}_{17}, \delta\widetilde{u}_{18}, \delta\widetilde{v}_{18}$

Table A.2: Relation between basis vectors and nodal displacement components for the 4-node ANS tetrahedron.

Rod length	**Rod basis 1**	**Rod basis 2**	**Rod basis 3**	**Nodes**	**Displacements**	
L_1	$\mathbf{e}^1$	$\mathbf{n}^1$	$\boldsymbol{\eta}^1$	$1 \to 2$	$\delta u_1, \delta v_1, \delta w_1$ $\delta u_2, \delta v_2, \delta w_2$	$\delta\widetilde{u}_1, \delta\widetilde{v}_1, \delta\widetilde{w}_1$ $\delta\widetilde{u}_2, \delta\widetilde{v}_2, \delta\widetilde{w}_2$
L_2	$\mathbf{e}^2$	$\mathbf{n}^2$	$\boldsymbol{\eta}^2$	$2 \to 3$	$\delta u_2, \delta v_2, \delta w_2$ $\delta u_3, \delta v_3, \delta w_3$	$\delta\widetilde{u}_3, \delta\widetilde{v}_3, \delta\widetilde{w}_3$ $\delta\widetilde{u}_4, \delta\widetilde{v}_4, \delta\widetilde{w}_4$
L_3	$\mathbf{e}^3$	$\mathbf{n}^3$	$\boldsymbol{\eta}^3$	$3 \to 1$	$\delta u_3, \delta v_3, \delta w_3$ $\delta u_1, \delta v_1, \delta w_1$	$\delta\widetilde{u}_5, \delta\widetilde{v}_5, \delta\widetilde{w}_5$ $\delta\widetilde{u}_6, \delta\widetilde{v}_6, \delta\widetilde{w}_6$
L_4	$\mathbf{e}^4$	$\mathbf{n}^4$	$\boldsymbol{\eta}^4$	$1 \to 4$	$\delta u_1, \delta v_1, \delta w_1$ $\delta u_4, \delta v_4, \delta w_4$	$\delta\widetilde{u}_7, \delta\widetilde{v}_7, \delta\widetilde{w}_7$ $\delta\widetilde{u}_8, \delta\widetilde{v}_8, \delta\widetilde{w}_8$
L_5	$\mathbf{e}^5$	$\mathbf{n}^5$	$\boldsymbol{\eta}^5$	$2 \to 4$	$\delta u_2, \delta v_2, \delta w_2$ $\delta u_4, \delta v_4, \delta w_4$	$\delta\widetilde{u}_9, \delta\widetilde{v}_9, \delta\widetilde{w}_9$ $\delta\widetilde{u}_{10}, \delta\widetilde{v}_{10}, \delta\widetilde{w}_{10}$
L_6	$\mathbf{e}^6$	$\mathbf{n}^6$	$\boldsymbol{\eta}^6$	$3 \to 4$	$\delta u_3, \delta v_3, \delta w_3$ $\delta u_4, \delta v_4, \delta w_4$	$\delta\widetilde{u}_{11}, \delta\widetilde{v}_{11}, \delta\widetilde{w}_{11}$ $\delta\widetilde{u}_{12}, \delta\widetilde{v}_{12}, \delta\widetilde{w}_{12}$

Table A.3: Relation between basis vectors and nodal displacement components for the 10-node ANS tetrahedron satellite tetrahedron number 1.

Rod length	**Basis 1**	**Basis 2**	**Basis 3**	**Nodes**	**Displacements**	
L_1	$\mathbf{e}^1$	$\mathbf{n}^1$	$\boldsymbol{\eta}^1$	$5 \to 7$	$\delta u_5, \delta v_5, \delta w_5$ $\delta u_7, \delta v_7, \delta w_7$	$\delta\widetilde{u}_1, \delta\widetilde{v}_1, \delta\widetilde{w}_1$ $\delta\widetilde{u}_2, \delta\widetilde{v}_2, \delta\widetilde{w}_2$
L_2	$\mathbf{e}^2$	$\mathbf{n}^2$	$\boldsymbol{\eta}^2$	$7 \to 8$	$\delta u_7, \delta v_7, \delta w_7$ $\delta u_3, \delta v_8, \delta w_8$	$\delta\widetilde{u}_3, \delta\widetilde{v}_3, \delta\widetilde{w}_3$ $\delta\widetilde{u}_4, \delta\widetilde{v}_4, \delta\widetilde{w}_4$
L_3	$\mathbf{e}^3$	$\mathbf{n}^3$	$\boldsymbol{\eta}^3$	$8 \to 5$	$\delta u_8, \delta v_8, \delta w_8$ $\delta u_5, \delta v_5, \delta w_5$	$\delta\widetilde{u}_5, \delta\widetilde{v}_5, \delta\widetilde{w}_5$ $\delta\widetilde{u}_6, \delta\widetilde{v}_6, \delta\widetilde{w}_6$
L_4	$\mathbf{e}^4$	$\mathbf{n}^4$	$\boldsymbol{\eta}^4$	$5 \to 1$	$\delta u_5, \delta v_5, \delta w_5$ $\delta u_1, \delta v_1, \delta w_1$	$\delta\widetilde{u}_7, \delta\widetilde{v}_7, \delta\widetilde{w}_7$ $\delta\widetilde{u}_8, \delta\widetilde{v}_8, \delta\widetilde{w}_8$
L_5	$\mathbf{e}^5$	$\mathbf{n}^5$	$\boldsymbol{\eta}^5$	$7 \to 1$	$\delta u_7, \delta v_7, \delta w_7$ $\delta u_1, \delta v_1, \delta w_1$	$\delta\widetilde{u}_9, \delta\widetilde{v}_9, \delta\widetilde{w}_9$ $\delta\widetilde{u}_{10}, \delta\widetilde{v}_{10}, \delta\widetilde{w}_{10}$
L_6	$\mathbf{e}^6$	$\mathbf{n}^6$	$\boldsymbol{\eta}^6$	$8 \to 1$	$\delta u_8, \delta v_8, \delta w_8$ $\delta u_1, \delta v_1, \delta w_1$	$\delta\widetilde{u}_{11}, \delta\widetilde{v}_{11}, \delta\widetilde{w}_{11}$ $\delta\widetilde{u}_{12}, \delta\widetilde{v}_{12}, \delta\widetilde{w}_{12}$

Table A.4: Relation between basis vectors and nodal displacement components for the 10-node ANS tetrahedron satellite tetrahedron number 2.

Rod length	**Basis 1**	**Basis 2**	**Basis 3**	**Nodes**	**Displacements**	
L_7	$\mathbf{e}^7$	$\mathbf{n}^7$	$\boldsymbol{\eta}^7$	$5 \rightarrow 6$	$\delta u_5, \delta v_5, \delta w_5$ $\delta u_6, \delta v_6, \delta w_6$	$\delta\widetilde{u}_{13}, \delta\widetilde{v}_{13}, \delta\widetilde{w}_{13}$ $\delta\widetilde{u}_{14}, \delta\widetilde{v}_{14}, \delta\widetilde{w}_{14}$
L_8	$\mathbf{e}^8$	$\mathbf{n}^8$	$\boldsymbol{\eta}^8$	$6 \rightarrow 9$	$\delta u_6, \delta v_6, \delta w_6$ $\delta u_9, \delta v_9, \delta w_9$	$\delta\widetilde{u}_{15}, \delta\widetilde{v}_{15}, \delta\widetilde{w}_{15}$ $\delta\widetilde{u}_{16}, \delta\widetilde{v}_{16}, \delta\widetilde{w}_{16}$
L_9	$\mathbf{e}^9$	$\mathbf{n}^9$	$\boldsymbol{\eta}^9$	$9 \rightarrow 5$	$\delta u_9, \delta v_9, \delta w_9$ $\delta u_5, \delta v_5, \delta w_5$	$\delta\widetilde{u}_{17}, \delta\widetilde{v}_{17}, \delta\widetilde{w}_{17}$ $\delta\widetilde{u}_{18}, \delta\widetilde{v}_{18}, \delta\widetilde{w}_{18}$
L_{10}	$\mathbf{e}^{10}$	$\mathbf{n}^{10}$	$\boldsymbol{\eta}^{10}$	$5 \rightarrow 2$	$\delta u_5, \delta v_5, \delta w_5$ $\delta u_2, \delta v_2, \delta w_2$	$\delta\widetilde{u}_{19}, \delta\widetilde{v}_{19}, \delta\widetilde{w}_{19}$ $\delta\widetilde{u}_{20}, \delta\widetilde{v}_{20}, \delta\widetilde{w}_{20}$
L_{11}	$\mathbf{e}^{11}$	$\mathbf{n}^{11}$	$\boldsymbol{\eta}^{11}$	$6 \rightarrow 2$	$\delta u_6, \delta v_6, \delta w_6$ $\delta u_2, \delta v_2, \delta w_2$	$\delta\widetilde{u}_{21}, \delta\widetilde{v}_{21}, \delta\widetilde{w}_{21}$ $\delta\widetilde{u}_{22}, \delta\widetilde{v}_{22}, \delta\widetilde{w}_{22}$
L_{12}	$\mathbf{e}^{12}$	$\mathbf{n}^{12}$	$\boldsymbol{\eta}^{12}$	$9 \rightarrow 2$	$\delta u_9, \delta v_9, \delta w_9$ $\delta u_2, \delta v_2, \delta w_2$	$\delta\widetilde{u}_{23}, \delta\widetilde{v}_{23}, \delta\widetilde{w}_{23}$ $\delta\widetilde{u}_{24}, \delta\widetilde{v}_{24}, \delta\widetilde{w}_{24}$

Table A.5: Relation between basis vectors and nodal displacement components for the 10-node ANS tetrahedron satellite tetrahedron number 3.

Rod length	**Basis 1**	**Basis 2**	**Basis 3**	**Nodes**	**Displacements**	
L_{13}	$\mathbf{e}^{13}$	$\mathbf{n}^{13}$	$\boldsymbol{\eta}^{13}$	$6 \rightarrow 7$	$\delta u_6, \delta v_6, \delta w_6$ $\delta u_7, \delta v_7, \delta w_7$	$\delta\widetilde{u}_{25}, \delta\widetilde{v}_{25}, \delta\widetilde{w}_{25}$ $\delta\widetilde{u}_{26}, \delta\widetilde{v}_{26}, \delta\widetilde{w}_{26}$
L_{14}	$\mathbf{e}^{14}$	$\mathbf{n}^{14}$	$\boldsymbol{\eta}^{14}$	$7 \rightarrow 10$	$\delta u_7, \delta v_7, \delta w_7$ $\delta u_{10}, \delta v_{10}, \delta w_{10}$	$\delta\widetilde{u}_{27}, \delta\widetilde{v}_{27}, \delta\widetilde{w}_{27}$ $\delta\widetilde{u}_{28}, \delta\widetilde{v}_{28}, \delta\widetilde{w}_{28}$
L_{15}	$\mathbf{e}^{15}$	$\mathbf{n}^{15}$	$\boldsymbol{\eta}^{15}$	$10 \rightarrow 6$	$\delta u_{10}, \delta v_{10}, \delta w_{10}$ $\delta u_6, \delta v_6, \delta w_6$	$\delta\widetilde{u}_{29}, \delta\widetilde{v}_{29}, \delta\widetilde{w}_{29}$ $\delta\widetilde{u}_{30}, \delta\widetilde{v}_{30}, \delta\widetilde{w}_{30}$
L_{16}	$\mathbf{e}^{16}$	$\mathbf{n}^{16}$	$\boldsymbol{\eta}^{16}$	$6 \rightarrow 3$	$\delta u_6, \delta v_6, \delta w_6$ $\delta u_3, \delta v_3, \delta w_3$	$\delta\widetilde{u}_{31}, \delta\widetilde{v}_{31}, \delta\widetilde{w}_{31}$ $\delta\widetilde{u}_{32}, \delta\widetilde{v}_{32}, \delta\widetilde{w}_{32}$
L_{17}	$\mathbf{e}^{17}$	$\mathbf{n}^{17}$	$\boldsymbol{\eta}^{17}$	$7 \rightarrow 3$	$\delta u_7, \delta v_7, \delta w_3$ $\delta u_3, \delta v_3, \delta w_3$	$\delta\widetilde{u}_{33}, \delta\widetilde{v}_{33}, \delta\widetilde{w}_{33}$ $\delta\widetilde{u}_{34}, \delta\widetilde{v}_{34}, \delta\widetilde{w}_{34}$
L_{18}	$\mathbf{e}^{18}$	$\mathbf{n}^{18}$	$\boldsymbol{\eta}^{18}$	$10 \rightarrow 3$	$\delta u_{10}, \delta v_{10}, \delta w_{10}$ $\delta u_3, \delta v_3, \delta w_3$	$\delta\widetilde{u}_{35}, \delta\widetilde{v}_{35}, \delta\widetilde{w}_{35}$ $\delta\widetilde{u}_{36}, \delta\widetilde{v}_{36}, \delta\widetilde{w}_{36}$

Table A.6: Relation between basis vectors and nodal displacement components for the 10-node ANS tetrahedron satellite tetrahedron number 4.

Rod length	**Basis 1**	**Basis 2**	**Basis 3**	**Nodes**	**Displacements**	
L_{19}	$\mathbf{e}^{19}$	$\mathbf{n}^{19}$	$\boldsymbol{\eta}^{19}$	$8 \rightarrow 9$	$\delta u_8, \delta v_8, \delta w_8$ $\delta u_9, \delta v_9, \delta w_9$	$\delta \widetilde{u}_{37}, \delta \widetilde{v}_{37}, \delta \widetilde{w}_{37}$ $\delta \widetilde{u}_{38}, \delta \widetilde{v}_{38}, \delta \widetilde{w}_{38}$
L_{20}	$\mathbf{e}^{20}$	$\mathbf{n}^{20}$	$\boldsymbol{\eta}^{20}$	$9 \rightarrow 10$	$\delta u_9, \delta v_9, \delta w_9$ $\delta u_{10}, \delta v_{10}, \delta w_{10}$	$\delta \widetilde{u}_{39}, \delta \widetilde{v}_{39}, \delta \widetilde{w}_{39}$ $\delta \widetilde{u}_{40}, \delta \widetilde{v}_{40}, \delta \widetilde{w}_{40}$
L_{21}	$\mathbf{e}^{21}$	$\mathbf{n}^{21}$	$\boldsymbol{\eta}^{21}$	$10 \rightarrow 8$	$\delta u_{10}, \delta v_{10}, \delta w_{10}$ $\delta u_8, \delta v_8, \delta w_8$	$\delta \widetilde{u}_{41}, \delta \widetilde{v}_{41}, \delta \widetilde{w}_{41}$ $\delta \widetilde{u}_{42}, \delta \widetilde{v}_{42}, \delta \widetilde{w}_{42}$
L_{22}	$\mathbf{e}^{22}$	$\mathbf{n}^{22}$	$\boldsymbol{\eta}^{22}$	$8 \rightarrow 4$	$\delta u_8, \delta v_8, \delta w_8$ $\delta u_4, \delta v_4, \delta w_4$	$\delta \widetilde{u}_{43}, \delta \widetilde{v}_{43}, \delta \widetilde{w}_{43}$ $\delta \widetilde{u}_{44}, \delta \widetilde{v}_{44}, \delta \widetilde{w}_{44}$
L_{23}	$\mathbf{e}^{23}$	$\mathbf{n}^{23}$	$\boldsymbol{\eta}^{23}$	$9 \rightarrow 4$	$\delta u_9, \delta v_9, \delta w_9$ $\delta u_4, \delta v_4, \delta w_4$	$\delta \widetilde{u}_{45}, \delta \widetilde{v}_{45}, \delta \widetilde{w}_{45}$ $\delta \widetilde{u}_{46}, \delta \widetilde{v}_{46}, \delta \widetilde{w}_{46}$
L_{24}	$\mathbf{e}^{24}$	$\mathbf{n}^{24}$	$\boldsymbol{\eta}^{24}$	$10 \rightarrow 4$	$\delta u_{10}, \delta v_{10}, \delta w_{10}$ $\delta u_4, \delta v_4, \delta w_4$	$\delta \widetilde{u}_{47}, \delta \widetilde{v}_{47}, \delta \widetilde{w}_{47}$ $\delta \widetilde{u}_{48}, \delta \widetilde{v}_{48}, \delta \widetilde{w}_{48}$